A DIFFERENTIAL CURVE OF GROWTH ANALYSIS OF THE SPECTRUM OF THE STAR THETA URSAE MAJORIS

By

EDWARD COVERT MANGOLD

Bachelor of Science
Rockhurst College
Kansas City, Missouri
1959

Master of Science
University of Maryland
College Park, Maryland
1964

Submitted to the faculty of the Graduate College
of the Oklahoma State University
in partial fulfillment of the requirements
for the degree of
DOCTOR OF PHILOSOPHY
July, 1968

A DIFFERENTIAL CURVE OF GROWTH ANALYSIS OF THE SPECTRUM OF THE STAR THETA URSAE MAJORIS

Thesis Approved:

Leon W. Schroeder
Thesis Adviser

Francis C. Todd

K. S. Mendenhall

N. N. Durham
Dean of the Graduate College

ACKNOWLEDGMENTS

The author wishes to express his appreciation to Dr. Leon Schroeder who initially suggested the problem, provided the intensitometer tracings, and gave direction and encouragement during the investigation.

Gratitude must be expressed to Dr. K. O. Wright who took the spectrograms of θ Ursae Majoris on which this study is based at the Dominion Astrophysical Observatory; also to Dr. Hugh O. Peebles for permission to use his measurements and for supplying his dispersions.

The Oklahoma State University Research Foundation provided financial support for obtaining the observations. Machine time for reduction of the observations was made available by the Oklahoma State University Computer Center.

The author's financial support during the time in which the thesis work was accomplished was provided by employment at the Oklahoma State University Research Foundation Electronics Laboratory. The author wishes to express his thankfulness to Mr. Richard F. Buck and Dr. Harold E. Harrington of the Laboratory for providing the position which has made a substantial contribution to the development of my professional career.

And finally I would like to express my deepest gratitude to my wife, Carolyn, whose long years of sacrifice, understanding and loyal support were a source of deep consolation in the preparation of this dissertation.

TABLE OF CONTENTS

Chapter		Page
I.	INTRODUCTION.	1
II.	THE CURVE OF GROWTH	5
	Basic Mechanism of the Formation of Lines in a Stellar Atmosphere	5
	Assumptions Made in the Curve of Growth Technique. .	7
	The Two Extreme Models of a Stellar Atmosphere . . .	9
	The Boltzmann Equation	10
	The Saha Equation.	12
	The f-values	13
	Doppler Effect and the Velocity of the Radiating Atoms.	14
	Damping Constant	15
	Criticism of the Curve of Growth Technique	16
	Absolute versus Differential Curve of Growth Techniques	17
	Cowley and Cowley's Solar Curve of Growth.	20
	Comparison of the Differential Curve of Growth and Model Atmosphere Techniques.	22
	Mathematical Development of the Curve of Growth. . .	23
	Application of the Curve of Growth Technique in the Differential Form.	28
	Summary of Steps Involved in a Differential Curve of Growth Analysis.	30
	Sources of Error in the Curve of Growth Technique. .	33
III.	OBSERVATIONAL MATERIAL.	37
	Spectrograms and Tracings.	37
	Location of the Continuum.	37
	Approximation of the Profiles.	40
	Identification of the Lines.	40
	Selection of Lines	41
	Effects of Blending.	41
	Number of Lines Available for a Particular Element .	42
	Determination of Equivalent Widths	42
	Comparison of Equivalent Width Measurements With Those of Greenstein.	61
IV.	RESULTS	63
	Influence of Model Atmospheres Concepts.	63

TABLE OF CONTENTS (Continued)

Chapter		Page
	Calculation of Abundances	64
	Statistical Weighting of Data	66
	Determination of Excitation Temperature by Differential Comparison With the Sun	72
	Partition Function	76
	Determination of Velocity Correction	76
	Determination of Electron Pressure	79
	Determination of the Correction for Continuous Optical Absorption	81
	Calculation of Abundance	82
	Factors Determining the Quality of the Data	84
	Results for Individual Elements	85
V.	CONCLUSIONS	155
	Summary of Physical Properties of θ Ursae Majoris	155
	Comparison with the Work of Peebles	158
	Comparison of the Results With Greenstein	159
REFERENCES		162
APPENDIX A.	REVIEW OF METHODS USED IN THE LITERATURE FOR DIFFERENTIAL CURVE OF GROWTH ANALYSIS	165
	Determination of Abundances	169
	Excitation Temperature	169
	Ionization Temperature	171
	Simultaneous Determination of Ionization Temperature and Electron Pressure	172
	Effective Temperatures	176
	Values of the Solar Parameters	178
	Absolute Techniques Using f-values	178
	Analysis by Both Curve of Growth and Model Atmosphere Methods	179
APPENDIX B.	STATISTICAL TECHNIQUES AND DETERMINATION OF ERRORS	184
	Statistical Methods	184
	Error Analysis	187

LIST OF TABLES

Table		Page
I.	Victoria Plate, Microphotometer, and Intensitometer Data for θ Ursae Majoris.	38
II.	List of Atoms and Ions Studied in This Investigation. .	43
III.	Line Intensities in the Spectrum of θ Ursae Majoris . .	47
IV.	Data Pertinent to Lines Located on the Wings of Hydrogen	60
V.	Model Atmosphere of the Sun	65
VI.	Curve of Growth Statistical Weights	68
VII.	Results of Least Squares Fits of Straight Lines to Plots of $[\eta]$ vs. Excitation Potential Data.	70
VIII.	Comparison of Excitation Temperatures Derived by the Differential Technique With Values Obtained by Peebles Weighted Data	71
IX.	Elements With Significant Values of Fisher's F.	74
X.	Experimental and Theoretical Determination of Log v^{o}/v^{*}	78
XI.	Determination of Electron Pressure of θ Ursae Majoris Relative to the Sun	80
XII.	Differential Curve of Growth Data Derived From Na I Lines	86
XIII.	Differential Curve of Growth Data Derived From Mg I Lines	87
XIV.	Differential Curve of Growth Data Derived From Mg II Lines	88
XV.	Differential Curve of Growth Data Derived From Si I Lines	89
XVI.	Differential Curve of Growth Data Derived From Si II Lines	90

LIST OF TABLES (Continued)

Table		Page
XVII.	Differential Curve of Growth Data Derived From Ca I Lines	91
XVIII.	Differential Curve of Growth Data Derived From Sc I Lines	93
XIX.	Differential Curve of Growth Data Derived From Sc II Lines	94
XX.	Differential Curve of Growth Data Derived From Ti I Lines	96
XXI.	Differential Curve of Growth Data Derived From Ti II Lines	99
XXII.	Differential Curve of Growth Data Derived From V I Lines	102
XXIII.	Differential Curve of Growth Data Derived From V II Lines	104
XXIV.	Differential Curve of Growth Data Derived From Cr I Lines	106
XXV.	Differential Curve of Growth Data Derived From Cr II Lines	109
XXVI.	Differential Curve of Growth Data Derived From Mn I Lines	111
XXVII.	Differential Curve of Growth Data Derived From Mn II Lines	113
XXVIII.	Differential Curve of Growth Data Derived From Fe I Lines	114
XXIX.	Differential Curve of Growth Data Derived From Fe II Lines	119
XXX.	Differential Curve of Growth Data Derived From Co I Lines	121
XXXI.	Differential Curve of Growth Data Derived From Ni I Lines	123
XXXII.	Differential Curve of Growth Data Derived From Cu I Lines	125

LIST OF TABLES (Continued)

Table		Page
XXXIII.	Differential Curve of Growth Data Derived From Zn I Lines.	126
XXXIV.	Differential Curve of Growth Data Derived From Sr I Lines.	127
XXXV.	Differential Curve of Growth Data Derived From Sr II Lines.	128
XXXVI.	Differential Curve of Growth Data Derived From Y I Lines.	129
XXXVII.	Differential Curve of Growth Data Derived From Y II Lines.	130
XXXVIII.	Differential Curve of Growth Data Derived From Zr II Lines.	131
XXXIX.	Differential Curve of Growth Data Derived From Ba II Lines.	132
XL.	Differential Curve of Growth Data Derived From La II Lines.	133
XLI.	Differential Curve of Growth Data Derived From Ce II Lines.	134
XLII.	Differential Curve of Growth Data Derived From Nd II Lines.	136
XLIII.	Differential Curve of Growth Data Derived From Sm II Lines.	137
XLIV.	Differential Curve of Growth Data Derived From Eu II Lines.	138
XLV.	Differential Curve of Growth Data Derived From Gd II Lines.	139
XLVI.	Physical Parameters of θ Ursae Majoris Determined From Curve of Growth Analyses.	157
XLVII.	Comparison of Values of Abundances Between Greenstein and This Work.	161
XLVIII.	Differential Curve of Growth Techniques Used by Other Authors in the Literature.	166

LIST OF TABLES (Continued)

Table		Page
XLIX.	Pseudo-Equivalent Widths for H γ	177
L.	Extremes of Excitation Temperature.	186

LIST OF FIGURES

Figure		Page
1.	The Equivalent Width, W, of a Spectral Line.	7
2.	The Four Theoretical Curves of Growth Used by Peebles. . .	11
3.	Cowley and Cowley's Curve of Growth of the Sun	21
4.	The Curve of Growth for the λ3933 Line of Ca II.	26
5.	Intensitometer Tracing of the Spectrum	39
6.	Comparison of Equivalent Widths Measured on Different Tracings with the Average Values	45
7.	Comparison of Equivalent Widths.	62
8.	Plot of [η] vs. Excitation Potential for Ca I.	92
9.	Plot of [η] vs. Excitation Potential for Sc II	95
10.	Plot of [η] vs. Excitation Potential for Ti I.	98
11.	Plot of [η] vs. Excitation Potential for Ti II	101
12.	Plot of [η] vs. Excitation Potential for V I	103
13.	Plot of [η] vs. Excitation Potential for V II.	105
14.	Plot of [η] vs. Excitation Potential for Cr I.	108
15.	Plot of [η] vs. Excitation Potential for Cr II	110
16.	Plot of [η] vs. Excitation Potential for Mn I.	112
17.	Plot of [η] vs. Excitation Potential for Fe I.	118
18.	Plot of [η] vs. Excitation Potential for Fe II	120
19.	Plot of [η] vs. Excitation Potential for Co I.	122
20.	Plot of [η] vs. Excitation Potential for Ni I.	124
21.	Plot of [η] vs. Excitation Potential for Ce II	135

CHAPTER I

INTRODUCTION

One of the most important analyses that can be performed on a stellar spectrum is a determination of the abundances of the elements from quantitative measurements of the intensities of the spectral lines. For an initial analysis it is customary to utilize the curve of growth which is the relationship between the observed line intensities and certain astrophysical parameters of the stellar atmosphere including the temperature, velocities of the radiating atoms and ions, and in particular, the abundances of the elements. In this paper the curve of growth technique will be applied to the analysis of spectral data from the star θ Ursae Majoris*.

An alternative procedure is the model atmospheres approach. For an assumed effective temperature, surface gravity, and chemical composition a detailed model of the variation with depth in the atmosphere of temperature, gas pressure, optical absorption coefficient and electron pressure is computed for the stellar atmosphere and the line profiles are calculated according to the postulated mechanism of formation. By comparing the observed contours with the theoretical ones, a good representation of the stellar atmosphere may be obtained.

---

*θ Ursae Majoris is listed by Johnson and Morgan (1953) as a subgiant (spectral type F6, luminosity class IV). Its visual magnitude is 3.3 and its coordinates are α (1900) = 9^h26^m, δ (1900) = $52^\circ8'$ (Keenan and Morgan, 1951).

The curve of growth analysis may be done either in an absolute sense, in which the abundances of the elements are calculated directly for the star under study, or by a differential technique in which the abundances of the elements in one star are determined relative to those in another star of similar spectral class. Curves of growth may be calculated from basic atomic theory and laboratory data on the transfer of radiation through gases or measured experimentally from observational material on a star.

The experimental approach has been used in a recent paper by Cowley and Cowley (1964) to determine a curve of growth for the sun. The equivalent widths of 612 lines of neutral Ca, Fe, Ti, V, Cr, Mn, and Co were photoelectrically determined from spectra taken of the center of the solar disk. The relative f-values of Corliss and Bozman (1962) were used to treat lines of more elements over a wider range of excitation potentials than had been used by previous investigators. The resulting curve of growth for the sun should be more accurate than any of the previously used curves because of the use of the photoelectrically determined equivalent widths and the use of a more consistent set of f-values extending over a wider range of excitation potentials.

In this paper photographically obtained spectral data from the star θ Ursae Majoris will be compared with the sun by the differential technique using the solar curve of the Cowleys.

Use of the differential technique requires, however, that the stars be sufficiently similar in temperature so that spectral lines of approximately the same excitation potentials are present. The corrections for velocity, partition function, and optical absorption that must be made require an accurate knowledge of the temperature. The final

results appear in the ratios of the abundances of the elements in the star with respect to the abundances in the sun instead of as an absolute determination.

In a previous study Peebles (1964) analyzed the spectrum of θ Ursae Majoris by an absolute technique using four theoretical curves of growth and the f-values of Corliss and Bozman (1962). A comparison was made between the results obtained using the four sets of theoretical curves. Comparison was also made with the results of Greenstein (1948) who analyzed θ Ursae Majoris by differential comparison with the sun using the Utrecht (1940) solar equivalent widths and a set of curves of growth devised by Pannekoek and van Albada (1946). Greenstein calls attention to the fact that the weakness of both the metallic lines and the hydrogen lines implies a high continuous optical absorption coefficient and, therefore, a high value of the effective surface gravity. A model atmosphere analysis was suggested but the availability of our data, covering a larger spectral range, and a new experimentally determined solar curve of growth justify another analysis to verify the spectroscopic properties of this subgiant. In this study all of the measurements of Peebles, as well as lines of other elements, are analyzed by the differential procedure instead of by the absolute method. Comparison of the results is made with those of Greenstein.

The equivalent widths of 444 lines of the following atoms and ions were utilized in this study: Na I, Mg I, Mg II, Si I, Si II, Ca I, Sc I, Sc II, Ti I, Ti II, V I, V II, Cr I, Cr II, Mn I, Mn II, Fe I, Fe II, Co I, Ni I, Cu I, Zn I, Sr I, Sr II, Y I, Y II, Zr II, Ba II, La II, Ce II, Nd II, Sm II, Eu II, and Gd II. Three hundred and fifty nine of these lines were measured by Peebles; the balance are new

measures. The lines ranged in wavelength from λ4000 to λ6500. For elements with many strong lines available, only those lines which were well resolved and unblended were used. For elements in which only a few lines were available, many cases existed in which poorly resolved lines were the only ones from which data could be obtained. The abundances of the elements relative to those in the sun, the electron pressure, and the difference in excitation temperatures between the sun and θ Ursae Majoris were determined.

CHAPTER II

THE CURVE OF GROWTH

In this chapter an explanation of the basic mechanism for the formation of lines in a stellar atmosphere will be given so that a better understanding may be obtained of the differential curve of growth technique. A mathematical derivation will also be given of the basic equations used in this study.

Basic Mechanism of the Formation of Lines in a Stellar Atmosphere

High dispersion spectrograms of starlight reveal the presence of atomic and molecular absorption lines which may number in the hundreds for stars of the proper spectral classes. Studies of these lines by astrophysicists have shown that the lines are formed by the removal of energy from the continuous background radiation through scattering and absorption by the atoms, ions and molecules that are present in the atmosphere of the star. The study of these spectra yields information concerning the composition and physical properties of the stellar atmosphere. Since the spectral lines appear as images which are darker than the continuum radiation they must be formed in the cooler upper regions of the stellar atmosphere. The basic physical processes responsible for the formation of these line spectra will now be described.

In the upper layers of a stellar atmosphere there is a net outward flow of radiation which interacts with the constituents of the atmosphere

through the thermodynamic laws of radiation transfer. Through the processes of absorption, scattering and emission, the continuum flux is modified and the Fraunhofer lines are formed. If the atmosphere is in a state of radiative equilibrium, the process of scattering occurs when a quantum is reemitted for each quantum that is absorbed. If the frequency of the quantum emitted is exactly equal to the frequency of the quantum absorbed the scattering is coherent, but if there is a small difference in the frequencies, the scattering is non-coherent. If the absorbing atom loses its acquired energy by some means other than a transition to the original level, the line is formed by the process of absorption. The actual mechanism of line formation in stars is a combination of the scattering and absorption processes.

To fully treat the problem of radiation flow in a stellar atmosphere a mathematical model of the radiation transfer processes must be set up and the equations solved. From assumed values of the appropriate absorption and emission coefficients the outward flow of radiation through the atmosphere of a star of assumed chemical composition, surface gravity, and effective temperature can be calculated. The line intensity calculations can achieve great levels of complexity as more elaborate features are introduced into the model. (An excellent review of model atmosphere procedures may be found in an article by Munch in the volume on Stellar Atmospheres edited by Greenstein [1960].) Although in principle the model atmospheres approach is the proper method by which to treat this very complicated problem of radiation transfer, in practice the large amount of labor involved and the high quality of the observational data necessary to justify the effort lead astrophysicists to seek a more simplified theory for the preliminary analysis of a

stellar atmosphere. Thus the curve of growth technique is usually used in an initial analysis to determine the abundances of the elements as well as average values of the temperature, electron pressure and state of ionization in the region of line formation.

Assumptions Made in the Curve of Growth Technique

In the curve of growth technique many simplified assumptions are made so that a relationship can be established between the amount of energy subtracted from the continuum radiation by an absorption line and the number of atoms of the particular element in the stellar atmosphere. The amount of energy removed is expressed in terms of the equivalent width of the line, W, which Aller (1963) defines as "the width of a perfectly black line of rectangular profile that would remove exactly the same amount of energy from the spectrum." Figure 1 illustrates the relation between an observed line profile and its equivalent width. The unit used in this thesis for the measurement of equivalent width is the milliangstrom (mA).

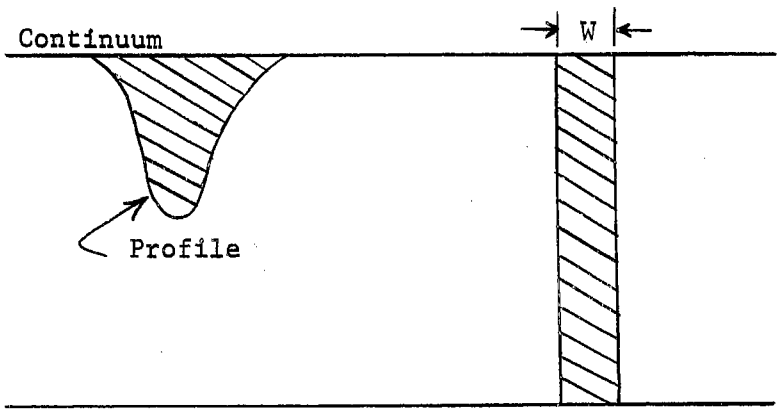

Figure 1. The Equivalent Width, W, of a Spectral Line. The Areas Enclosed by the Profile and the Rectangle are Identical.

The advantages of working with the equivalent widths of the lines are that it is not necessary to have an exact knowledge of the processes responsible for line formation, and the equivalent widths of the lines are not altered by the finite resolving power of the spectrograph. In contrast, procedures requiring computation of the line profile can lead to substantial errors if departures occur from the assumed conditions. Aller (1963) states that the "effect of accidental errors in the measurement of the equivalent width is minimized by using many lines."

It is further assumed that every line of a given element is formed at the same depth in the atmosphere, and that the same temperature, density and damping constant apply to all lines. The mechanism of radiative transfer in subordinate lines is assumed to be the same as within a resonance line, which implies that the same ratio of scattering to absorption holds for both. An atmospheric model, such as that of Schuster-Schwarzschild or of Milne-Eddington is postulated and a mechanism of line formation, pure scattering or pure absorption, is assumed to hold for the lines of all elements. The distribution of the electrons in the excited energy levels of the atom is assumed to follow a Boltzmann formula, with a unique excitation temperature, T_{exc}, which may differ from the ionization temperature, T_{ion}, or the effective temperature, T_{eff}. The fact that the excitation temperature does not equal the ionization temperature does not necessarily indicate deviation from local thermodynamic equilibrium but may simply be due to temperature stratification in the stellar atmosphere. The turbulent component of the velocity of the atoms is distributed in a Gaussian profile and all elements are assumed to possess the same mean turbulent velocity,

v_{turb}. The effective value of the surface gravity, which enters into the computation of the equivalent width, may differ from the gravitational value at the surface of the star. The ionization of all elements follows the Saha equation, without reference to the detailed ionization and recombination processes, at a single ionization temperature and electron pressure P_e. It is assumed that all lines of the same equivalent width have exactly the same shape, that each line follows the same curve of growth as every other line regardless of excitation potential or stage of ionization. The continuous absorption of the background radiation is taken to be the same for all lines irrespective of the wavelength or of the depth from which they originate.

The Two Extreme Models of a Stellar Atmosphere

Models of stellar atmospheres may range between two extreme assumptions regarding the regions in which line formation is thought to occur. In the Schuster-Schwarzschild (S-S) model an absorbing region, called the reversing layer, of depth H is presumed to overlay the photosphere from which the continuum is radiated. The processes of radiation of the continuous spectrum and formation of the line spectrum are strictly segregated into separate regions of the atmosphere. On the other hand, in the Milne-Eddington (M-E) model, formation of the lines and the continuum takes place in the same region. At each optical depth the ratio of the line absorption coefficient to the continuous absorption coefficient is assumed to be constant. In actuality, line absorption and continuous absorption take place together in the stellar atmosphere and the ratio of the line absorption coefficient to the continuous absorption coefficient varies with depth in a different way for

different elements. The absorption of continuous radiation in solar-type stars is primarily a function of the concentration of the negative hydrogen ion which varies with depth in the atmosphere. For very hot stars, electron scattering and absorption by neutral atoms of helium and hydrogen are very important; for late-type stars, molecular absorption is significant.

Several other atmospheric models have been proposed but the S-S and M-E models represent the two extreme cases. The four model atmospheres used by Peebles, representing S-S pure absorption, S-S pure scattering, M-E pure absorption and M-E pure scattering, are illustrated in Figure 2 which is taken directly from Peebles (1964) thesis. The curves are drawn for values of log a = -1.8 where a is the damping parameter or ratio of natural line width to the Doppler width, b.

The Boltzmann Equation

The atoms in the stellar atmosphere are assumed to have their electrons distributed over the available energy levels in accordance with the Boltzmann equation,

$$N_s = \frac{N g_s}{u} \exp(-\chi_e/kT), \qquad (2\text{-}1)$$

where

N_s = number of atoms per unit volume in level s,

N = total number of atoms per unit volume of the element in question,

g_s = $2J + 1$ = statistical weight of level s,

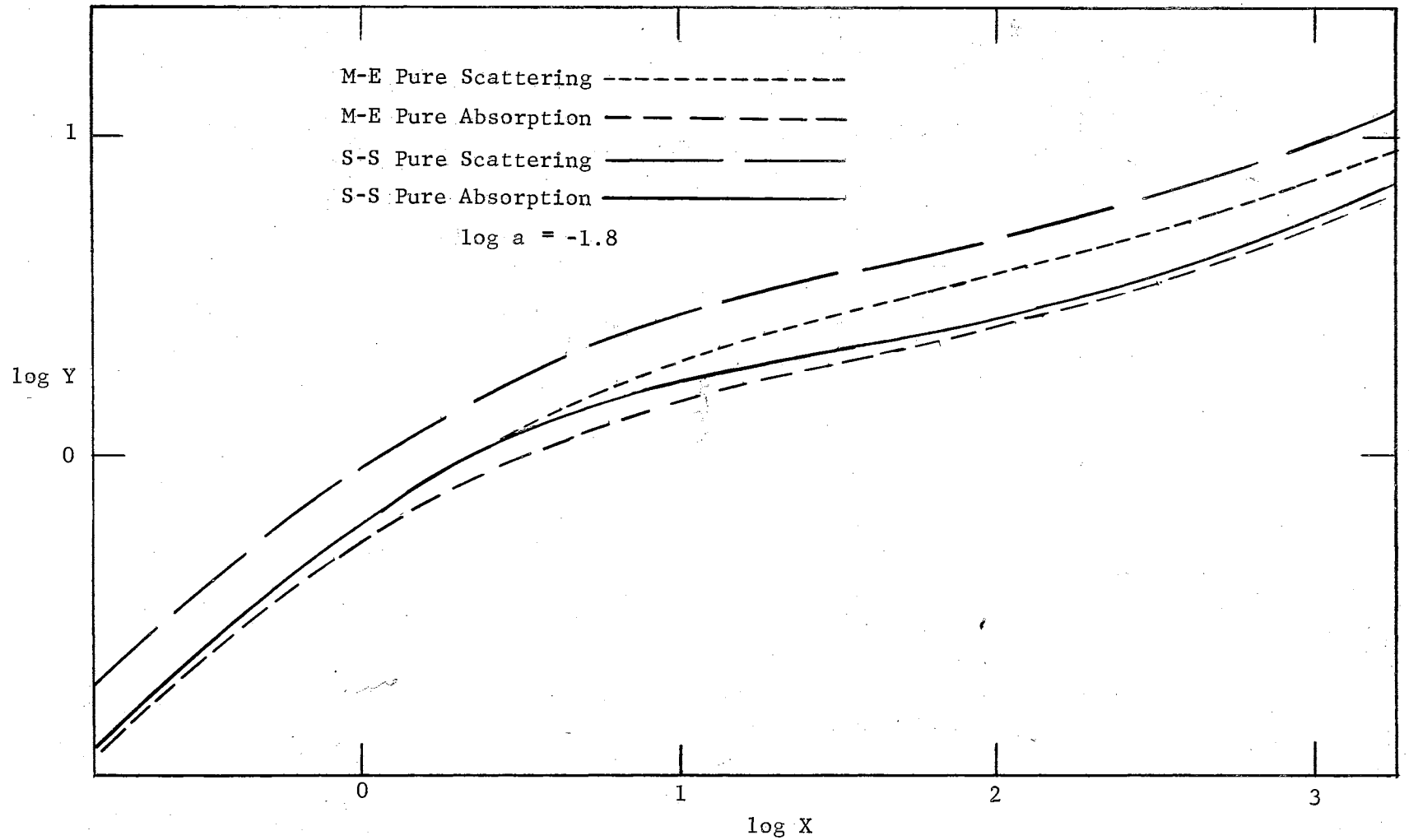

Figure 2. The Four Theoretical Curves of Growth Used by Peebles.
For M-E Pure Scattering, $X = \eta_o$, $Y = W/b$. For M-E Pure Absorption, $X = \eta_o$, $Y = W/2R_c b$.
For S-S Pure Scattering, $X = \tau_o$, $Y = W/b$. For S-S Pure Absorption, $X = 3\tau_o/2$, $Y = W/2R_c b$.

χ_e = excitation potential of level s,

k = Boltzmann's constant,

T = excitation temperature, and

u = the partition function $= \sum g_i \, w \exp(-\chi_{e,i}/kT)$ summed over all levels in the atom. w is a correction for pressure effects.

The Saha Equation

If the element being studied exists in several stages of ionization, then the total abundance is given by the Saha equation. In logarithmic form,

$$\log N_1/N_o = -\log P_e - \theta\chi_i + 2.5 \log T - 0.48 + \log 2u_1/u_o, \qquad (2\text{-}2)$$

where

χ_i = ionization potential in electron volts,

P_e = electron pressure in dynes per cm^2,

N_1 = number of singly ionized atoms per cm^3,

N_o = number of neutral atoms per cm^3,

u_1 = partition function of the singly ionized atoms,

u_o = partition function of the neutral atoms,

T = ionization temperature, and $\theta = 5040/T$.

The equation may be successively applied to include all significant stages of ionization. In this study the principle application of the Saha equation is made in the differential form which is derived in Appendix A.

The f-values

The f-values are important atomic constants which are required for the calculation of curves of growth and represent the quantum mechanical probabilities, as defined by Weisskopf and Wigner, for transitions between the energy levels in an atom or ion. Aller (1963) gives the following relationships between the f-value for a transition from state n' to n and the more commonly known Einstein transition coefficients $A_{nn'}$ and $B_{n'n}$:

$$A_{nn'} = \frac{g_{n'}}{g_n} \frac{8\pi^2 e^2 \nu^2}{mc^3} f_{n'n}, \tag{2-3}$$

$$B_{n'n} = \frac{4\pi^2 e^2}{mch\nu} f_{n'n}, \tag{2-4}$$

where

e = charge on the electron,

m = mass of the electron,

ν = frequency of the radiation involved in the transition,

c = velocity of light,

h = Planck's constant,

$A_{nn'}$ = Einstein probability of spontaneous emission,

$B_{n'n}$ = transition probability for absorption.

The f-values may be either theoretically calculated from the principles of quantum mechanics or experimentally measured in the laboratory. The experimental technique is the more accurate but large errors are still experienced, especially in the determination of the f-values

from the ionized stages of the elements, or for lines arising from a high excitation potential. The lack of accurately determined f-values is one of the greatest obstacles to a more widespread use of the curve of growth technique.

Doppler Effect and the Velocity of the Radiating Atoms

The Doppler effect plays an important role in broadening the line and determining the amount of energy which the line subtracts from the continuum. The total velocity of the radiating atom, v, is the parameter of significance and is composed of a thermal motion component and a component due to large scale turbulent motion of the stellar atmosphere in convective eddies. These velocities are combined in root mean square fashion.

$$v = \sqrt{v_{th}^2 + v_{turb}^2} \, . \qquad (2\text{-}5)$$

The turbulent velocity is assumed to have a Gaussian distribution with v_{turb} being the mean value of the velocity. The thermal component of the velocity is related to the kinetic temperature of the gas by the Boltzmann relation

$$v_{th} = \sqrt{\frac{2kT}{M}} \, , \qquad (2\text{-}6)$$

where

v_{th} = most probable value of the thermal velocity,

k = Boltzmann constant,

T = absolute value of the kinetic temperature,

M = mass of the radiating atom.

The effect of an increase in the velocity of the atoms or ions in a stellar atmosphere, either because of a higher temperature or a larger turbulent velocity, is to elevate the "flat" region of the curve of growth. The increased equivalent widths of the lines are due to more Doppler broadening. The place where the curve of growth departs from linearity is called the "knee" and is illustrated in Figure 3. Increasing the total velocity tends to make the knee occur higher on the curve of growth.

Damping Constant

For stars with physical conditions similar to those in the sun, the value of the damping constant is determined primarily by collisional damping and pressure broadening. Other factors influencing the value of the damping constant are the temperature, degree of ionization of the atoms and radiation damping. The position of the curve of growth at the upper end is markedly influenced by the value of the damping constant and large errors in the analysis can result for lines of large equivalent width if a curve of growth with the wrong damping constant is used. Since the value of the damping constant can easily vary by large amounts from the star under analysis to the star with which it is being compared, it may often be necessary to exclude data from lines with large values of equivalent width to avoid errors. Figure 4(b) illustrates the change in the damping region of a curve of growth for two different values of the damping constant.

In addition to the damping parameter a, which is defined as the ratio of the effective natural line width to the Doppler width, another

term, Γ, is referred to as the effective damping constant. It can be shown that the relationship between the two is given by

$$a = \frac{c}{4\pi\nu_o} \sqrt{\frac{M}{2kT}}\,\Gamma , \qquad (2\text{-}7)$$

where ν_o is the frequency at the center of the line and the other quantities have been previously identified.

Criticism of the Curve of Growth Technique

In criticism of the curve of growth technique it should be noted that the actual line formation process takes place over a span of the stellar atmosphere in which the temperature, pressure and other physical parameters are continuously varying. An increase of the temperature and pressure with optical depth is characteristic of all stellar atmospheres. Because of this, the state of ionization of the elements and the occupation numbers of the energy levels also change with depth and the single layer approximation does not accurately describe the true state of the stellar atmosphere. Lines originating from levels of high excitation potential are formed at greater depths than those from lower energy levels because the high level energy states are not sufficiently populated at the lower temperatures to permit a significantly large number of transitions to occur.

Since higher temperatures are required to produce ionization of an element, the lines from the ionized state will, in general, come from deeper layers which are characterized by a different set of physical parameters than the lines from the same element in the unionized state.

Making allowance for the fact that physical conditions change in

the stellar atmosphere over the region of line formation some authors have improved upon the single-parameter type assumptions by using separate curves of growth for the neutral and ionized lines. This permits the use of different values of excitation temperature and damping constant for lines formed in the shallow and deep regions of the atmosphere and allows for a variation of the turbulent velocity with height. The assumption of two separate curves of growth for neutral and ionized lines can be justified from model atmosphere theory.

Additional considerations resulting from the variation of the physical parameters with depth in the stellar atmosphere include the fact that the centers of strong lines are formed at higher levels than are the wings. It must be remembered that in using the Saha equation it is assumed that the ionized lines come from the same level as do the unionized lines and that the region can be characterized by a single value of ionization temperature and electron pressure.

Absolute Versus Differential Curve of Growth Techniques

Absolute Curves of Growth

If accurate absolute f-values are known for the lines of the elements under study a curve of growth analysis may be used to obtain the total abundance of the element above the photosphere determined on an absolute basis. However, it must be recognized that the "absolute" abundances contain terms describing properties of the atmosphere that cannot be evaluated with adequate precision.

In the M-E model the abscissa of the curve of growth contains the average density of the atmosphere and the average value of the continu-

ous absorption coefficient, while the S-S model involves the depth of the reversing layer.

Other advantages of the absolute method are that the total velocity of each atomic species may be determined from the vertical shift required to fit the observed to the theoretical curve of growth, and the excitation temperature and the damping constant may be determined directly.

Differential Curves of Growth

If accurately determined f-values are not available, a differential curve of growth technique can be employed. In the differential procedure the star under study is compared to a reference star of similar physical properties and spectral class, which is assumed to have similar line formation processes in its atmosphere and therefore a similar curve of growth. The chemical composition and average values of the temperature, electron pressure and gas pressure of the standard star will usually be known. In addition to not requiring f-values for the individual lines under study, the differential curve of growth technique also reduces the effects of errors due to the improper choice of the line formation process and assumptions concerning the physical state of the atmosphere. It should be noted, however, that this thesis is based upon the empirical curve of growth of Cowley and Cowley (1964) which was derived using the experimental f-values of Corliss and Bozman (1962). If a theoretical curve of growth would have been used, the use of f-values would not have been necessary. In using a differential curve of growth technique, abundances are only determined on a relative basis, and no information is directly obtained on the total velocity of each

species which must be determined from another source. Only the difference between the reciprocal temperatures of the standard and the comparison stars is obtained from the variation of the shift of the abscissa with excitation potential, and large errors will result for data based on lines of large equivalent width if the damping constants of the two stars are not the same.

Comparison of Differential and Absolute Curve of Growth Techniques

The biggest difference between the two curve of growth techniques is that the differential method does not require knowledge of the f-values of the elements since they are assumed the same in both stars, or in the star and the sun if the sun is used for comparison purposes. In addition, errors arising from stratification, or the wrong choice of model atmosphere, or systematic errors in the choice of the physical parameters of the atmosphere, or departures from idealized situations, such as local thermodynamic equilibrium, tend to cancel in the differential approach since they should occur in the sun and in the star in nearly the same way.

However, the differential curve of growth approach does not result in an absolute determination of the abundances of the elements but only gives the abundance relative to the standard star used in the comparison. It is advantageous to be able to use the sun as the reference for comparison because as Aller and Greenstein (1960) state: "Conditions in the sun are much better known than in the stars, and relative abundances of spectroscopically similar elements, with respect to the sun, may easily be modified with improved knowledge of the solar model." In this study a differential curve of growth technique will be used to

compare the spectrum of θ Ursae Majoris with that of the sun.

Cowley and Cowley's Solar Curve of Growth

In addition to the calculation of a curve of growth from laboratory absorption data, one may be experimentally determined from the measured values of the equivalent widths if the f-values of the lines are known. Of particular importance to this study is the empirically determined curve of growth of the sun made by Cowley and Cowley (1964). Using photoelectrically determined equivalent widths from spectra of the center of the solar disk for 612 lines of neutral Ca, Fe, Ti, Cr, Mn and Co, and the absolute f-values of Corliss and Bozman (1962), a solar curve of growth was constructed based on the lines of chromium which covered almost the full extent of the curve. Through the use of this recently determined set of f-values, more lines of more elements over a wider range of excitation potential could be employed than had been used by any previous workers. An average excitation temperature of 5143°K, which corresponds to $\theta_{exc} = 0.98$, was found to produce the minimum amount of scatter in fitting lines of different excitation potential to a curve of growth for all of the elements which the Cowleys studied. The resulting curve of growth is reproduced in Figure 3 where the ordinate, log W/λ , is plotted against an abscissa of log $gf\lambda - \theta_{exc}\chi_e$. The abscissa gives the values for chromium with λ in Angstroms. Notice that the Cowleys have made no correction on the ordinate for the velocities of the emitting atoms and ions. In view of the fact that any differentially made velocity correction between the sun and θ Ursae Majoris would be small, no such correction will be made to the experimental data for θ Ursae Majoris. The new solar curve of growth of the

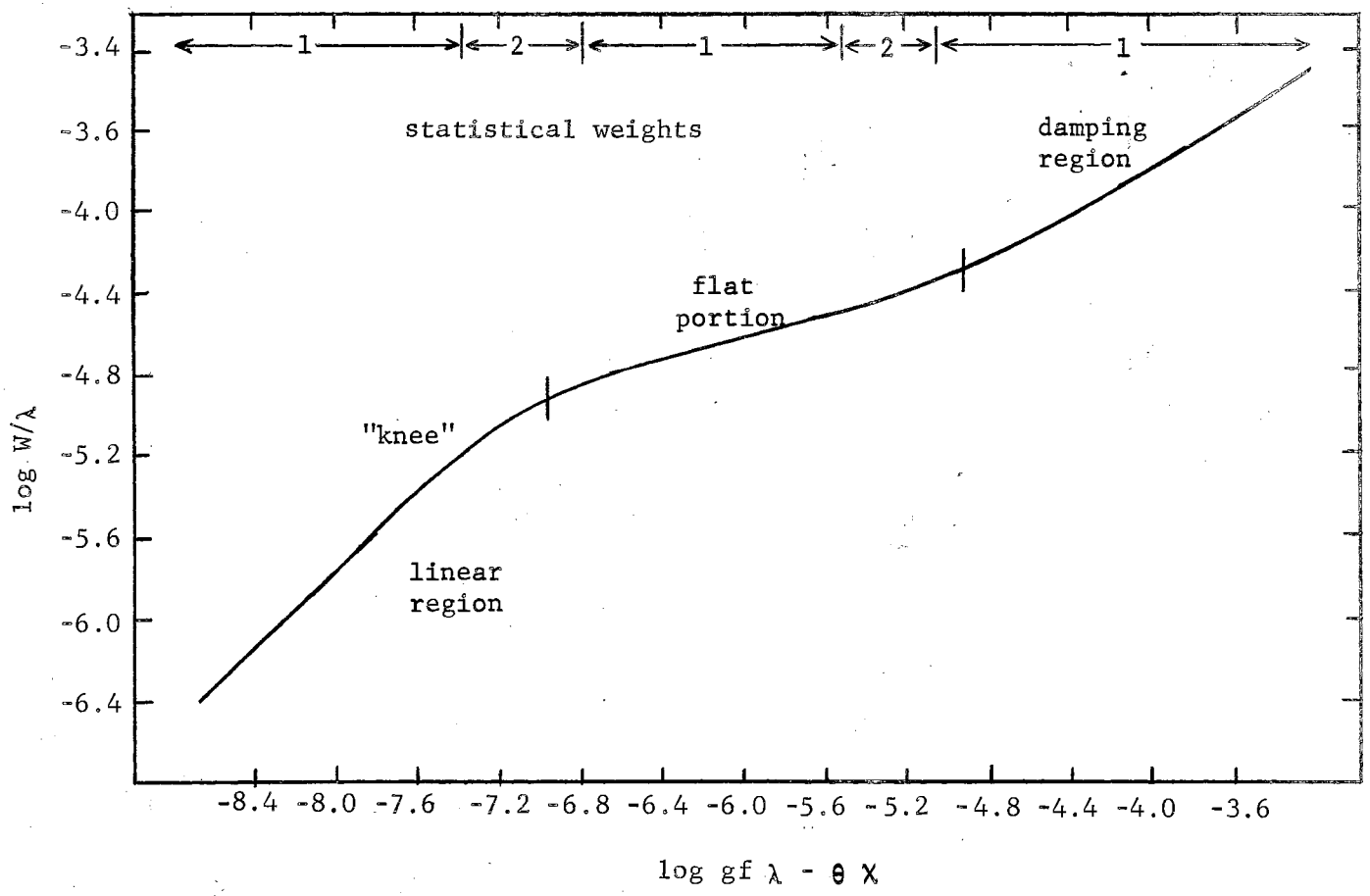

Figure 3. Cowley and Cowley's Curve of Growth of the Sun.

Cowleys will be used in this study to relate the line intensities to the abundances of the elements in θ Ursae Majoris relative to the sun.

Comparison of the Differential Curve of Growth and Model Atmosphere Techniques

Aller (1963) lists the advantages and disadvantages of the curve of growth technique relative to the model atmospheres approach. The curve of growth is a statistical procedure in which a large number of the lines arising from an element are analyzed to provide estimates of the average values of the electron pressure, excitation temperature, ionization temperature, and abundances of the elements. These results are obtainable with a smaller investment in labor than through the use of model atmospheres. One advantage of the curve of growth technique is that the equivalent widths of the lines are far less subject to errors arising from the effects of the observing instruments than are the line profiles. Small errors made in the model atmospheres approach, either computationally or observationally, can result in substantial errors in the final result. The chief disadvantage to the curve of growth is that it ignores information contained in the shape of the line.

An often-used model atmospheres technique is that of line profile analysis in which the observed profile is matched against a set of profiles computed for a variety of assumed physical conditions. As a result of the distortion of the true profile by the finite resolution of the spectrograph this technique is usually only applied to lines having large equivalent widths. Because of their immense size, the analysis of the hydrogen line profiles for the determination of the effective

temperature is especially well suited to this procedure.

Another method employing model atmospheres involves calculating the width of the line at half of the maximum depression and comparing the results with the observational data. Information can be obtained on the turbulence in the stellar atmosphere and on Doppler broadening of the line due to the kinetic temperature with the results not severely influenced by the effects of blending with neighboring lines.

Even if the very high quality data required to justify the use of a model atmosphere calculation is available, a curve of growth analysis may still first be performed to provide preliminary values of the abundances, temperatures, electron pressure, and state of ionization of the star. Initial estimates of these quantities are necessary if the analysis is to be continued by the model atmospheres approach. The chief limitation to the application of the model atmosphere technique is the lack of high quality data, although for some stars such as late model supergiants no adequate theory exists on which to base model atmosphere calculations.

Mathematical Development of the Curve of Growth

Absorption lines may be studied in the laboratory by passing a collimated beam of white light through an absorption tube filled with a gas at a known temperature and pressure. The reduction in the intensity of the continuous spectrum follows an exponential absorption law

$$I = I_o \, e^{-k_\lambda x}, \tag{2-8}$$

where

I_o = initial intensity of the light,

k_λ = optical absorption coefficient at wavelength λ,

x = distance the light travels through the absorbing gas.

The variation of the absorption coefficient with frequency (or wavelength) about the center of the line is determined by:

1) The natural, radiation damping due to the finite breadth of the energy levels in the atom. The width of the energy level and the lifetime of the state are related by the uncertainty principle.

2) Doppler broadening due to the thermal motion of the atoms. If the kinetic temperature of the gas is known the average thermal velocity of the atoms may be calculated.

3) Pressure broadening of the lines due to disturbance of the energy levels by electric fields when an atom in the excited state collides with other atoms and ions.

Laboratory measurements show that for gas pressures less than 0.01 dynes/cm^2 the wings of a line are poorly developed and the intensity of the line is determined by the natural width and Doppler motions. At pressures greater than 10 dynes/cm^2, the line intensity is determined almost entirely by the wings which are due to radiation damping and collisional broadening.

Minnaert and Slob (1931) applied the theory of radiation absorption to stellar problems in 1931. Numerous authors (Menzel, 1936; Baker, 1936; Unsold, 1938; Wrubel, 1949; Hunger, 1956) since then have developed the theory for different types of stellar atmospheres.

The development of the curve of growth and its characteristic features can be understood if consideration is given to the increase of the equivalent width of a line as the number of absorbing atoms is

increased. For a small concentration of N atoms per unit volume, the value of Nf, the number of absorbers per unit volume, is small and the amount of energy removed from the continuous spectrum increases linearly with Nf. If the logarithm of the equivalent width is plotted against the logarithm of the number of absorbing atoms a linear portion results with a slope of 45°. As the amount of absorbing gas is increased the center of the line becomes black and ceases to absorb further. The increase in the equivalent width with the value of Nf diminishes and the curve of growth displays a flat portion known as the transition region. Finally, as the amount of absorbing gas is further increased, the equivalent width of the line begins to increase due to the development of wings on the line. This portion of the curve of growth is known as the damping region and the logarithm of the equivalent width increases as the square root of $Nf\Gamma$, where Γ is the effective damping constant listed in Equation (2-7). The exact shape of the curve of growth in this region is dependent upon the value of the damping constant.

Figure 4, taken from p. 371 of Aller (1963), displays both the line profiles and the curves of growth which have been theoretically calculated for the "K" line of Ca II at λ3933. Note the development of the broad wings as the concentration of atoms is increased beyond one thousand times the initial concentration, N_o. The calculations were made on the Schuster-Schwarzschild pure scattering model with pure radiation damping.

In laboratory studies the concentration of gas in an absorption tube can be systematically increased as measurements are made of the absorption. The resulting curve relating equivalent width W, to the concentration of absorbers Nf, is called a "curve of growth."

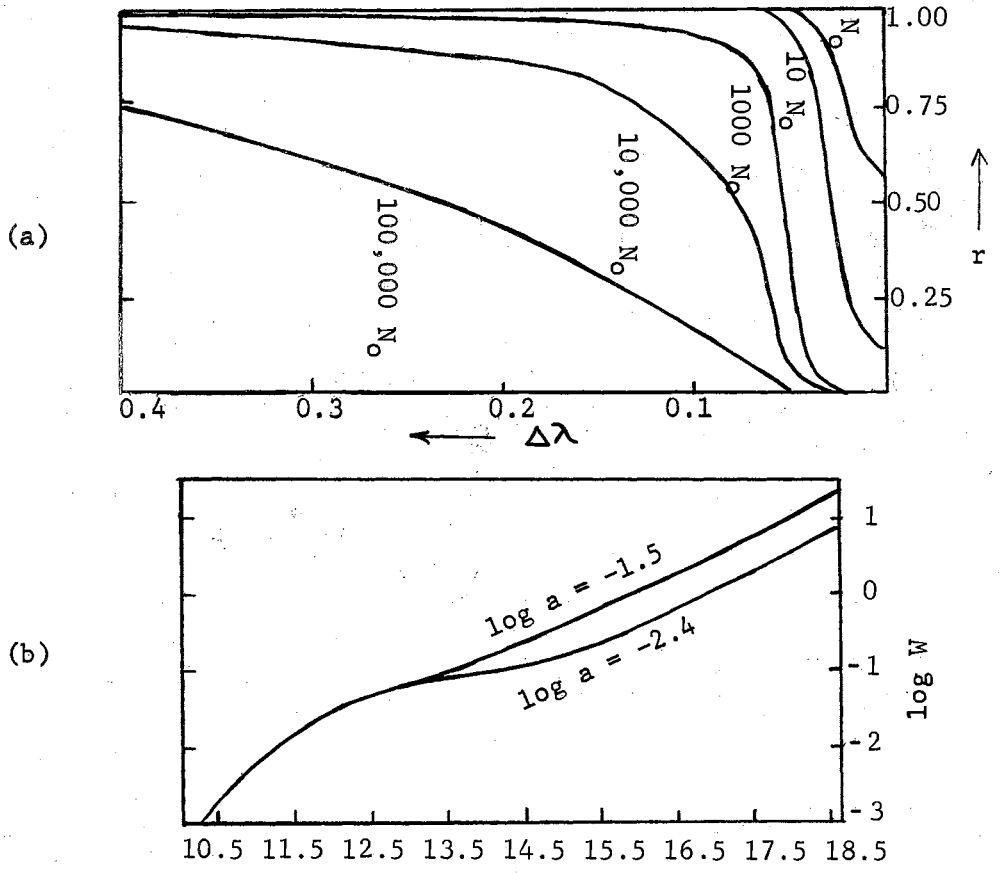

Figure 4. The Curve of Growth for the λ3933 Line of Ca II.

(a) Theoretical profiles calculated for the Schuster-Schwarzschild model and pure radiation damping.

(b) From the integration of the profiles of Fig. 4a we obtain log W which we plot against the number of atoms above the photosphere. Curves are given for log a = -1.5 and -2.4.

Calculation of the intensity of an absorption line is accomplished by evaluating the following integral for the equivalent width.

$$W = \int_0^\infty 1 - \frac{I_\nu}{I_o} \, d\nu \, . \qquad (2\text{-}9)$$

The intensity of a point on the line profile is expressed as a ratio of the intensity I_ν at the frequency ν of the point to the intensity I_o of the adjacent continuous spectrum. The integral may be evaluated from the solution of the equation describing the transfer of radiation through a stellar atmosphere under different sets of assumptions concerning the atmospheric model and the mechanism of line formation. Details concerning the performance of the computations may be found in Aller (1963) on pages 371-378. The determination of the curve of growth is accomplished by plotting log $Wc/\lambda\nu$ as ordinate against an abscissa which Aller gives as

$$\log \eta = \log N_{r,s} + \log \alpha_o - \log k_\lambda \, , \qquad (2\text{-}10)$$

where W is the equivalent width of the line of wavelength λ, $N_{r,s}$ is the number of atoms per gram of stellar material in the sth level of the rth stage of ionization, α_o is the absorption coefficient at the center of the line if there were zero damping, and k_λ is the continuum optical absorption coefficient

Assuming that the excited electrons in the atoms are distributed over the energy states in a Boltzmann distribution, Equation (2-1) may be rewritten in logarithmic form to substitute for $N_{r,s}$.

$$\log N_{r,s} = \log N_r + \log g_{r,s} - \log u(T) - \theta \chi_{r,s} \qquad (2\text{-}11)$$

where $\theta = 5040/T$, the excitation potential is expressed in electron volts, and the temperature is in degrees Kelvin. Aller also shows that the zero damping absorption coefficient may be expressed as

$$\alpha_o = \frac{\sqrt{\pi}\, e^2}{m\, c} \quad \frac{f\,\lambda}{v} \,. \tag{2-12}$$

Substituting Equations (2-11) and (2-12) into Equation (2-10), an expression is obtained for log η in terms of the number density of the atoms of the element forming the lines and the physical parameters describing the stellar atmosphere.

$$\log \eta = \log N_r + \log g_{r,s} - \log u(T) - \theta\, \chi_{r,s} + \log \left\{ \sqrt{\pi}\, e^2/mc \right\} + \log f\lambda - \log v - \log k_\lambda \,. \tag{2-13}$$

$$\log \eta = \log N_r + \log gf\lambda - \theta\, \chi_{r,s} - \log \left\{ v(T)\, u(T) \right\} - \log k_\lambda\ (T, P_e) - 1.824, \tag{2-14}$$

where P_e is the electron pressure, $\log \sqrt{\pi}\ e^2/mc = -1.824$, and the subscript on g is suppressed for convenience.

Application of the Curve of Growth Technique in the Differential Form

Equation (2-14) may be used to derive a relationship which will enable a comparison to be made between a line which is present in the star under investigation and in the comparison star, which for this study is the sun. This equation holds for the line both in the sun and in the star. If the superscript ^{o} is used to designate the value of a quantity as it exists in the sun and the superscript * for the star, Equation (2-14) may be rewritten for the sun as

$$\log \eta^{o} = \log N_r^{o} + \log gf\lambda - \theta^{o}\chi_{r,s} - \log [\, v^{o}u^{o}(T)] - 1.824 - \log k_\lambda^{o}\,(T^{o},\, P_e^{o}), \tag{2-15}$$

and for the star,

$$\log \eta^{*} = \log N_r^{*} + \log gf\lambda - \theta^{*}\chi_{r,s} - \log [\, v^{*}u^{*}(T)] - 1.824 - \log k_\lambda^{*}\,(T^{*},\, P_e^{*}). \tag{2-16}$$

Subtracting Equation (2-16) from Equation (2-15), the constant term and the log $gf\lambda$ terms cancel because they are the same for both the sun and the star and Equation (2-17) is obtained:

$$\log \eta^{o}/\eta^{*} = \log N_r^{o}/N_r^{*} - \chi_{r,s}\,(\theta^{o} - \theta^{*}) - \log [v^{o}u^{o}(T)/v^{*}u^{*}(T)] - \log k_\lambda^{o}\,(T,\, P_e^{o})/k_\lambda^{*}(T,\, P_e^{*}). \tag{2-17}$$

This equation may be expressed in a more economical notation by letting

$$[\xi] = \log \xi^{o}/\xi^{*}$$

for any quantity ξ. The logarithm of the abundance ratio is then given in the new notation by rearranging the terms in Equation (2-17):

$$[N_r] = [\eta] + \chi_{r,s}\,(\theta^{o} - \theta^{*}) + [v] + [u(T)] + [k_\lambda(T,\, P_e)]. \tag{2-18}$$

If the terms on the right hand side of Equation (2-18) can now be evaluated, we will be able to determine the abundance ratio of the particular stage of ionization of the element in question.

The first term on the right hand side of Equation (2-18) is determined from the measurements of the equivalent widths in the following manner. From the average value of the equivalent width for each line of an ionic species for the star the term $\log W^{*}/\lambda$ is formed. This term

is entered as an ordinate onto the selected curve of growth and the corresponding value of $\log \eta^*$ is read off of the abscissa. The equivalent width of the same line in the sun, as determined from an atlas, is also entered into the curve of growth, chosen as representative of both sun and star, and the two abscissa values are subtracted to form $[\eta]$.

If all of the values of $[\eta]$ for the lines of a particular ionic species are plotted against the excitation potentials of the states from which they arose, appropriate statistical weights may be assigned and a straight line fitted to the data. The slope of the line gives the value of the term $(\theta^o - \theta^*)$. The factor $\chi_{r,s}\ (\theta^o - \theta^*)$ is then added onto the value of $[\eta]$ for each line and the average value of $[\eta] + \chi_{r,s}\ (\theta^o - \theta^*)$ for all observed lines of the ionic species determined. If the temperature of the star is known, the partition function term u(T) may be interpolated from Table 3-24 in Aller (1963) and the thermal velocity of the ionic species calculated from Equation (2-6). Estimates of the turbulent velocity v_{turb}, can be made by methods described in Appendix A and the total velocity then may be calculated with Equation (2-5).

From a knowledge of the electron pressure and temperature the optical absorption coefficient may be determined from tables in Allen (1963). The values are very sensitive to changes in electron pressure so it is important that this quantity be well determined. All of the quantities on the right hand side of Equation (2-18) are now evaluated, and their summation gives the logarithm of the ratio of the number of absorbing atoms per gram in the sun to that in the star, $\log N_r^o/N_r^*$.

Summary of Steps Involved in a Curve of Growth Analysis

1) Obtain spectrograms of the star to be investigated.--It is necessary to use spectra of the highest dispersion possible so that effects of blending will be minimized.

2) From these plates obtain microphotometer tracings.--Microphotometer tracings are plots of the density of the spectral image versus the wavelength.

3) Obtain intensitometer tracings.--The intensitometer converts the density of the image into intensity. Calibration involves the use of sources of known intensity. The central portion of the density-intensity curve for the plate is used.

At the Dominion Astrophysical Observatory steps two and three were performed separately. At other observatories, Mt. Wilson for example, the two may be combined into a single operation. Line profiles may also be obtained by photoelectric spectrophotometry. The instruments and procedures used in these various techniques have been described by Wright (1962).

4) Draw in the continuum.--The location of the continuum is a great source of error. The continuum can be drawn directly on the intensitometer tracing or first drawn on the microphotometer tracing and then transferred. The procedure employed depends upon which seems to be the most reliable for the wavelength region concerned.

5) Identify the lines and approximate the profiles.--If the apparent line profile is irregular or asymmetric, several tracings may be compared to determine if the variations are real. A possible cause for irregularities and asymmetry is blending. In drawing the profiles these possible effects of blending should be taken into account. For the additional lines in this work that were not drawn in by Peebles the

same procedure was used of drawing a line contour in which the profile of the wings is inversely proportional to distance from the line center as is indicated by theory. The alternative is to assume a triangular profile which is simpler to draw, especially when the wings of moderate to strong lines are influenced by blending.

6) Determine equivalent widths.--The following steps are needed: a) planimeter the lines to determine the area enclosed by the profile and the continuum, b) measure the height of the continuum, c) measure the dispersion, and d) calculate the equivalent width.

7) Look up the equivalent width of the same line in the sun from the Utrecht Atlas (1960). Form the term log W/λ for the equivalent widths of the line in both the star and the sun. Enter the values of log W^*/λ and log W^o/λ as ordinates into the Cowleys' solar curve of growth and obtain the corresponding values of log η^* and log η^o.

8) Form the term $[\eta]$ by subtracting log η^* from log η^o. Plot the resulting value of $[\eta]$ against the excitation potential of the lower level in electron volts.

9) Assign statistical weights to each line according to the number of tracings on which the profile occurs, the consistency of the measured values, and the region of the curve of growth on which the line falls. Fit a straight line to the data by the least squares technique. The slope of the line gives the best estimate of the term $(\theta^o - \theta^*)$.

10) Using the value for the difference in excitation temperatures determined in step 9, and employing the same statistical weights, obtain a value for the quantity $[\eta] + \chi(\theta^o - \theta^*)$ to be used in Equation (2-18). The appropriate value of $[\eta]$ must be combined with the value of χ for each line in taking the average.

11) After determining θ and the electron pressure for the sun and the star by techniques described in Appendix A, obtain numerical values of the optical absorption coefficient and partition function from tables in reference works such as Allen (1963).

12) Using values of v_{turb} which have been determined by other investigators, calculate the total velocity according to Equation (2-5) for each ionic species for both the sun and the star. Subtract the logarithms to form the $[v]$ term.

13) Calculate the relative abundance of the elements in the star with respect to the sun from Equation (2-18).

14) Apply the differential Saha equation to determine the total relative abundances of all of the observed elements.

Sources of Error in the Curve of Growth Technique

The sources of error which arise from the spectrophotometry are described in detail by Wright (1948). Errors due to improper focus, ghosts, and scattered light in the spectograph are of the same order of magnitude as the errors involved in the calibration of the photographic plate and the development process. The effect of the microphotometer slit width can be significant if it is large relative to the width of the line but the largest errors arise in the reduction of the tracings themselves due to the effects of the grain of the photographic film, the difficulties involved in accurately locating the continuum, and blending with neighboring lines. Comparison of equivalent width data taken by different authors on the same star using different equipment shows typical errors of $\pm$20 percent in the equivalent width of small (less than 20 mA) lines and $\pm$10 percent for the equivalent width of

medium lines (up to 50 mA); the different measures usually tend to differ in a systematic fashion. The equivalent widths of faint or seriously blended lines are often so affected by error that it is impossible to derive information from them. Observers have noted that high dispersion spectra tend to show smaller equivalent widths than those taken on instruments of low dispersion. Dispersions of 10 A/mm or better are necessary to do a good quantitative analysis. In order to average out the errors arising from the above mentioned sources, it is good procedure to secure several plates covering the same wavelength region and to compute the average of the equivalent widths of the individual measurements.

The accuracy achievable with the curve of growth technique for a particular element depends strongly upon the region of the curve of growth upon which the data lines fall. Lines falling on the linear part of the curve have small values of equivalent width which can be subject to large systematic errors. Medium strong lines may have more accurately determined values of equivalent width, but fall on the flat portion of the curve where a small error in the equivalent width can produce a large shift in the abscissa. The equivalent widths of strong lines can be more accurately measured, but use of a curve of growth with the wrong value of damping constant will cause a serious error. The most accurate results come from lines at the top end of the linear region just before the knee, but in practice lines falling on all parts of the curve must usually be used due to scarcity of data in the linear region.

Some authors, such as Wright (1966), have fit standard profiles to the observational tracings, or have used measurements of the half width

and central depth of the line. However, the procedure adopted in this study has been to draw in the line profile by hand and use a rolling disk planimeter to measure the enclosed area. The principal factor limiting the accuracy with which the profile could be estimated was the effect of blending upon the wings of the line.

By measuring the vertical shift between the observed and theoretical curves of growth a measurement can be made of the total velocity of a radiating atom or ion. For a differential comparison of two stars a difference in velocity determined in this fashion would be subject to the sum of the errors made in each determination. An alternative technique is to calculate the velocity of each atomic species for each of the two stars under study from previously determined turbulent velocities and kinetic temperatures. This latter approach is used here to compare the velocities in the sun and θ Ursae Majoris.

In the absolute curve of growth technique the excitation temperature is determined from the difference in the horizontal shift on the log η axis required to fit the lines coming from different excitation potentials to the curve of growth. The accuracy with which the excitation temperature for an element can be determined is a function of the number of lines available for the element, the scatter of the lines about the curve of growth, and the range of excitation potential covered by the lines from different spectral terms. Since the observable lines of iron are far more numerous than the lines of other elements, and are spread over a large range of excitation potential, Fe I is often the only element used to determine the excitation temperature. The scatter in the data is often large enough to limit the accuracy to ± 0.05 in the value of θ_{exc}. In general, lines from ionized elements will have a

higher excitation temperature than those in the neutral state. Since the ionization temperature is a measure of the ionization process and relates to processes taking place over levels where both ionized and unionized lines are formed, its value is often higher than the excitation temperature, which is usually obtained from information relating to the excitation process of only unionized elements. In practice, model atmosphere calculations can be used to relate the ionization and excitation temperatures to the effective temperature, which can be accurately measured by multicolor photometry or photoelectric scans of the continuum.

Use of the Saha equation to determine average values of the ionization temperature and the electron pressure usually results in inadequate determinations of these parameters. In principle both the ionization temperature and the electron pressure can be determined from observational data of more than one element in both the ionized and neutral state, but in practice the elements for which good observational data are available have ionization potentials that are so close together that the solution is indeterminate. It is better to assume values of the ionization temperature from information on the effective temperature and use the observational data in the Saha equation to calculate an average value of the electron pressure (Aller, 1963).

CHAPTER III

OBSERVATIONAL MATERIAL

Spectrograms and Tracings

The θ Ursae Majoris spectrograms used in this study were taken at the Cassegrain focus of the 72-inch telescope of the Dominion Astrophysical Observatory by Dr. K. O. Wright.

The dispersion varied with the spectrograph used. For the Littrow spectrograph with the Wood grating (15,000 lines/inch) the dispersion was approximately 7.5 A/mm for the second order spectra in the range λλ4800-6750; for third order spectra in the range λλ3750-4500, the dispersion was about 4.5 A/mm. When the Bausch and Lomb grating No. 496 (30,000 lines/inch) was used in the second order, the dispersion was about 3.2 A/mm. For the three-prism spectrograph the dispersion varied from about 5 A/mm to 15 A/mm over the wavelength range studied.

The microphotometer and intensitometer tracings were made at Victoria by Dr. Leon W. Schroeder. The magnification of the tracings is 200. Details of the spectrograms and tracings are given in Table I.

Figure 5 is a reproduction of a portion of one of the intensitometer tracings showing the estimated position of the continuum and the profiles of some representative lines.

Location of the Continuum

For the most part, the continuum was drawn directly on the intensi-

TABLE I

VICTORIA PLATE, MICROPHOTOMETER, AND INTENSITOMETER DATA FOR θ URSAE MAJORIS

Victoria Plate Number	Microphotometer & Intensitometer Tracing Number	Spectrograph	Wavelength Range (Angstroms)
55224	1808	Grating*-2nd Order	3900-4080
55053	1828	Grating*-2nd Order	3990-4085
38157	1827	Grating -3rd Order	4000-4210
50092	1797	Prism	4120-4250
55225	1793	Grating*-2nd Order	4180-4315
55054	1811	Grating*-2nd Order	4210-4340
50092	1796	Prism	4250-4580
34599	1807	Grating -3rd Order	4275-4455
55225	1792	Grating*-2nd Order	4300-4480
37111	1914	Grating*-2nd Order	4310-4900
37075	1915	Grating*-2nd Order	4310-4900
55054	1810	Grating*-2nd Order	4335-4495
31421	1799	Prism	4600-5020
38133	1816	Grating -2nd Order	4700-4830
38133	1815	Grating -2nd Order	4825-5180
31421	1798	Prism	5015-5710
37111	1812	Grating -3rd Order	5130-5450
37074	1800	Grating -2nd Order	5160-5450
34800	1814	Grating -2nd Order	5165-5510
36796	1818	Grating -2nd Order	5600-6010
34799	1817	Grating -2nd Order	6000-6325
36795	1819	Grating -2nd Order	6200-6700

*The asterisk refers to grating spectra made with the Bausch and Lomb grating No. 496, or 169 in the cases of plates 37112 and 37075. All other grating spectra were made with the Wood grating. Prism spectrograms were made with the three prism spectrograph.

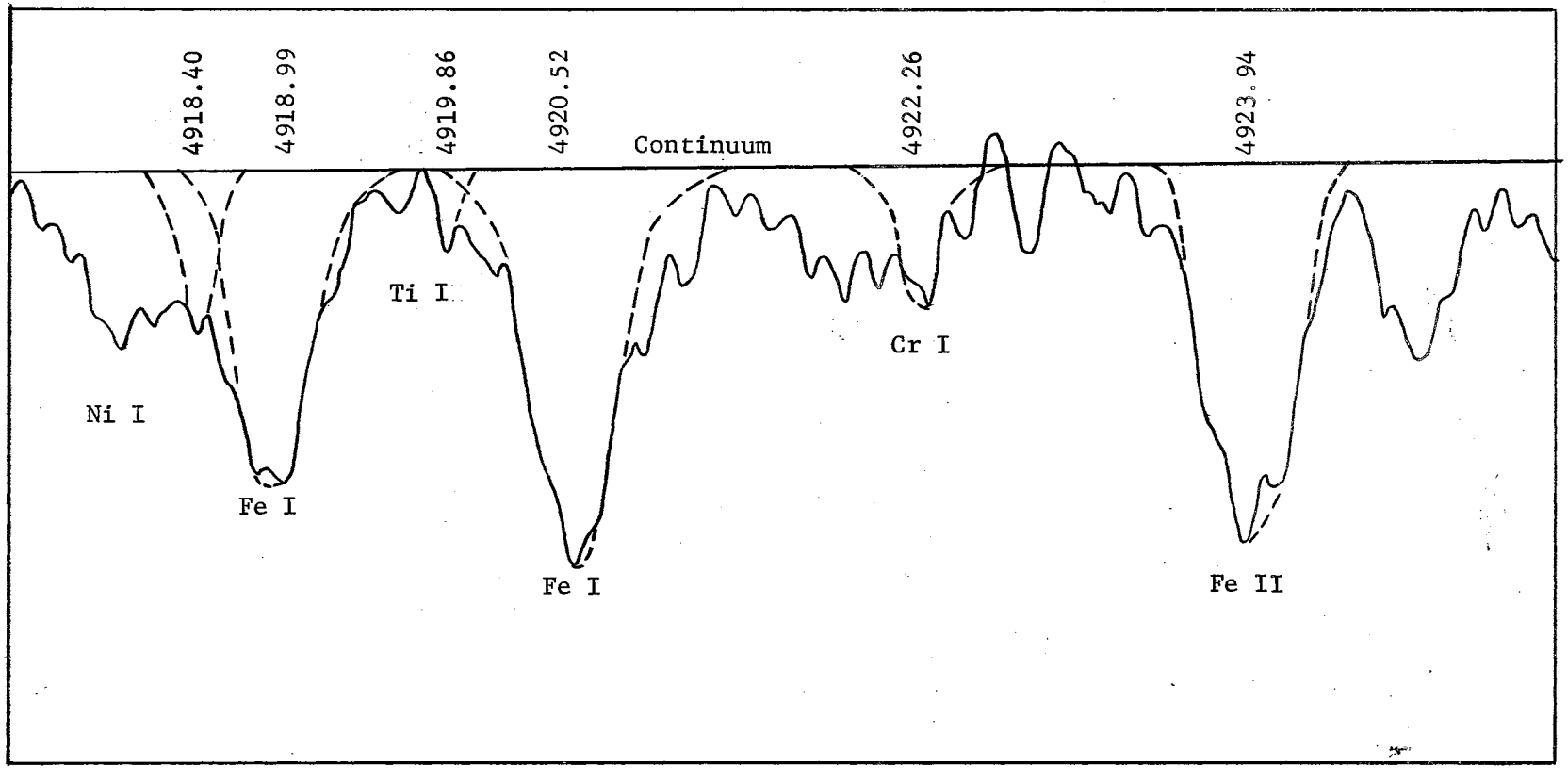

Figure 5. Intensitometer Tracing of the Spectrum of θ Ursae Majoris in the Region λλ 4918-4924. A line has been drawn indicating the estimated position of the continuum and the profiles are drawn in dashed lines for six absorption lines whose equivalent widths were measured.

tometer tracings as the average of the galvanometer deflections due to plate grain in the regions between the lines. In a few cases, however, the position of the continuum was more apparent on the microphotometer tracing and hence was first drawn there and then transferred to the intensitometer tracing.

Approximation of the Profiles

Theory indicates that the shape of the wings exhibited by the stronger lines should be inversely proportional to the square of the distance from the line center in units of the Doppler width. An attempt was made to take this into account when drawing the profiles of the stronger lines. The shapes of the wings were readily apparent for very strong lines, especially when there were no nearby lines to produce blending effects in the wings. When blending was serious the wings were roughly approximated.

Identification of the Lines

The lines were identified by referring to the tables published by Swensson (1946) in his paper "The Spectrum of Procyon." Identifications could be made in this way because the spectrum of Procyon (spectral type F5, luminosity class IV) is quite similar to that of θ Ursae Majoris. Also, the θ Ursae Majoris tracings were compared with similar ones for Procyon which were used by Schroeder (1958) in his study of that star. The work by Charlotte E. Moore (1945), A Multiplet Table of Astrophysical Interest, Revised Edition, was also consulted for purposes of line identification.

Selection of Lines

Peebles (1964) performed his selection of lines on the basis of the following criteria: the effects of blending, the availability of f-values, and the number of lines available for a particular element. The selection of the lines used in this study differed in one major respect since knowledge of the f-values is unnecessary in a differential curve of growth analysis. Desiring to include as many elements as possible in this analysis, the standards of quality for selection of lines were reduced, particularly in the areas of blending and the acceptance of lines of small equivalent width. Therefore, any lines that appeared free from substantial blending in both the sun and the star were considered suitable for comparison and analysis.

Since the spectrum on the short wavelength side of 4000A is very complex and the continuum is unidentifiable, no lines were used from this region.

Effects of Blending

Although it would have been desirable to have measured the equivalent widths of only those lines which were substantially free of the effects of blending, it was necessary to utilize blended lines from elements for which the number of observable lines was small. If an adequate number of lines of good quality were available, the blended lines were rejected in the statistical weighting process. Swensson's (1946) line identifications for Procyon were used not only for the identification of lines but also for the rejection of blended components.

Number of Lines Available for a Particular Element

The reliability of the results obtained in a curve of growth analysis depends strongly upon the number of lines available for the element being investigated because of the statistical nature of the procedure. Therefore, Peebles was careful to select only those elements for which an adequate number of lines were available so that a reliable analysis would result. Of the elements which Peebles studied, Co I, with 12 lines, had the fewest number, but for the differential curve of growth analysis performed in this work, such selectivity was not required and some elements are represented by only one line.

In Table II are listed the 34 atoms and ions studied, in order of increasing atomic weight, and the number of lines available for each element.

Determination of Equivalent Widths

Equivalent Widths for θ Ursae Majoris

The determination of the equivalent widths of the lines was accomplished by the following procedure. The areas on the intensitometer tracings enclosed by the line profiles and the continuum were measured with an Ott rolling disk planimeter. At least two measurements were made of the area of each profile, and, if mutually consistent, the average of the two was taken as the equivalent width in the computations. However, some lines, especially those of small equivalent width, had large enough variations in area that several repeated measurements were made until the operator was satisfied that the average of certain selected values represented a valid measurement of the area of the line.

TABLE II

LIST OF ATOMS AND IONS STUDIED IN THIS INVESTIGATION

Atom or Ion	Atomic Weight	Number of Lines	Atom or Ion	Atomic Weight	Number of Lines
Na I	22.99	4	Fe I*	55.85	115
Mg I	24.31	7	Fe II	55.85	31
Mg II	24.31	1	Co I*	58.94	12
Si I	28.09	4	Ni I*	58.71	32
Si II	28.09	2	Cu I	63.55	1
Ca I*	40.08	21	Zn I	65.37	2
Sc I	44.96	3	Sr I	87.63	1
Sc II	44.96	11	Sr II	87.63	2
Ti I*	47.90	55	Y I	88.91	2
Ti II*	47.90	27	Y II	88.91	6
V I	50.94	18	Zr II	91.22	6
V II	50.94	11	Ba II	137.35	2
Cr I*	52.00	65	La II	138.92	4
Cr II	52.00	17	Ce II	140.13	11
Mn I*	54.94	22	Nd II	144.25	3
Mn II	54.94	4	Sm II	150.36	2
Eu II	151.96	1	Gd II	157.25	1

*Elements marked with an asterisk are those for which the equivalent widths were measured by Peebles (1964).

The continuum height was taken as the average of the measurements taken to the right and to the left of the line. The value of the dispersion was read from graphs of dispersion measurements taken at various points along the tracing and plotted against wavelength.

The equivalent width was then calculated in milliangstroms according to the formula

$$W = \frac{A\ C\ D}{\frac{1}{2}\ (H_l + H_r)}\ , \qquad (3\text{-}1)$$

where A = the area enclosed by the line profile, measured in planimeter units,

C = the planimeter conversion factor, in in^2/planimeter unit,

D = dispersion of the spectrum, in mA/inch,

$H_{l,r}$ = height of the continuum above the reference line to the left and right of the profile being measured, in inches.

Due to overlapping and duplication of the spectrograms, some lines were represented by as many as seven profiles, others by only one. The equivalent width was taken as an equally weighted average of all of the tracings, in most cases, with certain selected points given zero weight if a particular measurement exhibited a gross deviation from the average. In Figure 6 are plotted equivalent widths measured on different tracings against the corresponding average values for the lines that were used in this study but were not used in Peebles' work. Figure 6 in Peebles' study gives a similar plot for the lines which he used. Comparison of the two figures shows that the higher quality of his data is reflected in a smaller dispersion of the points about the average due to the selectivity which he was able to employ in choosing the lines.

If a line does not occur too deeply into the wing of one of the

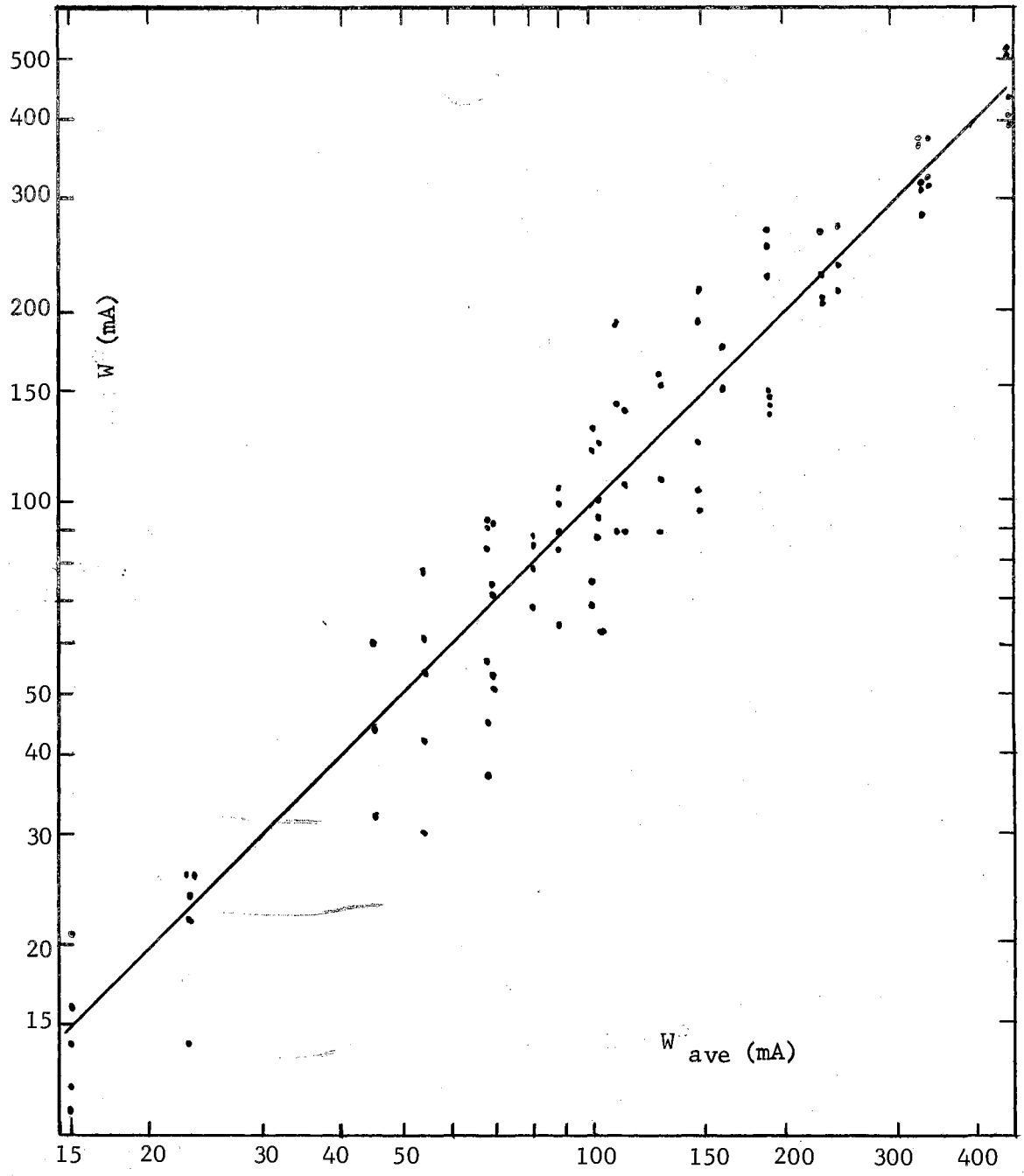

Figure 6. Comparison of Equivalent Widths Measured on Different Tracings With the Average Values for a Representative Group of Lines. Data Points are for Elements Measured by Mangold.

large hydrogen profiles an acceptable correction can be made using Thackery's (1936) relation

$$W = \frac{W_b}{r_w}, \qquad (3\text{-}2)$$

which gives an expression for W, the equivalent width which the line would have if no blending occured in terms of W_b, the measured equivalent width referred to the wing as the continuum, and r_w, the ratio of the intensity of the wing to the intensity of the true continuum at the center of the line being studied.

The equivalent widths of the lines used in this study are listed in Table III along with other information which is useful in the analysis. The data in this table, together with several other physical constants which characterize the sun and θ Ursae Majoris, constitute the basic observational data on which this study is based. The data for the eight ionic species which were measured by Peebles are taken directly from his work. As a check on the consistency of the procedure for determining the equivalent widths, several lines that were measured by Peebles were remeasured by the author. There was excellent agreement between the two sets of independent measures.

The elements in Table III are listed according to increasing atomic weight and within the tabulation for each element the lines are listed according to increasing wavelength.

Column 1 lists the wavelength in Angstroms as given by Miss Moore (1959) in the Revised Multiplet Table (RMT).

Column 2 gives the RMT multiplet number.

Column 3 lists the excitation potential of the lower level of the

TABLE III

LINE INTENSITIES IN THE SPECTRUM OF THETA URSAE MAJORIS

λ RMT	Multiplet RMT	χ_e	Number of Measures	W
	Na I			
5682.633	6	2.09	1	85
5688.193	6	2.10	1	120
5889.953	1	0.00	1	378
5895.923	1	0.00	1	296
	Mg I			
4167.27	15	4.33	2	117
4702.9909	11	4.33	4	228
4730.0285	10	4.33	3	43
5172.6843	2	2.70	5	450
5183.6042	2	2.70	4	566
5528.4094	9	4.33	1	194
5711.0912	8	4.33	1	41
	Mg II			
4427.995	9	9.95	2	5
	Si I			
5708.437	10	4.93	1	54
5772.258	17	5.06	1	38
5948.584	16	5.06	1	59
6237.34	28	5.59	2	34
	Si II			
6347.091	2	8.09	1	87
6371.359	2	8.09	1	47
	Ca I			
4226.728	2	0.00	3	400
4283.010	5	1.88	3	119
4289.364	5	1.87	3	114
4298.986	5	1.88	3	137
4425.441	4	1.87	5	132
4434.960	4	1.88	4	167
4435.688	4	1.88	4	134

TABLE III (Continued)

λ RMT	Multiplet RMT	χ_e	Number of Measures	W
	Ca I (Continued)			
4526.935	36	2.70	2	69
4578.558	23	2.51	2	80
5262.244	22	2.51	3	119
5512.979	48	2.92	1	106
5581.971	21	2.51	1	79
5588.757	21	2.51	1	177
5590.120	21	2.51	1	66
5601.285	21	2.51	2	123
6102.722	3	1.87	1	121
6122.219	3	1.88	1	173
6162.172	3	1.89	1	183
6166.443	20	2.51	1	36
6439.073	18	2.51	1	181
6493.780	18	2.51	1	121
	Sc I			
4023.688	7	0.02	3	17
4743.814	14	1.44	2	9
	Sc II			
4246.829	7	0.31	3	160
4294.767	15	0.60	4	99
4314.084	15	0.62	7	188
4320.745	15	0.60	2	104
4354.609	14	0.60	5	88*
4415.559	14	0.59	5	147
5239.823	26	1.45	4	60
5526.809	31	1.76	1	131
5667.164	29	1.49	1	39
5669.030	29	1.49	1	34
6245.629	28	1.50	1	36
	Ti I			
4008.046	187	2.11	3	38
4008.926	12	0.02	3	108
4016.264	186	2.13	2	7
4060.263	80	1.05	2	15
4166.311	163	1.87	1	8
4169.330	163	1.88	2	6
4186.119	129	1.50	1	21
4265.723	162	1.87	2	4
4281.371	44	0.81	1	7
4286.006	44	0.82	4	79
4287.405	44	0.83	5	37
4305.910	44	0.84	5	200
4321.655	235	2.23	7	28

TABLE III (Continued)

λ RMT	Multiplet RMT	χ_e	Number of Measures	W
	Ti I (Continued)			
4326.359	43	0.82	4	15
4417.274	161	1.88	6	14
4427.098	128	1.50	1	14
4453.708	160	1.87	4	19
4465.807	146	1.73	4	18
4518.022	42	0.82	4	59
4533.238	42	0.84	4	151
4534.782	42	0.83	4	108
4548.764	42	0.82	2	42
4555.486	42	0.84	4	66
4617.269	145	1.74	3	44
4623.098	145	1.73	2	22
4639.369	145	1.73	2	19
4639.669	145	1.74	2	11
4645.193	145	1.73	2	15
4656.468	6	0.00	4	38
4681.908	6	0.05	4	92
4758.120	233	2.24	3	22
4759.272	233	2.25	3	25
4799.797	242	2.26	3	30
4805.416	260	2.33	3	12
4820.410	126	1.50	2	19
4840.874	53	0.90	3	23
4913.616	157	1.87	1	18
4919.867	200	2.15	1	11
4981.732	38	0.84	2	123
5016.162	38	0.84	2	54
5024.842	38	0.81	2	74
5025.570	173	2.03	2	41
5039.959	5	0.02	2	66
5043.578	38	0.83	2	14
5152.185	4	0.02	1	11
5173.742	4	0.00	5	74
5194.043	183	2.09	2	8
5201.096	183	2.08	1	8
5210.386	4	0.05	4	62
5224.301	183	2.13	2	18
5689.465	249	2.29	1	12
5713.895	249	2.28	1	13
5766.330	309	3.28	1	14
5866.453	72	1.06	1	14
5918.548	71	1.06	1	14
	Ti II			
4300.052	41	1.18	4	218
4301.928	41	1.16	4	152

TABLE III (Continued)

λ RMT	Multiplet RMT	χ_e	Number of Measures	W
	Ti II (Continued)			
4312.861	41	1.18	7	176
4316.807	94	2.04	7	55
4337.916	20	1.08	6	159*
4344.291	20	1.08	4	104*
4394.057	51	1.22	6	110
4395.031	19	1.08	6	223
4395.848	61	1.24	6	87
4409.517	61	1.23	2	37
4417.718	40	1.16	6	129
4421.949	93	2.05	6	63
4443.802	19	1.08	5	173
4450.487	19	1.08	5	137
4468.493	31	1.13	5	189
4533.966	50	1.23	3	253
4563.761	50	1.22	3	194
4568.312	60	1.22	2	46
4571.971	82	1.56	3	245
4708.663	49	1.23	2	68
4779.986	92	2.04	3	84
4805.105	92	2.05	2	155
5129.143	86	1.88	2	137
5185.90	86	1.88	4	76
5336.809	69	1.57	4	85
5381.020	69	1.56	3	72
5418.802	69	1.57	3	59
	V I			
4095.486	41	1.06	1	19*
4111.785	27	0.30	1	46*
4113.518	52	1.21	1	15*
4115.185	27	0.29	2	24*
4342.832	103	1.86	3	20*
4379.238	22	0.30	5	69
4389.974	22	0.27	5	54
4406.641	22	0.30	4	24
4408.204	22	0.27	2	26
4437.837	21	0.29	4	10
4444.207	21	0.27	3	19
4452.008	87	1.86	1	18
4469.710	87	1.85	2	10
4553.056	133	2.35	1	26
4560.710	109	1.94	1	16
4577.173	4	0.00	1	41
4686.926	93	1.86	1	8
5234.088	131	2.35	1	17

TABLE III (Continued)

λ RMT	Multiplet RMT	χ_e	Number of Measures	W
	V II			
4002.940	9	1.42	2	78
4005.712	32	1.81	3	112
4023.388	32	1.80	3	63
4036.779	9	1.47	2	48
4039.574	32	1.81	1	20
4065.070	215	3.78	1	39
4178.390	25	1.68	1	26
4183.435	37	2.04	1	57
4225.228	37	2.02	1	30
4232.065	225	3.96	2	23
4234.251	24	1.68	2	11
	Cr I			
4001.444	268	3.87	2	36
4022.263	268	3.87	3	15
4039.100	251	3.83	2	29
4065.716	279	4.09	1	6
4120.613	65	2.70	1	16
4126.521	35	2.53	2	15
4197.234	249	3.83	3	11
4208.357	249	3.83	1	4
4209.368	248	3.83	1	15
4211.349	133	3.00	2	11
4254.346	1	0.00	3	180
4272.910	96	2.89	3	16
4274.803	1	0.00	3	172
4289.721	1	0.00	4	219
4337.566	22	0.96	6	93*
4339.450	22	0.98	4	54*
4339.718	22	0.96	4	25*
4344.507	22	1.00	2	97*
4346.833	104	2.97	5	29*
4351.051	22	0.96	2	48
4373.254	22	0.98	4	10
4381.112	64	2.70	1	5
4384.977	22	1.03	3	46
4387.496	103	2.99	4	37
4410.304	129	3.00	2	7
4412.250	22	1.03	4	12
4458.538	127	3.00	3	35
4511.903	150	3.07	4	37
4535.146	33	2.53	2	15
4545.956	10	0.94	4	84
4591.394	21	0.96	5	58
4600.752	21	1.00	5	86
4616.137	21	0.98	4	70

TABLE III (Continued)

λ RMT	Multiplet RMT	χ_e	Number of Measures	W
	Cr I (Continued)			
4626.188	21	0.96	4	65
4639.538	186	3.10	1	35
4646.174	21	1.03	4	132
4649.461	32	2.53	2	15
4651.285	21	0.98	4	61
4652.158	21	1.00	4	76
4708.040	186	3.15	5	40
4718.429	186	3.18	5	56
4724.416	145	3.07	2	12
4730.711	145	3.07	2	29
4745.308	61	2.70	2	11
4756.113	145	3.09	5	55
4764.294	231	3.54	2	24
4836.857	144	3.09	3	13
4922.267	143	3.09	2	156
4936.334	166	3.10	2	41
4954.811	166	3.11	2	60
4964.928	9	0.94	1	30
5110.751	60	2.70	2	11
5206.039	7	0.94	4	164
5238.971	59	2.70	1	20
5243.395	201	3.38	4	27
5247.564	18	0.96	4	55
5296.686	18	0.98	4	76
5297.360	94	2.89	4	82
5298.269	18	0.98	4	146
5329.12	94	2.90	4	57
5345.807	18	1.00	4	84
5348.319	18	1.00	4	55
5390.394	191	3.35	3	26
5409.791	18	1.03	3	119
5712.778	119	3.00	1	9
	Cr II			
4242.38	31	3.85	3	119
4252.62	31	3.84	3	42
4261.92	31	3.85	2	73
4275.57	31	3.84	2	105
4555.02	44	4.05	2	97
4558.659	44	4.06	3	145
4588.217	44	4.05	3	113
4592.09	44	4.06	1	61
4616.64	44	4.05	2	49
4634.11	44	4.05	2	82
4812.35	30	3.85	3	52
4848.24	30	3.85	3	103*

TABLE III (Continued)

λ RMT	Multiplet RMT	χ_e	Number of Measures	W
	Cr II (Continued)			
4876.41	30	3.85	3	121*
5237.35	43	4.06	1	51
5305.85	24	3.81	2	44
5334.88	43	4.05	2	35
5502.05	50	4.15	1	42
	Mn I			
4018.102	5	2.11	4	143
4030.755	2	0.00	4	286
4033.073	2	0.00	4	225
4034.490	2	0.00	4	181
4055.543	5	2.13	3	113
4059.392	29	3.06	2	31
4070.279	5	2.18	4	33
4079.422	5	2.18	2	87
4082.944	5	2.17	3	55
4257.659	23	2.94	3	15
4265.924	23	2.93	2	23
4453.005	22	2.93	2	18
4457.045	28	3.06	2	11
4470.138	22	2.93	4	23
4502.220	22	2.91	3	28
4709.715	21	2.88	4	30
4739.108	21	2.93	4	25
4754.042	16	2.27	4	129
4765.859	21	2.93	3	67
4766.430	21	2.91	4	85
4783.420	16	2.29	4	158
4823.516	16	2.31	4	180
	Mn II			
4530.034	17	10.62	1	27
4652.816	18	10.74	1	5
4755.728	5	5.37	1	20
5299.278	11	9.82	1	37
	Fe I			
4005.246	43	1.55	3	284
4009.714	72	2.21	3	103
4045.815	43	1.48	4	558
4062.446	359	2.83	3	98
4063.597	43	1.55	4	372
4071.740	43	1.60	4	329
4107.492	354	2.82	2	85*
4132.681	357	2.82	1	123
4143.871	43	1.55	2	265

TABLE III (Continued)

λ RMT	Multiplet RMT	χ_e	Number of Measures	W
	Fe I (Continued)			
4147.673	42	1.48	1	103
4154.502	355	2.82	1	123
4175.640	354	2.83	3	102
4181.758	354	2.82	3	154
4187.044	152	2.44	3	129
4187.802	152	2.41	2	180
4191.436	152	2.46	2	150
4199.098	522	3.03	3	133
4202.031	42	1.48	3	228
4206.702	3	0.05	3	116
4216.186	3	0.00	3	137
4219.364	800	3.56	3	141
4222.219	152	2.44	3	120
4227.434	693	3.32	3	231
4233.608	152	2.47	3	140
4235.942	152	2.41	3	207
4238.816	693	3.38	3	139
4247.432	693	3.35	3	154
4248.228	482	3.06	3	93
4250.125	152	2.46	3	156
4250.790	42	1.55	3	177
4260.479	152	2.39	2	223
4271.159	152	2.44	3	184
4271.764	42	1.48	3	276
4282.406	71	2.17	4	144
4291.466	3	0.05	4	89
4325.765	42	1.60	4	372
4337.049	41	1.55	4	158*
4352.737	71	2.21	6	159
4369.774	518	3.03	5	131
4375.932	2	0.00	4	139
4383.547	41	1.48	4	397
4389.244	2	0.05	4	44
4404.752	41	1.55	4	313
4415.125	41	1.60	4	276
4427.312	2	0.05	4	156
4430.618	68	2.21	4	118
4442.343	68	2.19	3	138
4443.197	350	2.85	3	120
4447.722	68	2.21	3	134
4454.383	350	2.82	3	109
4461.654	2	0.09	3	197
4466.554	350	2.82	3	152
4489.741	2	0.12	3	113
4494.568	68	2.19	1	161
4531.152	39	1.48	1	265

TABLE III (Continued)

λ RMT	Multiplet RMT	χ_e	Number of Measures	W
	Fe I (Continued)			
4602.944	39	1.48	2	119
4736.780	554	3.20	3	137
4859.748	318	2.86	4	145*
4871.323	318	2.85	4	195*
4872.144	318	2.87	4	191*
4890.762	318	2.86	4	193
4891.496	318	2.84	4	235
4918.999	318	2.85	2	203
4910.509	318	2.82	2	269
5001.871	965	3.86	2	170
5005.720	984	3.87	1	145
5006.126	318	2.82	1	145
5049.825	114	2.27	2	144
5051.636	16	0.91	2	155
5068.774	383	2.93	2	117
5083.342	16	0.95	2	119
5110.414	1	0.00	2	161
5133.692	1092	4.16	3	142
5191.460	383	3.03	4	152
5192.350	383	2.99	4	145
5194.943	36	1.55	4	106
5216.278	36	1.60	4	122
5225.533	1	0.11	1	59
5232.946	383	2.93	4	194
5250.650	66	2.19	4	82
5266.562	383	2.99	4	142
5269.541	15	0.86	4	202
5281.796	383	3.03	4	106
5283.628	553	3.23	3	161
5307.365	36	1.60	4	75
5324.185	553	3.20	4	167
5328.042	15	0.91	4	265
5339.935	553	3.25	4	102
5364.874	1146	4.43	3	92
5367.470	1146	4.40	3	95
5369.965	1146	4.35	3	117
5383.374	1146	4.29	3	136
5393.174	553	3.23	3	109
5397.131	15	0.91	3	170
5404.144	1165	4.42	3	183
5405.778	15	0.99	3	167
5410.913	1165	4.45	3	107
5424.072	1146	4.30	3	156
5429.699	15	0.95	3	228
5434.527	15	1.01	3	160
5445.045	1163	4.37	3	103

TABLE III (Continued)

λ RMT	Multiplet RMT	χ_e	Number of Measures	W
	Fe I (Continued)			
5446.920	15	0.99	3	222
5497.519	15	1.01	2	174
5501.469	15	0.95	2	146
5506.782	15	0.99	1	154
5569.625	686	3.40	1	124
5572.849	686	3.38	1	146
5576.097	686	3.42	1	86
5586.763	686	3.35	1	193
5615.652	686	3.32	2	215
5762.992	1107	4.19	1	113
6024.066	1178	4.53	1	76
6065.487	207	2.60	1	99
6137.696	207	2.58	1	114
6230.728	207	2.55	2	134
6246.334	816	3.59	2	77
6252.561	169	2.39	2	108
6265.140	62	2.17	2	64
6301.515	816	3.64	2	103
6318.022	168	2.44	2	79
6393.605	168	2.42	1	117
6411.658	816	3.64	1	124
6421.355	111	2.27	1	93
6430.851	62	2.17	1	93
6494.985	168	2.39	1	129
	Fe II			
4122.638	28	2.57	1	134
4128.735	27	2.57	2	50
4178.855	28	2.57	2	90
4273.317	27	2.69	3	94
4303.166	27	2.69	3	100
4369.404	28	2.77	2	49
4384.33	32	2.65	2	157
4416.817	27	2.77	5	109
4491.401	37	2.84	4	127
4508.283	38	2.84	2	139
4576.331	38	2.83	3	112
4583.829	38	2.79	3	210
4620.513	38	2.82	1	63
4666.750	37	2.82	1	106
4731.439	43	2.88	2	132
4923.921	42	2.88	2	246
5018.437	42	2.88	2	294
5132.67	35	2.79	1	31
5169.030	42	2.88	5	329
5197.569	49	3.22	4	125

TABLE III (Continued)

λ RMT	Multiplet RMT	χ_e	Number of Measures	W
	Fe II (Continued			
5234.620	49	3.21	3	119
5264.801	48	3.22	2	61
5284.092	41	2.88	2	70
5325.559	49	3.21	3	60
5362.864	48	3.19	4	101
5414.089	48	3.21	1	28
5425.269	49	3.19	1	57
6247.562	74	3.87	2	72
6416.905	74	3.87	1	59
6432.654	40	2.88	1	63
6456.376	74	3.89	1	144
	Co I			
4020.898	16	0.43	3	29
4092.386	29	0.92	2	112*
4110.532	29	1.04	2	38*
4121.318	28	0.92	2	90
4517.094	150	3.11	2	23
4693.190	156	3.22	2	18
4727.936	15	0.43	2	14
5156.366	180	4.04	1	50
5212.699	170	3.50	1	15
5342.703	190	4.00	2	9
5343.383	190	4.01	3	24
5369.591	39	1.73	1	17
	Ni I			
4462.460	86	3.45	3	57
4470.483	86	3.38	3	67
4604.994	98	3.47	2	72
4606.231	100	3.58	2	23
4648.659	98	3.40	3	75
4686.218	98	3.58	2	35
4714.421	98	3.37	4	136
4715.778	98	3.53	4	53
4756.519	98	3.47	4	67
4806.996	163	3.66	4	35
4829.028	131	3.53	4	99
4866.267	111	3.52	4	66*
4873.437	111	3.68	4	52*
4904.413	129	3.53	3	58
4918.363	177	3.82	2	51
4935.830	177	3.92	2	26
4980.161	112	3.59	2	96
4984.126	143	3.78	1	91
5000.335	145	3.62	1	78

TABLE III (Continued)

λ RMT	Multiplet RMT	χ_e	Number of Measures	W
	Ni I (Continued			
5012.464	111	3.68	2	55
5017.591	111	3.52	2	97
5035.374	143	3.62	2	85
5080.523	143	3.64	2	102
5081.111	194	3.83	2	67
5084.081	162	3.66	2	73
5099.946	161	3.66	2	78
5115.397	177	3.82	2	65
5146.478	162	3.69	3	100
5155.764	210	3.88	3	65
5176.565	209	3.88	5	33
5578.734	47	1.67	1	27
5592.283	69	1.94	1	22
	Cu I			
5218.202	7	3.80	2	38
	Zn I			
4722.159	2	4.01	2	50
4810.534	2	4.06	4	80
	Sr I			
4607.331	2	0.00	1	25
	Sr II			
4077.714	1	0.00	3	337
4215.524	1	0.00	3	242
	Y I			
4047.64	8	0.00	1	9
4477.45	14	1.35	1	15
	Y II			
4358.73	5	0.10	2	41
4398.02	5	0.13	6	68
4883.69	106	1.08	4	110
5087.42	20	1.08	2	69
5200.42	20	0.99	3	44
5402.85	35	1.83	2	21
	Zr II			
4050.32	43	0.71	3	35
4096.63	15	0.56	1	24*
4156.24	29	0.74	1	133
4208.99	41	0.71	2	45
4317.32	40	0.71	5	15

TABLE III (Continued)

λ RMT	Multiplet RMT	χ_e	Number of Measures	W
	Zr II (Continued)			
4333.28	132	2.40	2	16*
	Ba II			
4554.033	1	0.00	2	272
6496.896	2	0.60	1	170
	La II			
4042.91	66	0.92	3	28
4086.72	10	0.00	2	58
4238.38	41	0.40	2	24
4333.76	24	0.17	2	55
	Ce II			
4014.899	157	0.53	2	12
4073.477	4	0.00	3	12
4083.233	60	0.70	2	12
4113.726	137	0.49	1	10*
4137.646	2	0.04	1	16
4399.203	81	0.33	2	7
4418.784	2	0.38	3	10
4486.909	57	0.23	1	11
4562.360	1	0.00	2	36
4628.160	1	0.04	2	16
5274.244	15	0.56	2	10
	Nd II			
4021.330	36	0.32	1	12
4358.169	10	0.32	3	20
4462.985	50	0.56	1	13
	Sm II			
4334.153	27	0.28	1	15
4467.342	53	0.66	2	8
	Eu II			
4129.73	1	0.00	1	36
	Gd II			
4130.372	19	0.60	1	14

transition, in electron volts.

Column 4 lists the number of profiles measured for the line.

Column 5 gives the equivalent width in milliangstroms. Equivalent widths of lines found in the wings of the Balmer lines have been corrected according to Thackeray's ralation and are indicated by an asterisk. A listing of these lines and the raw data are given in Table IV.

TABLE IV

DATA PERTINENT TO LINES LOCATED ON WINGS OF HYDROGEN

λ (A)	Element	Wing Location	r_w	W_b (mA)	W(mA)
4092.386	Co I	Hδ	0.904	102	112
4095.486	V I	Hδ	0.834	16	19
4096.63	Zr II	Hδ	0.812	20	24
4107.492	Fe I	Hδ	0.832	71	85
4110.532	Co I	Hδ	0.891	34	38
4111.785	V I	Hδ	0.920	42	46
4113.518	V I	Hδ	0.957	14	15
4113.726	Ce II	Hδ	0.962	10	10
4115.185	V I	Hδ	0.989	24	24
4333.28	Zr II	Hγ	0.896	14	16
4337.049	Fe I	Hγ	0.808	127	158
4337.566	Cr I	Hγ	0.769	71	93
4337.916	Ti II	Hγ	0.739	117	159
4339.450	Cr I	Hγ	0.561	30	54
4339.718	Cr I	Hγ	0.519	13	25
4342.832	V I	Hγ	0.676	14	20
4344.291	Ti II	Hγ	0.811	84	104
4344.507	Cr I	Hγ	0.832	81	97
4346.833	Cr I	Hγ	0.899	26	29
4354.609	Sc II	Hγ	0.956	84	88
4848.24	Cr II	Hβ	0.947	100	103
4859.748	Fe I	Hβ	0.602	87	145
4866.267	Ni I	Hβ	0.821	54	66
4871.323	Fe I	Hβ	0.894	174	195
4872.144	Fe I	Hβ	0.902	172	191
4873.144	Ni I	Hβ	0.913	48	52
4876.41	Cr II	Hβ	0.971	117	121

Equivalent Widths for the Sun

The primary source of data on solar equivalent widths was the

Utrecht Atlas (1960); a secondary source was from the Commonwealth Solar Observatory (Allen 1934, 1938). Both sources used dispersions which were considerably higher than that of the θ Ursae Majoris data used in this study. Dispersions for the Utrecht Atlas ranged from 3 mm/A to 1.5 mm/A while the data for the Commonwealth Solar Observatory varied from 0.5 mm/A to 2.2 mm/A. Solar equivalent width data are tabulated in Tables XII through XLV in Chapter IV.

Comparison of Equivalent Width Measurements With Those of Greenstein

A comparison of the equivalent widths of spectral lines measured in this work and the widths of the same lines measured by Greenstein (1948) at a dispersion of 2.8 A/mm at HY is plotted in Figure 7. The dispersion of the points for the lines unique to this paper is greater than the dispersion for the lines measured by Peebles. The greater dispersion results from the fact that many of the lines unique to this paper are of lower quality than those selected by Peebles for this study. As Peebles noted, the values of the small equivalent widths measured by Greenstein tended to be larger than the equivalent widths measured in his paper and an inspection of Figure 7 in this paper indicates a similar trend. This tendency could be due to an instrumental effect, or this could be due to the difference in methods used to convert the microphotometer tracings into equivalent width data.

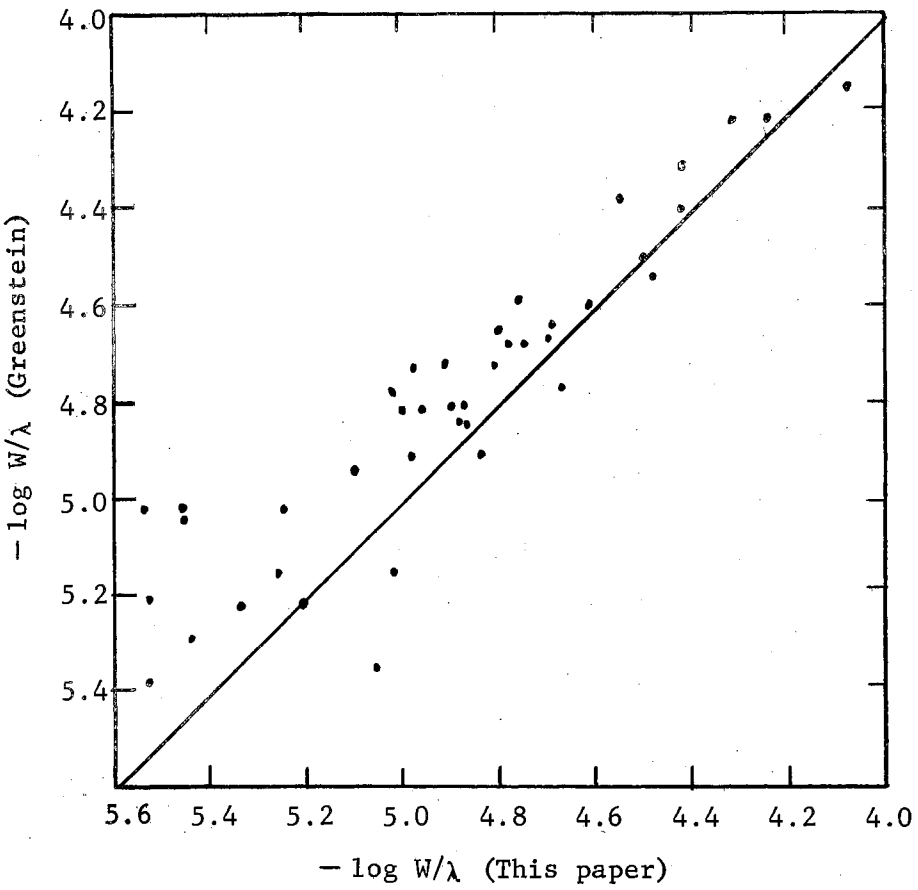

Figure 7. Comparison of Equivalent Widths for Lines in This Paper Measured by Mangold, and Their Counterparts as Measured by Greenstein.

CHAPTER IV

RESULTS

The results of the differential curve of growth analysis performed on the data listed in Table III for θ Ursae Majoris will be given in this chapter. The primary result of the analysis is the relative abundances of the elements in θ Ursae Majoris as compared with the sun. The absolute abundances of the elements in the star can be obtained from a determination of the absolute abundance in the sun. Other values which are determined are the difference between the excitation temperatures of the sun and star, the total velocity of each atomic and ionic species, and the value of the relative electron pressure.

Influence of Model Atmospheres Concepts

Analysis of a stellar atmosphere by the differential curve of growth technique involves use of some concepts from the theory of model atmospheres. The mechanism of the line formation process must be understood. The value of the continuous absorption coefficient depends upon the values of the ionization temperature and electron pressure that are used; both quantities are functions of the optical depth. The effective temperature of a star is representative of the physical state at an optical depth of $\tau = 0.6$ whereas line formation takes place at about half this depth. A powerful method for the determination of the ionization temperature makes use of model atmosphere calculations to study the

profiles of the hydrogen lines.

In order to give a specific example of a model atmosphere, a model atmosphere of the sun from Aller's (1963) text is now given. In Table V are listed the value of θ , electron pressure, gas pressure, and linear depth in the solar atmosphere as a function of optical depth.

Calculation of Abundances

The calculation of the abundances of the elements from the experimental data will be done using Equation (2-17), which will now be repeated, and the significant factors to be considered in calculating each term will be discussed.

$$\log \eta^o/\eta^* = \log N^o/N^* - \chi(\theta^o-\theta^*) - \log \frac{v^o u^o(T)}{v^* u^*(T)} - \log \frac{k_\lambda^o(T,P_e^o)}{k_\lambda^*(T,P_e^*)}. \quad (4\text{-}1)$$

Determination of $\log \eta^o/\eta^*$

The term $\log \eta^o/\eta^*$ is evaluated according to the procedure described in Chapter II in the section "Summary of Steps Involved in a Curve of Growth Analysis." After determining the location of the continuum described in step 4), the profile of each selected line is drawn on the microphotometer tracing according to step 5), and the area under the curve is measured with a planimeter as described in step 6). The error of the measurement of the area under the curve is very small and only amounts to about 0.02 to 0.05 in the value of $[\eta]$.

Although it was obvious from the inspection of the individual tracings that the quality of the plates varied markedly, there was no good way of knowing which plate gave the most accurate value of the

TABLE V

MODEL ATMOSPHERE OF THE SUN

Log τ_o	θ (5040/T)	Log P_g	Log P_e	X (km)
-2.0	1.073	4.290	-0.030	-115
-1.9	1.069	4.330	+0.005	-105
-1.8	1.065	4.372	+0.042	- 95
-1.7	1.059	4.417	+0.087	- 85
-1.6	1.052	4.464	+0.136	- 74
-1.5	1.044	4.512	+0.190	- 62
-1.4	1.033	4.562	+0.250	- 50
-1.3	1.021	4.612	+0.311	- 38
-1.2	1.007	4.663	+0.375	- 26
-1.1	0.991	4.715	+0.460	- 13
-1.0	0.977	4.766	+0.550	0
-0.9	0.957	4.815	+0.658	+ 12
-0.8	0.940	4.861	+0.763	+ 24
-0.7	0.922	4.906	+0.865	+ 36
-0.6	0.904	4.949	+0.971	+ 48
-0.5	0.885	4.990	+1.094	+ 59
-0.4	0.865	5.029	+1.213	+ 70
-0.3	0.845	5.066	+1.338	+ 81
-0.2	0.825	5.101	+1.478	+ 91
-0.1	0.804	5.133	+1.619	+101
0.0	0.782	5.162	+1.793	+110
+0.1	0.759	5.187	+1.983	+117
+0.2	0.736	5.209	+2.147	+125
+0.3	0.706	5.229	+2.328	+132
+0.4	0.687	5.248	+2.485	+139
+0.5	0.660	5.264	+2.718	+144
+0.6	0.631	5.277	+3.020	+149

Hydrogen/metal ratio = 7.37×10^{-5} or log A = 4.133.

Fraction by weight of H = 0.613.

$\tau_o = \tau(\lambda_o)$. λ_o = 5000A.

P_g and P_e are measured in dynes/cm^2.

equivalent width. Therefore, no attempt was made to weight the tracings in determining the equivalent width, other than by completely omitting a measurement if the value of equivalent width was definitely inconsistent with all of the other measured values; this omission was done infrequently. The number of times that an individual line was measured varied from one to seven. The net effect of these error sources is to produce data that may have as much as a factor of two separating the maximum and minimum values of W for an individual line for which several measurements are available.

As a measure of the accuracy with which the $[\eta]$ term in step 8) can be calculated, analysis of the θ Ursae Majoris data indicates that a one-standard-deviation spread in the values of the equivalent width for a single line can generate differences of 0.20 to 0.50 in the values of $[\eta]$.

Statistical Weighting of Data

Due to the large number of sources of error to which the data are subject, it is desirable to use statistical techniques to treat the data in such a fashion that the results are more strongly influenced by those lines which are more reliably determined. The lines will be statistically weighted according to five criteria:

1) the number of individual measurements of a particular line,
2) the deviation in the measurements of the equivalent width from the average,
3) the position of the line on the curve of growth,
4) the absolute magnitude of the equivalent width of the line, and
5) agreement on values of solar equivalent width between the

Utrecht Tables (1960) and the data of the Commonwealth Solar Observatory (Allen, 1934, 1938).

After examining figures in which the values of $[\eta]$ are plotted against excitation potential, several instances are noted where points with highly singular values of $[\eta]$ are observed relative to other points of approximately the same excitation potential. An examination of Figures 11, 15, 17, and 18 reveals several instances where points of this type occur.

On the assumption that these extreme values arise from the sources of error mentioned above, as well as inadvertent computational errors which might have been made in data reduction, the rejection of such points is permissible if they are inconsistent with the statistical spread of data exhibited by the other points. This is accomplished by assigning these points zero statistical weight.

The weighting of the lines which were retained was done by the following procedure. A statistical weight of one or two was assigned to a line depending upon the number of spectra on which it appeared and the consistency of the equivalent width measurements. A line was given a weight of two only if three or more measurements of its equivalent width were available and if the variations among the measurements were small. An additional statistical weight of one or two was then assigned to the line on the basis of its position on the curve of growth. The line was given a weight of one if the equivalent width were so small that measurement errors were thought to be significant, if the change in $[\eta]$ were excessively large, or if the line were well into the damping portion of the curve. These weighted regions are illustrated in the top part of Figure 3. In Table VI are listed the statistical weights of the

various portions of the curve of growth, the average change in $[\eta]$ which results from a change of 0.02 in log W/λ, and comments concerning reasons for reduced weight in the three regions.

TABLE VI

CURVE OF GROWTH STATISTICAL WEIGHTS

Range of η	$\Delta\eta$	Weight	Comments
-8.4 to -7.4	0.02	1	Equivalent width less than 15 mA
-7.4 to -7.0	0.03	2	
-7.0 to -6.8	0.04	2	
-6.8 to -6.6	0.06	1	Flat portion of the curve
-6.6 to -5.5	0.08	1	Flat portion of the curve
-5.5 to -5.0	0.05	2	
-5.0 to -3.7	0.03	1	Damping portion of the curve

The total statistical weight of a line is then determined by adding together the weights from the number of measures and the position on the curve of growth, and subtracting unity. A numerical value of one, two, or three was thus obtained; if the value of $[\eta]$ were completely rejected because of gross inconsistency with the other data, it was given a weight of zero. In Figures 9 through 22 the statistical weight of a data point is indicated by the following system of symbols. A line assigned a statistical weight of zero is represented by an open circle, a weight of unity by a solid circle, a weight of two by an open square, and a line of statistical weight three by an open triangle.

The weighted data were than used to fit straight lines to plots of $[\eta]$ versus excitation potential for all of the elements for which

sufficient data existed to justify the procedure. In Table VII are shown the values of the slopes of the lines, the standard errors of the slopes, the standard error of estimate of the points from the regression lines calculated from both weighted and unweighted data and the value of Fisher's F. Comparison of the values shows that the introduction of the weighting procedure produced no substantial changes in the values of the calculated quantities. In Table VIII the values of θ_{exc} for eight elements obtained by the differential curve of growth technique have been converted into excitation temperatures and can be compared with the maximum and minimum values of Peebles obtained by the absolute method using f-values.

One additional factor was used to help assign statistical weights. The primary source of equivalent widths for the solar lines was the Utrecht tables (1960). If the value of $[\eta]$ obtained from the use of this solar equivalent width did not seem consistent with the values obtained from the other lines of the element, the equivalent width from the Commonwealth Solar Observatory (Allen, 1934, 1938) was compared with the Utrecht value. If the Commonwealth Observatory value differed greatly from the Utrecht value used in the calculation, a consequent reduction in the weighting of the line was indicated due to unreliability in the value of the solar equivalent width.

The value of $[\eta]$ which is used for the calculation of the electron pressure term (to be described later in the section on Determination of Electron Pressure) is taken to be the weighted average of the values of $[\eta]$ for the individual lines.

TABLE VII

RESULTS OF LEAST SQUARES FITS OF STRAIGHT LINES TO PLOTS OF $[\eta]$ VS. EXCITATION POTENTIAL

	Unweighted Data			Weighted Data		
Element	Fisher's F Test	Standard Error of Estimate	Slope (eV^{-1})	Fisher's F Test	Standard Error of Estimate	Slope (eV^{-1})
Ca I	1.39	$\pm$0.23	-0.17 $\pm$0.14	0.44	$\pm$0.22	-0.08 $\pm$0.12
Sc II	0.26	$\pm$0.37	0.11 $\pm$0.22	0.64	$\pm$0.36	0.14 $\pm$0.18
Ti I	5.2**	$\pm$0.32	0.135 $\pm$0.06	8.55**	$\pm$0.32	0.12 $\pm$0.04
Ti II	3.92*	$\pm$0.24	0.27 $\pm$0.14	9.08**	$\pm$0.24	0.27 $\pm$0.09
V I	-	-	-	9.51**	$\pm$0.37	-0.38 $\pm$0.12
V II	-	-	-	19.90**	$\pm$0.18	0.25 $\pm$0.06
Cr I	0.01	$\pm$0.29	-0.003 $\pm$0.03	0.66	$\pm$0.66	-0.02 $\pm$0.02
Cr II	0.035	$\pm$0.49	-0.20 $\pm$1.07	0.05	$\pm$0.41	-0.15 $\pm$0.68
Mn I	3.93*	$\pm$0.27	0.12 $\pm$0.06	5.32**	$\pm$0.28	0.10 $\pm$0.04
Fe I	16.7**	$\pm$0.30	0.10 $\pm$0.02	13.9**	$\pm$0.29	0.08 $\pm$0.02
Fe II	0.21	$\pm$0.35	0.10 $\pm$0.22	0.14	$\pm$0.34	0.07 $\pm$0.18
Co I	-	-	-	3.29*	$\pm$0.51	-0.16 $\pm$0.09
Ni I	-	-	-	0.07	$\pm$0.23	-0.02 $\pm$0.08
Y II	0.008	$\pm$0.34	0.026 $\pm$0.28	0.016	$\pm$0.33	-0.03 $\pm$0.23
Zr II	-	-	-	0.28	$\pm$0.20	0.07 $\pm$0.13
Ce II	-	-	-	1.55	$\pm$0.26	-0.40 $\pm$0.32

*Data significant at the 10% level.

**Data significant at the 5% level.

TABLE VIII

COMPARISON OF EXCITATION TEMPERATURES DERIVED BY DIFFERENTIAL TECHNIQUE WITH VALUES OBTAINED BY PEEBLES-WEIGHTED DATA

	Weighted Data			Values Obtained by Peebles	
Element	θ^* ($^oK^{-1}$)	Standard Derivation of θ^* ($^oK^{-1}$)	Excitation Temperature (^oK)	Excitation Temperature (^oK)	Atmospheric Model
Ca I	0.81	±0.12	6230±810	minimum 4532± 23	S-S Scatt.
				maximum 5607± 99	M-E Abs.
Fe I	0.97	±0.03	5190±160	minimum 5219±279	M-E Scatt.
				maximum 5522±511	M-E Abs.
Cr I	0.87	±0.01	5810± 80	minimum 6071±242	S-S Scatt.
				maximum 6239±352	M-E Abs.
Co I	0.73	±0.09	6900±730	minimum 5142±425	M-E Scatt.
				maximum 5259±517	S-S Abs.
Ni I	0.87	±0.08	5810±500	minimum 5625±383	S-S Scatt.
				maximum 6004±619	M-E Abs.
Mn I	0.99	±0.04	5080±200	minimum 4678±164	S-S Scatt.
				maximum 4752± 95	M-E Abs.
Ti I	1.01	±0.04	4980±190	minimum 4667±206	M-E Abs.
				maximum 4728±240	S-S Scatt.
Ti II	1.16	±0.09	4350±360	minimum 5933±309	S-S Scatt.
				maximum 8141±614	M-E Abs.

Determination of Excitation Temperature by Differential Comparison With the Sun

The value of the term $(\theta^{o} - \theta^{*})$ in Equation (4-1) is determined by plotting $[\eta] = \log \eta^{o} - \log \eta^{*}$ against the excitation potential (electron volts) of the lower energy level involved in the transition. A straight line was fitted to the data by the least squares technique with the aid of a standard linear regression program of the Oklahoma State Uniersity Computing Center. The results of the computations are listed in Table VII. Three quantities are tabulated for each calculation:

1) The slope of the best least squares straight line fit to the data (and its probable error), which gives the best estimate of $(\theta^{*} - \theta^{o})$.
2) The standard error of the estimate gives the deviation of the data points from the regression line and serves as an indication of the overall accuracy of the data reduction technique.
3) The value of a statistical parameter known as Fisher's F (Steel and Torrie; 1960) is calculated for each regression line.

In fitting a straight line to the data by the least squares technique, the assumption is made that a statistically significant reduction is made in the sums of squares of the deviations of the data points from the straight line as compared to the sums of squares of the deviations from a horizontal line that passes through the mean value of $[\eta]$. If this assumption cannot be verified, then there is no statistical justification for claiming that the slope of the line that is calculated from the least squares technique is any better representation of the

data than a horizontal line which passes through the mean value of $[\eta]$. In order to test the hypothesis that the straight line calculated by the least squares method gives a statistically significant reduction in the sum of squares of the deviations, the Fisher's F test is employed. The test is made by comparing the calculated values of Fisher's F with tabulated values such as may be found in statistics books like Steel and Torrie's "Principles and Procedures of Statistics" (1960). The computed value of F is compared against the tabulated value for the appropriate number of degrees of freedom, a quantity which is determined by the number of data points composing the graph. A significance level of five percent was chosen for these tests which means that there is a probability of one chance in twenty that the conclusion drawn from the test is erroneous. The larger the calculated value of Fisher's F the greater is the certainty that the calculated value of the regression line will produce a statistically significant reduction in the sum of squares of the deviations of the data points. Two sets of calculations were made for the elements Ca I, Fe I, Cr I, Mn I, Ti I, and Ti II. One set was made with all of the lines given equal weight, except for lines of weight zero which were excluded. The second calculation was made with the statistical weights given in the last column of Tables XII through XLV. For the other elements, no unweighted computations were made because the weights that were given to the lines were not considered to be of enough significance to change the results noticeably. A comparison of the computed values for the weighted and unweighted data shows that the weighting procedure did not make any substantial changes in the computed slopes or standard deviations. The largest change in slope was an increase of 0.09 for Ca I from -0.17 to -0.08. Since no radical

changes were produced in the results by adopting the weighting procedure, this may be taken as an indication that no undue emphasis was placed on singular data points in the weighting procedure. Should large deviations in the quantities have been noted in the results computed from weighted data, the validity of the weighting process would have been questionable. In the rest of the thesis, computations and conclusions will be made with the weighted data. Of the slopes that were obtained from plots of $[\eta]$ versus the excitation potential to determine the value of $(\theta^{o} - \theta^{*})$, Fisher's F test shows that only the four singly ionized elements listed in Table IX have slopes that are statistically significant at the five percent level.

TABLE IX

ELEMENTS WITH SIGNIFICANT VALUES OF FISHER'S F

Element	$(\theta^{o} - \theta^{*})$	Fisher's F
Fe I	0.08 ± 0.02	13.90
Mn I	0.10 ± 0.04	5.32
Ti I	0.12 ± 0.04	8.55
V I	0.38 ± 0.12	9.51

Consideration should also be given to Co I which just misses being statistically significant at the five percent level and has a slope of -0.16. The data for the two elements having negative slopes is not considered as reliable as that for the first three listed elements. Only eleven lines were available for V I and the analysis of Co I was based on twelve lines as opposed to twenty or more lines for the other elements. Another indication that the data is of lower quality is that the

standard deviations of the data points from the regression lines are larger for V I and Co I than for the other three elements.

The average of the slopes for Fe I, Mn I, and Ti I will therefore be taken as the difference in excitation temperature between θ Ursae Majoris and the sun. Setting $(\theta^{\circ} - \theta^{*}) = +0.10 \pm 0.03$ and adopting the Cowleys' value of $\theta^{\circ} = 0.98$, which corresponds to an excitation temperature of 5140°K, an excitation temperature of 5730°K is obtained, which corresponds to $\theta^{*}_{exc} = 0.88$. This value of $(\theta^{\circ} - \theta^{*})$ will be used as the reciprocal temperature difference for neutral atoms of all of the elements.

It is of significance to note in Table VII that the values of the standard deviation of a typical measurement about the regression line are fairly well clustered about the average value of $\pm$ 0.30. (The comparable value for unweighted data is $\pm$0.32.) The uniformity of the average deviation for almost all of the elements seems to be an indication of the basic accuracy of the differential curve of growth technique and was used in the Error Analysis section, Appendix A, to calculate the probable error in the determination of the abundance.

The determination of the value of $(\theta^{\circ} - \theta^{*})$ which should be used for elements in the ionized state is not as straightforward as for the unionized state of the elements. Examination of Table VII shows that only Ti II and V II have slopes which are significant at the five percent level. However, the lines of Ti II only cover a low range of excitation potential, and the large positive slope for V II is due to only two points which are separated in excitation potential from the large cluster. (See Table XXIII.) The data for Y II is based on only six

lines. Cr II, Ce II, and Zr II also show a low range of excitation potential. In addition, the deviations about the regression line for Cr II are very large which make one question the quality of the data.

Regarding the slopes of Fe II, Sc II, and Ti II as being indicative of the best quality data for the ionized elements, it would seem appropriate to use the same value of the difference in reciprocal temperatures as was used for the unionized elements. With the value of $(\theta^{o} - \theta^{*}) = +0.10$ now determined, the correction to $[\eta]$ for excitation potential may now be computed for each line of the ionized elements.

Partition Function

Since the lines of the elements are formed at different temperatures in the solar and stellar atmospheres the distribution of electrons among the available energy levels are different and a correction must be made for the relative numbers of electrons in the populated states. The partition function correction term, $\log u^{o}(T^{o})/u^{*}(T^{*})$, is computed from the values of the excitation temperature since these are the most representative of the occupation levels of the atoms and ions. The values of the partition function were obtained by graphing the data given in Table 3-1 of Aller (1963) and interpolating for the excitation temperatures of 5730^{o}K for θ Ursae Majoris and 5140^{o}K for the sun.

Determination of the Velocity Correction

The next correction to be made is for the difference in the total velocity between a radiating atom of an element in the sun and the star. The log c/v term may be determined experimentally from an absolute curve

of growth analysis from the amount of vertical shift that is necessary to fit the observational data to the theoretical curve of growth. Numerical values of log c/v are available for θ Ursae Majoris from Peebles' study and for the sun from the paper of Wright (1948). However, there are significant differences in the values of log c/v obtained from the four models used by Peebles, and the solar curve of growth used by Wright is based on yet a fifth curve of growth, which was plotted from the experimentally determined f-values obtained by King and King (1938) and the observed values of equivalent widths of the sun. If the experimentally determined values of the velocity were to be used, the selection of the proper curve of growth from the four available for θ Ursae Majoris would be a problem. The number of elements for which solar velocity data from Wright is available is limited to the neutral elements Ca I, Ti I, Cr I, Fe I, Ni I and the ionized atoms of Sc II, Ti II, Cr II and Fe II. The average value of log c/v for the four model atmospheres used by Peebles and the average of the velocities given by Wright were used to compute the [v] term given in Table X.

The correction term for the total velocity may be theoretically computed from the kinetic velocity, which is a function of the temperature and the atomic weight of the species, and the turbulent velocities, which are already known for the sun and θ Ursae Majoris. Taking the kinetic temperatures equal to the effective temperatures for all of the elements, and turbulent velocities of 1.4 ± 0.2 km/sec for the sun and 2.4 ± 0.2 km/sec for θ Ursae Majoris, the values of the velocity correction term listed in Table X were calculated.

An inspection of the table shows that the experimental values of log v^o/v^* for Fe I, Ca I and Ti II agree quite well with the theoretical

TABLE X

EXPERIMENTAL AND THEORETICAL DETERMINATION OF LOG v^o/v^*

Element	Atomic Weight	Experimental Values of log c/v						log v^o/v^*	
		Sun (Wright)	M-E Scatt.	M-E Abs.	S-S Scatt.	S-S Abs.	Average for θUM	Experimentally Determined	Theoretically Calculated
Na	22.99	-	-	-	-	-	-	-	-0.12
Ca I	40.08	5.18	5.06	5.00	5.07	5.05	5.045	-0.135	-0.15
Ti I	47.90	5.20	4.90	4.75	4.95	4.85	4.86	-0.34	-0.16
Ti II	47.90	5.20	4.95	4.05	5.00	5.07	5.02	-0.18	-0.16
Cr I	52.00	5.15	4.70	4.65	4.95	4.80	4.775	-0.375	-0.164
Fe I (NBS)	55.85	5.18	5.06	5.00	5.07	5.05	5.045	-0.145	-0.17
Ni I	58.71	5.08	5.06	5.00	5.07	5.05	5.045	-0.035	-0.17
Zn	65.37	-	-	-	-	-	-	-	-0.173
Y	88.91	-	-	-	-	-	-	-	-0.185
Ba	137.35	-	-	-	-	-	-	-	-0.20

computations (Equations 2-5 and 2-6) but those for Ti I, Cr I and Ni I show a large variation. Since values of log v^o/v^* will also be needed for 28 other elements, the theoretically computed velocities will be used in the abundance determinations.

Determination of Electron Pressure

In order to obtain the continuous absorption coefficient from tabular data it is necessary to have both the ionization temperature and the electron pressure. Some of the techniques described in the literature for the determination of the ionization temperature and the electron pressure are reviewed in Appendix A. In Appendix A is described an attempt to apply the pseudo-equivalent width technique to the Hγ profiles. This produced effective temperature data which show a large amount of dispersion. The procedure that was adopted is recommended on page 379 of Aller (1963) and assumes that the ionization temperature is equal to the effective temperature. The values of $[\eta]$ for the neutral and first ionized states of several elements are used to calculate the electron pressure of θ Ursae Majoris relative to that of the sun with the aid of the differential Saha equation in the single-layer approximation. The derivation is to be found in Appendix A and the resulting equation is

$$[\eta_1] - [\eta_o] = (\theta^* - \theta^o)\,\chi_i + 2.5 \log T^o/T^* - \log P_e^o/P_e^*, \qquad (4-2)$$

where χ_i is the ionization potential of the element in question. Using values of $\theta^o_{eff} = 0.8796$ corresponding to $T^o = 5725^oK$ and $\theta^*_{eff} = 0.8112$ or $T^* = 6210^oK$ (Hynek; 1951) the relative electron pressures were calculated using data from the neutral and singly ionized

stages of the elements Fe, Ti, Cr, V and Si. Calculations were also attempted with data from the elements Si, Sc, Mn, Sr and Y, but the values of the relative electron pressure which resulted were sufficiently removed from those values obtained from the better quality data that they were given zero weight. Using weights assigned on the basis of the quality of the data for the element in both the unionized and ionized states, an average value of $P_e^* = 1.17\ P_e^o$ is calculated from the information given in Table XI.

TABLE XI

DETERMINATION OF ELECTRON PRESSURE OF
θ URSAE MAJORIS RELATIVE TO THE SUN

Element	$[\eta_o]$	$[\eta_1]$	χ_i (eV)	Weighting Factor	$\log \frac{P_e^o}{P_e^*}$	P_e^* (in units of P_e^o)
Si	+0.26	-0.42	8.15	0	+0.02	0.955
Sc	+0.33	-0.27	6.54	0	+0.97	0.0073
Ti	+0.20	-0.36	6.82	2	0.0	1.00
V	+0.34	-0.13	6.74	1	-0.09	1.23
Cr	+0.23	-0.42	6.76	1	+0.09	0.81
Mn	+0.55	+0.67	7.43	0	-0.55	0.28
Fe	+0.16	-0.34	7.87	3	-0.14	1.38
Sr	+0.24	-0.02	5.69	0	+0.57	0.27
Y	+0.02	-0.42	6.38	0	+0.80	0.159

The relative electron pressure may be converted to absolute pressure units if the electron pressure in the sun is known. It is at this point that a knowledge of the theory of model atmospheres is required

since the electron pressure in the solar atmosphere varies continuously with the optical depth. At a representative depth for line formation the electron pressure must be chosen from an appropriate model atmosphere for the sun. Reference to the literature reviewed in Appendix A shows that authors have taken the depth of line formation to be in the range $\tau \approx 0.25 - 0.35$ and values of $\log P_e^o = 0.80$ to 1.30. Following the recent work of Koelbloed (1967), an intermediate value of $\log P_e^o = 1.00$ is assumed, and the value of the average electron pressure in θ Ursae Majoris is calculated to be

$$\begin{aligned} \log P_e^* &= \log 1.17 + \log P_e^o, \\ &= 0.07 + 1.00, \\ &= 1.07, \end{aligned} \qquad (4-3)$$

where P_e is in dynes/cm^2. Using a solar electron pressure of $\log P_e^o = 0.80$, Greenstein (1948) calculated the electron pressure in θ Ursae Majoris using the differential Saha equation in the single-layer approach from Fe, Cr and Ti data. Interpolating in his Table 9 for $\theta_{ion} = 0.81$, a mean value of $\log P_e^* = 1.11$ is obtained, which is in good agreement with the value obtained above. Using the same equivalent width data for titanium on which this study was based, Peebles obtained values of 1.36, 1.30, 1.27 and 1.32 for $\log P_e^*$ using four different atmospheric models.

Determination of the Correction for Continuous Optical Absorption

Now that the ionization temperature and the electron pressure have

been chosen, subject to the variation induced by the choice of model atmosphere and the choice of optical depth at which line formation occurs, the correction can be made for the difference in optical absorption between θ Ursae Majoris and the sun. It is extremely important for the determination of the abundance of the element that this correction be made accurately since the optical absorption coefficient is very sensitive to the values of both temperature and electron pressure. Using the effective temperature values and the weighted average electron pressure, the values of log k_λ are obtained from the tables on pages 96-98 of Allen (1963) for the sun and θ Ursae Majoris and subtracted to form the $[k_\lambda]$ term. In spite of the fact that spectral data extend over the wavelength range from 4000A - 6500A, no variation of the optical absorption with wavelength was taken into account. The vast majority of the lines come from the 4000A - 5500A wavelength region and the variation of the optical absorption coefficient with wavelength is much smaller than the uncertainty due to lack of knowledge of the proper values of the ionization temperature and electron pressure.

Calculation of Abundance

Tables XII through XLV list the observational data for the 34 elements and ions studied in this work, and certain other quantities necessary for the determination of the abundances, derived from this data. For each spectral line the tables list the wavelength, the values of log W/λ for both the sun and star, the corresponding values of log η from the Cowleys' photoelectrically determined curve of growth for the sun illustrated in Figure 3, and the difference in log η values, i.e., $\log \eta^\circ/\eta^* = \log \eta^\circ - \log \eta^*$. Using the value $(\theta^\circ - \theta^*) = +0.10$

for all of the elements, both neutral and singly ionized, the correction for the difference in excitation temperature is added to the log η°/η^{*} term and the value of $[\eta] + \chi(\theta^{\circ} - \theta^{*})$ is listed for each line in the next to the last column of the tables. Using the statistical weights for each point given in the last column, determined according to the procedure explained in the section of this chapter entitled "Statistical Weighting of Data", the weighted average values of $[\eta] = \log \eta^{\circ}/\eta^{*}$ were calculated for the elements Fe, Ti, Cr, V, Si, Sc, Mn and Sr which occurred in both the unionized and ionized states. These values of $[\eta]$ were used to calculate the relative electron pressure of θ Ursae Majoris with respect to the sun as described in the section on "Determination of Electron Pressure." A similar weighted average of $[\eta] + (\theta^{\circ} - \theta^{*})$ was made for all of the elements for use in the abundance analysis. Numerical calculations of the partition function correction, $[u]$, were made from graphical data using the values of excitation temperature for the sun and star. Comparison of the numerical values of the partition function correction with the numerical values of the other terms in the abundance equation (Equation 2-17) shows that the partition function term is the smallest. The values of the velocity correction term $[v]$ were calculated from the excitation temperatures and the turbulent velocities and have been given in Table X. The variation of the relative correction for optical absorption coefficient with wavelength was ignored in view of the much larger uncertainty due to the error in the values of ionization temperature and electron pressure from which the term was calculated. Also, since the term is applied in a differential fashion, small errors will tend to cancel. Assuming that the ionization temperature is equal to the effective temperature and using log $P_e^{\circ} = 1.00$,

the $[\ k_\lambda]$ term was calculated from the tables in Allen (1963).

Factors Determining the Quality of the Data

Before going into an element-by-element description of the data in detail, the significant factors influencing the quality of the data will be briefly reviewed. Of primary importance are the number of lines which are observable for an element and the number of measures of each line on intensitometer tracings. Because the spectra vary in quality, numerous measurements of the equivalent width of the line will produce an average value which is more reliable than a single measurement. The quality of the data may be judged from the magnitude of the standard deviation about the average. Other factors which affect the accuracy with which the equivalent width can be measured are the clarity of the profile, the dispersion of the spectrum, and the size of the line in milliangstroms, since weak lines are subject to larger systematic errors in the measurement of the equivalent width. The amount of change in log $[\eta]$ which is obtained for a given increment in values of log W/λ for the sun and star depends upon whether the line falls on the linear, flat, or damping portions of the curve of growth and is one of the factors taken into account in the weighting procedure.

For an accurate determination of the difference in excitation temperature between the sun and the star for an element the lines must cover a sufficiently large range of excitation potentials and have a low value for the sum of squares of the deviations about the regression line.

From the values of $[\eta]$ for the elements Fe, Ti, Cr, V, Si, Sc, Mn, and Sr, which occur in two stages of ionization, it is possible to

deduce the relative electron pressure using the Saha equation in the single layer approximation if the ionization temperature is assumed to be equal to the effective temperature. With the number of lines available for each element and the quality of the data varying by a considerable margin, the statistical weights in Table X were assigned to the determinations, with four of the elements given zero weight. Aside from differences in value due to error in the data, it should be expected that variations will arise in the values of the calculated electron pressure from element to element because the lines are formed in different strata of the atmosphere and the electron pressure varies with the optical depth in the atmosphere. In addition to having different ionization potentials for the formation of the ionized stage, the excitation potentials for both neutral and ionized stages vary between the elements, and the data for each element will therefore sample the conditions from a different set of layers in the atmosphere.

Results for Individual Elements

Results for Na I

Only four lines of Na I are observable and are listed in Table XII. Since each line appeared on only one tracing, the reliability of the data is low. The two lines arising from a level at 2.0 eV lie on the flat portion of the curve of growth while the two sodium D lines from 0.0 eV have very large equivalent widths and lie far out on the damping portion. Consequently these lines have been assigned statistical weights of zero and the results for Na I are based only upon the two lines from the flat region.

TABLE XII

DIFFERENTIAL CURVE OF GROWTH DATA DERIVED FROM Na I LINES

λ RMT	$\log \frac{W^*}{\lambda}$	$\log \eta^*$	$\log \frac{W^o}{\lambda}$	$\log \eta^o$	$\log \eta^o/\eta^*$	$\log \eta^o/\eta^* + \chi(\theta^o-\theta^*)$	Statistical Weight
5682.633	-4.82	-6.72	-4.74	-6.47	0.25	0.46	1
5688.193	-4.68	-6.26	-4.67	-6.24	0.02	0.23	1
5889.953	-4.19	-4.75	-3.90	-4.21	0.54	-0.54	0
5895.923	-4.30	-5.00	-4.02	-4.42	0.58	-0.58	0

Weighted Average $[\eta] + \chi(\theta^o-\theta^*) = 0.34$

Partition Function $\mu^o(T = 5140^oK) = 2.29$ $\mu^*(T = 5730^oK) = 2.41$

$[\mu] = \log 2.29/2.41 = -0.02$

Total Velocity $[v] = -0.12$

Continuous Absorption Coefficient $[k_\lambda] = 0.06$

Relative Abundance

$$\log \frac{N^o}{N^*} = 0.34 - 0.02 - 0.12 + 0.06 = 0.26$$

TABLE XIII

DIFFERENTIAL CURVE OF GROWTH DATA DERIVED FROM Mg I LINES

λ RMT	$\log \frac{W^*}{\lambda}$	$\log \eta^*$	$\log \frac{W^o}{\lambda}$	$\log \eta^o$	$\log \eta^o/\eta^*$	$\log \eta^o/\eta^* + \chi(\theta^o-\theta^*)$	Statistical Weight
4167.27	-4.55	-5.77	-4.32	-5.05	0.72	1.15	2
4702.9909	-4.31	-5.03	-4.16	-4.68	0.75	1.18	1
4730.0285	-5.02	-7.11	-4.86	-6.82	0.29	0.72	2
5172.6843	-4.06	-4.50	-3.62	-3.73	0.74	1.11	1
5183.6042	-3.96	-4.32	-3.49	-3.56	0.76	1.03	1
5528.4094	-4.35	-5.38	-4.28	-4.94	0.44	0.87	1
5711.0912	-5.14	-7.30	-4.73	-6.43	0.87	1.03	1

Weighted Average $[\eta] + \chi(\theta^o-\theta^*) = 1.00$

Partition Function $\mu^o(T = 5140^oK) = 1.04$ $\mu^*(T = 5730^oK) = 1.05$

$[\mu] = \log 1.04/1.05 = 0.00$

Total Velocity $[v] = -0.12$

Continuous Absorption Coefficient $[k_\lambda] = 0.06$

Relative Abundance

$$\log \frac{N^o}{N^*} = 1.00 + 0.00 - 0.12 + 0.06 = 0.94$$

TABLE XIV

DIFFERENTIAL CURVE OF GROWTH DATA DERIVED FROM Mg II LINES

λ RMT	$\log \frac{W^*}{\lambda}$	$\log \eta^*$	$\log \frac{W^o}{\lambda}$	$\log \eta^o$	$\log \eta^o/\eta^*$	$\log \eta^o/\eta^* + \chi(\theta^o-\theta^*)$	Statistical Weight
4427.995	-5.94	-8.18	-5.56	-7.86	+0.32	+1.32	1

Weighted Average	$[\eta] + \chi(\theta^o-\theta^*) = +1.32$
Partition Function	Not Available
Total Velocity	$[v] = -0.12$
Continuous Absorption Coefficient	$[k_\lambda] = +0.06$

Relative Abundance

$$\log \frac{N^o}{N^*} = +1.32 - 0.12 + 0.06 = +1.26$$

TABLE XV

DIFFERENTIAL CURVE OF GROWTH DATA DERIVED FROM Si I LINES

λ RMT	$\log \frac{W^*}{\lambda}$	$\log \eta^*$	$\log \frac{W^o}{\lambda}$	$\log \eta^o$	$\log \eta^o/\eta^*$	$\log \eta^o/\eta^* + \chi(\theta^o-\theta^*)$	Statistical Weight
5708.437	-5.02	-7.11	-4.87	-6.84	0.27	0.76	1
5772.258	-5.18	-7.36	-5.09	-7.23	0.13	0.85	1
5948.584	-5.00	-7.08	-4.83	-6.74	0.34	0.86	1
6237.34	-5.26	-7.48	-5.02	-7.18	0.30	0.64	1
Weighted Average		$[\eta] = 0.26$					
Weighted Average		$[\eta] + \chi(\theta^o-\theta^*) = 0.78$					
Partition Function		$\mu^o(T = 5140^oK) = 9.34$ $\mu^*(T = 5730^oK) = 9.51$ $[\mu] = \log 9.34/9.51 = -0.01$					
Total Velocity		$[v] = -0.13$					
Continuous Absorption Coefficient		$[k_\lambda] = 0.06$					
Relative Abundance		$\log \frac{N^o}{N^*} = 0.78 - 0.01 - 0.13 + 0.06 = 0.70$					

TABLE XVI

DIFFERENTIAL CURVE OF GROWTH DATA DERIVED FROM Si II LINES

λ RMT	$\log \frac{W^*}{\lambda}$	$\log \eta^*$	$\log \frac{W^o}{\lambda}$	$\log \eta^o$	$\log \eta^o/\eta^*$	$\log \eta^o/\eta^* + \chi(\theta^o-\theta^*)$	Statistical Weight
6347.091	-4.86	-6.82	-5.17	-7.35	-0.53	-0.28	1
6371.359	-5.13	-7.29	-5.36	-7.59	-0.30	0.51	1
Weighted Average		$[\eta]$ = -0.42					
Weighted Average		$[\eta] + \chi(\theta^o-\theta^*)$ = 0.40					
Partition Function		μ^o(T = 5140°K) = 5.67 μ^*(T = 5730°K) = 5.70 $[\mu]$ = log 5.67/5.70 = 0.0					
Total Velocity		$[v]$ = -0.13					
Continuous Absorption Coefficient		$[k_\lambda]$ = 0.06					
Relative Abundance		$\log \frac{N^o}{N^*}$ = 0.40 + 0.0 - 0.13 + 0.06 = 0.33					

TABLE XVII

DIFFERENTIAL CURVE OF GROWTH DATA DERIVED FROM Ca I LINES

λ RMT	log $\frac{W^*}{\lambda}$	log η^*	log $\frac{W^o}{\lambda}$	log η^o	log η^o/η^*	log $\eta^o/\eta^* + \chi(\theta^o-\theta^*)$	Statistical Weight
4226.728	-4.02	-4.02	-3.46	-3.48	0.94	0.94	0
4283.010	-4.56	-5.80	-4.51	-5.58	0.22	0.41	2
4289.364	-4.58	-5.87	-4.52	-5.60	0.27	0.46	2
4298.986	-4.50	-5.55	-4.58	-5.85	−0.30	-0.11	2
4425.441	-4.53	-5.68	-4.48	-5.47	0.21	0.40	2
4434.960	-4.42	-5.30	-4.41	-5.28	0.02	0.21	2
4435.688	-4.52	-5.63	-4.54	-5.71	−0.08	0.11	2
4526.935	-4.78	-6.72	-4.78	-6.60	0.12	0.39	1
4578.558	-4.76	-6.53	-4.80	-6.66	−0.13	0.12	1
5262.244	-4.64	-6.11	-4.62	-6.01	0.10	0.35	2
5512.979	-4.71	-6.38	-4.77	-6.56	−0.18	0.11	1
5581.971	-4.85	-6.80	-4.79	-6.62	0.18	0.07	1
5588.757	-4.50	-5.55	-4.60	-5.94	−0.39	−0.14	1
5590.120	-4.93	-6.96	-4.81	-6.70	0.26	0.51	2
5601.285	-4.66	-6.20	-4.75	-6.49	−0.29	−0.04	1
6102.722	-4.70	-6.34	-4.65	-6.18	0.16	0.35	1
6122.219	-4.55	-5.76	-4.44	-5.35	0.41	0.60	1
6162.172	-4.53	-5.68	-4.44	-5.35	0.33	0.52	1
6166.443	-5.23	-7.44	-5.06	-7.18	0.26	0.51	2
6439.073	-4.55	-5.76	-4.52	-5.66	0.10	0.35	1
6493.780	-4.73	-6.44	-4.64	-6.12	0.32	0.57	1

Weighted Average $[\eta] + \chi(\theta^o-\theta^*) = 0.25$

Partition Function $\mu^o(T = 5140^oK) = 1.25$ $\mu^*(T = 5730^oK) = 1.32$

$[\mu] = \log 1.25/1.32 = -0.02$

Total Velocity $[v] = -0.15$

Continuous Absorption Coefficient $[k_\lambda] = 0.06$

Relative Abundance $\log \frac{N^o}{N^*} = 0.25 - 0.02 - 0.15 + 0.06 = 0.14$

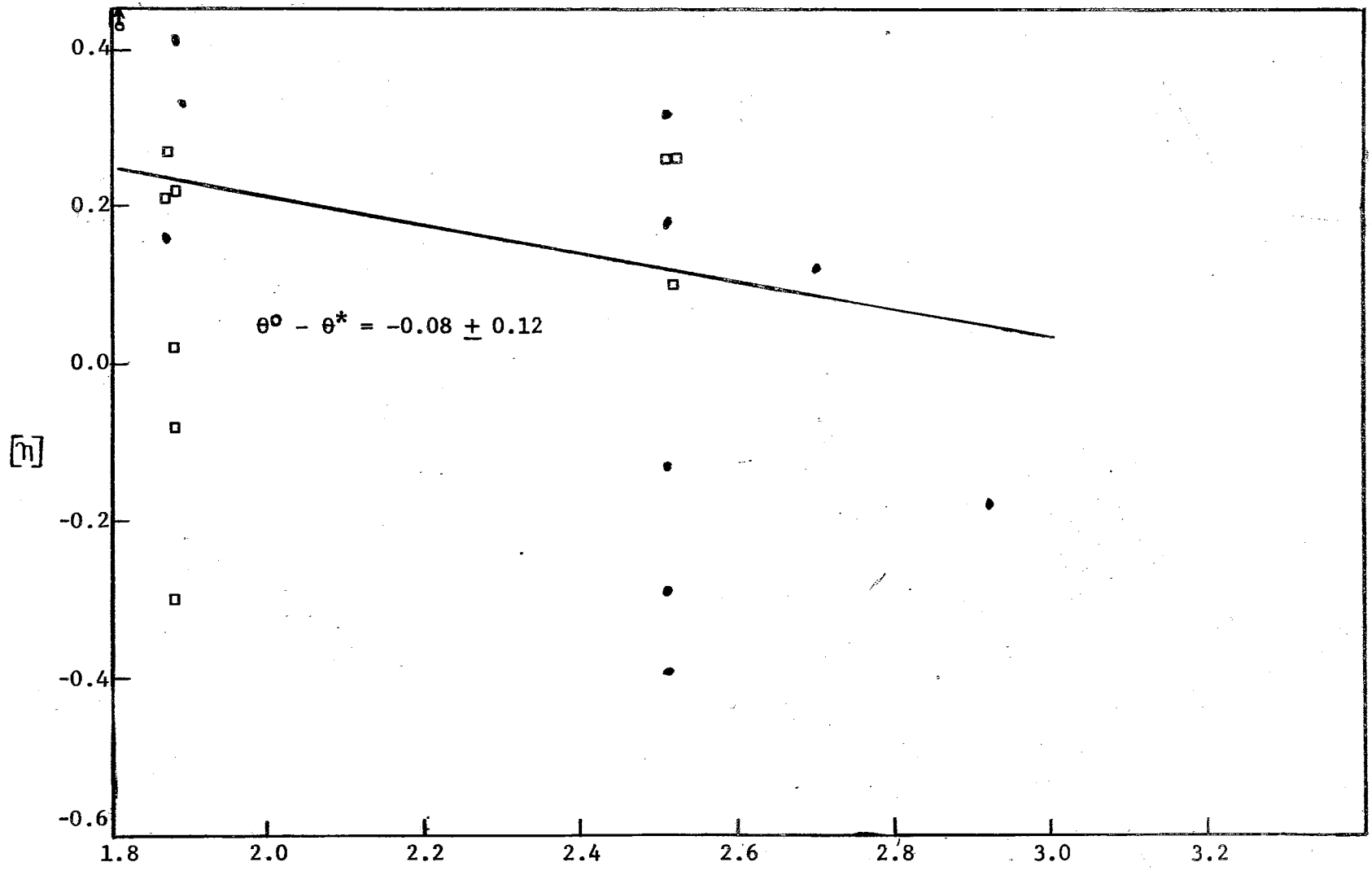

Figure 8. Plot of $[\eta]$ vs. Excitation Potential for Ca I.

TABLE XVIII

DIFFERENTIAL CURVE OF GROWTH DATA DERIVED FROM Sc I LINES

λ RMT	$\log \frac{W^*}{\lambda}$	$\log \eta^*$	$\log \frac{W^o}{\lambda}$	$\log \eta^o$	$\log \eta^o/\eta^*$	$\log \eta^o/\eta^* + \chi(\theta^o-\theta^*)$	Statistical Weight
4023.688	-5.37	-7.60	-5.04	-7.14	0.46	0.46	2
4743.814	-5.72	-7.96	-4.80	-6.66	1.30	0.06	1
4753.152	-5.68	-7.92	-6.18	-8.42	0.50	-0.50	0
Weighted Average		$[\eta] = 0.31$					
Weighted Average		$[\eta] + \chi(\theta^o-\theta^*) = 0.33$					
Partition Function		$\mu^o(T = 5140^oK) = 13.75$ $\mu^*(T = 5730^oK) = 13.84$					
		$[\mu] = \log 13.75/13.84 = 0.00$					
Total Velocity		$[v] = -0.16$					
Continuous Absorption Coefficient		$[k_\lambda] = 0.06$					
Relative Abundance		$\log \frac{N^o}{N^*} = 0.33 + 0.00 - 0.16 + 0.06 = 0.23$					

TABLE XIX

DIFFERENTIAL CURVE OF GROWTH DATA DERIVED FROM Sc II LINES

λ RMT	$\log \frac{W^*}{\lambda}$	$\log \eta^*$	$\log \frac{W^o}{\lambda}$	$\log \eta^o$	$\log \eta^o/\eta^*$	$\log \eta^o/\eta^* + \chi(\theta^o-\theta^*)$	Statistical Weight
4246.829	-4.42	-5.30	-4.40	-5.24	0.06	0.09	2
4294.767	-4.64	-6.11	-4.84	-6.77	-0.66	-0.60	1
4314.084	-4.36	-5.15	-4.60	-5.95	-0.80	-0.72	2
4320.745	-4.62	-6.03	-4.66	-6.20	-0.17	-0.11	1
4354.609	-4.70	-6.32	-4.79	-6.64	-0.32	-0.26	2
4415.559	-4.48	-5.45	-4.71	-6.37	-0.92	-0.86	2
5239.823	-4.94	-6.98	-4.98	-7.04	-0.06	0.08	2
5526.809	-4.62	-6.05	-4.86	-6.82	-0.77	-0.59	1
5667.164	-5.16	-7.33	-5.35	-7.58	-0.25	-0.10	2
5669.030	-5.22	-7.42	-5.22	-7.42	0.00	0.15	1
6245.629	-5.24	-7.45	-5.32	-7.55	-0.10	0.05	1

Weighted Average	$[\eta] = -0.33$
Weighted Average	$[\eta] + \chi(\theta^o-\theta^*) = -0.27$
Partition Function	$\mu^o(T = 5140^oK) = 23.17 \quad \mu^*(T = 5730^oK) = 24.04$ $[\mu] = \log 23.17/24.04 = -0.02$
Total Velocity	$[v] = -0.16$
Continuous Absorption Coefficient	$[k_\lambda] = 0.06$
Relative Abundance	$\log \frac{N^o}{N^*} = -0.27 - 0.02 - 0.16 + 0.06 = -0.39$

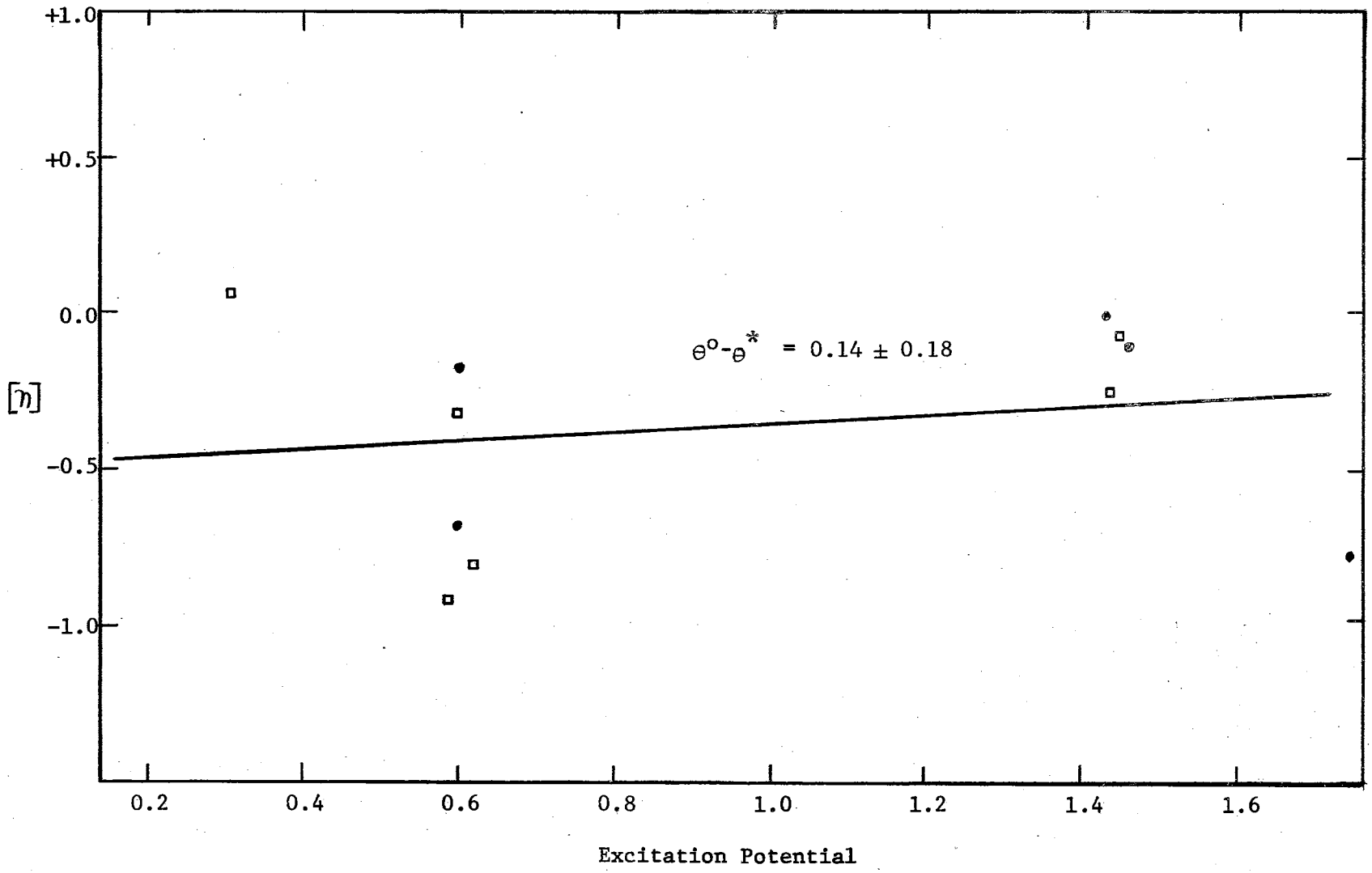

Figure 9. Plot of $[\eta]$ vs. Excitation Potential for Sc II.

TABLE XX

DIFFERENTIAL CURVE OF GROWTH DATA DERIVED FROM Ti I LINES

λ RMT	log $\frac{W^*}{\lambda}$	log η^*	log $\frac{W^o}{\lambda}$	log η^o	log η^o/η^*	log $\eta^o/\eta^* + \chi(\theta^o-\theta^*)$	Statistical Weight
4008.046	-5.03	-7.14	-5.16	-7.33	-0.19	0.02	3
4008.926	-4.57	-5.80	-4.58	-5.87	-0.07	-0.07	2
4016.264	-5.77	-8.00	-5.49	-7.73	0.27	0.48	1
4060.263	-5.44	-7.68	-5.08	-7.21	0.47	0.57	1
4166.311	-5.70	-7.94	-5.32	-7.55	0.39	0.58	1
4169.330	-5.82	-8.06	-5.62	-7.86	0.20	0.39	1
4186.119	-5.30	-7.51	-5.00	-7.08	0.43	0.58	1
4265.723	-6.03	-8.23	-5.24	-7.45	0.78	0.97	0
4281.371	-5.79	-8.03	-5.33	-7.56	0.47	0.55	1
4286.006	-4.73	-6.47	-4.56	-5.80	0.67	0.75	3
4287.405	-5.06	-7.17	-4.87	-6.84	0.21	0.29	3
4305.910	-4.33	-5.07	-4.44	-5.34	0.27	0.35	3
4321.655	-5.19	-7.37	-5.22	-7.42	0.05	0.27	3
4326.359	-5.45	-7.68	-5.30	-7.53	0.15	0.23	3
4417.274	-5.51	-7.75	-4.99	-7.06	0.69	0.88	2
4427.098	-5.49	-7.73	-4.84	-6.77	0.97	1.13	0
4453.708	-5.38	-7.62	-5.09	-7.23	0.39	0.58	2
4465.807	-5.41	-7.64	-5.17	-7.34	0.30	0.47	2
4518.022	-4.88	-6.87	-4.86	-6.82	0.05	0.13	2
4533.238	-4.48	-5.45	-4.70	-6.34	-0.89	-0.81	1
4534.782	-4.62	-6.00	-4.75	-6.50	-0.50	-0.42	2
4548.764	-5.03	-7.13	-4.86	-6.82	-0.31	-0.23	2
4555.486	-4.84	-6.77	-4.93	-6.96	-0.19	-0.11	2
4617.269	-5.02	-7.13	-4.08	-7.03	0.10	0.27	3
4623.369	-5.33	-7.55	-5.00	-7.08	0.47	0.64	1
4639.369	-5.39	-7.63	-5.11	-7.25	0.38	0.55	1
4639.669	-5.65	-7.90	-5.10	-7.24	0.66	0.83	1
4645.193	-5.51	-7.75	-5.46	-7.69	0.06	0.23	1
4656.468	-5.08	-7.19	-4.86	-6.85	0.34	0.34	3
4681.908	-4.71	-6.39	-4.86	-6.82	-0.43	-0.43	3
4758.120	-5.33	-7.55	-5.08	-7.20	0.35	0.57	2
4759.272	-5.27	-7.46	-5.06	-7.18	0.28	0.50	2
4799.797	-5.21	-7.38	-4.80	-6.67	0.71	0.94	2
4805.416	-5.62	-7.87	-5.11	-7.26	0.61	0.84	2
4820.410	-5.42	-7.65	-5.04	-7.14	0.51	0.66	2
4840.874	-5.33	-7.55	-4.91	-6.92	0.63	0.72	2
4913.616	-5.45	-7.68	-5.00	-7.08	0.60	0.79	1
4919.867	-5.64	-7.90	-5.31	-7.54	0.36	0.58	1
4981.732	-4.61	-6.00	-4.64	-6.11	-0.11	-0.03	1
5016.162	-4.97	-7.02	-4.92	-6.94	0.08	0.00	2
5024.842	-4.83	-6.73	-4.91	-6.92	-0.19	-0.11	1
5025.576	-5.09	-7.22	-4.99	-7.06	0.16	0.36	2
5039.959	-4.88	-6.87	-4.88	-6.88	-0.01	0.00	2
5043.578	-5.55	-5.78	-4.56	-5.78	0.00	0.08	1
5152.185	-5.67	-7.92	-5.13	-7.29	0.63	0.63	0

TABLE XX (Continued)

λ RMT	$\log \frac{W^*}{\lambda}$	$\log \eta^*$	$\log \frac{W^o}{\lambda}$	$\log \eta^o$	$\log \eta^o/\eta^*$	$\log \eta^o/\eta^* + \chi(\theta^o-\theta^*)$	Statistical Weight
5173.742	-4.84	-6.77	-4.89	-6.88	-0.11	-0.11	2
5194.043	-5.86	-6.85	-4.71	-6.39	0.46	0.67	1
5201.096	-5.83	-8.07	-5.67	-7.91	0.16	0.37	1
5210.386	-4.93	-6.95	-4.78	-6.60	0.35	0.35	3
5224.301	-5.46	-7.70	-5.16	-7.33	0.37	0.58	1
5689.465	-5.68	-7.93	-5.71	-7.95	-0.02	0.21	1
5713.895	-5.65	-7.90	-6.06	-8.30	-0.40	-0.17	0
5766.330	-5.60	-7.85	-5.83	-8.07	-0.22	0.11	1
5866.453	-5.62	-7.87	-5.17	-7.34	0.53	0.64	1
5918.548	-5.61	-7.86	-5.62	-7.86	0.00	0.11	1

Weighted Average $[\eta] = 0.20$

Weighted Average $[\eta] + \chi(\theta^o-\theta^*) = 0.33$

Partition Function μ^o (T = 5140°K) = 29.8 μ^* (T = 5730°K) = 34.0

$[\mu] = \log 29.8/34.0 = -0.057$

Total Velocity $[v] = -0.16$

Continuous Absorption Coefficient $[k_\lambda] = 0.06$

Relative Abundance $\log \frac{N_o^o}{N_o^*} = 0.33 - 0.057 - 0.16 + 0.06 = 0.173$

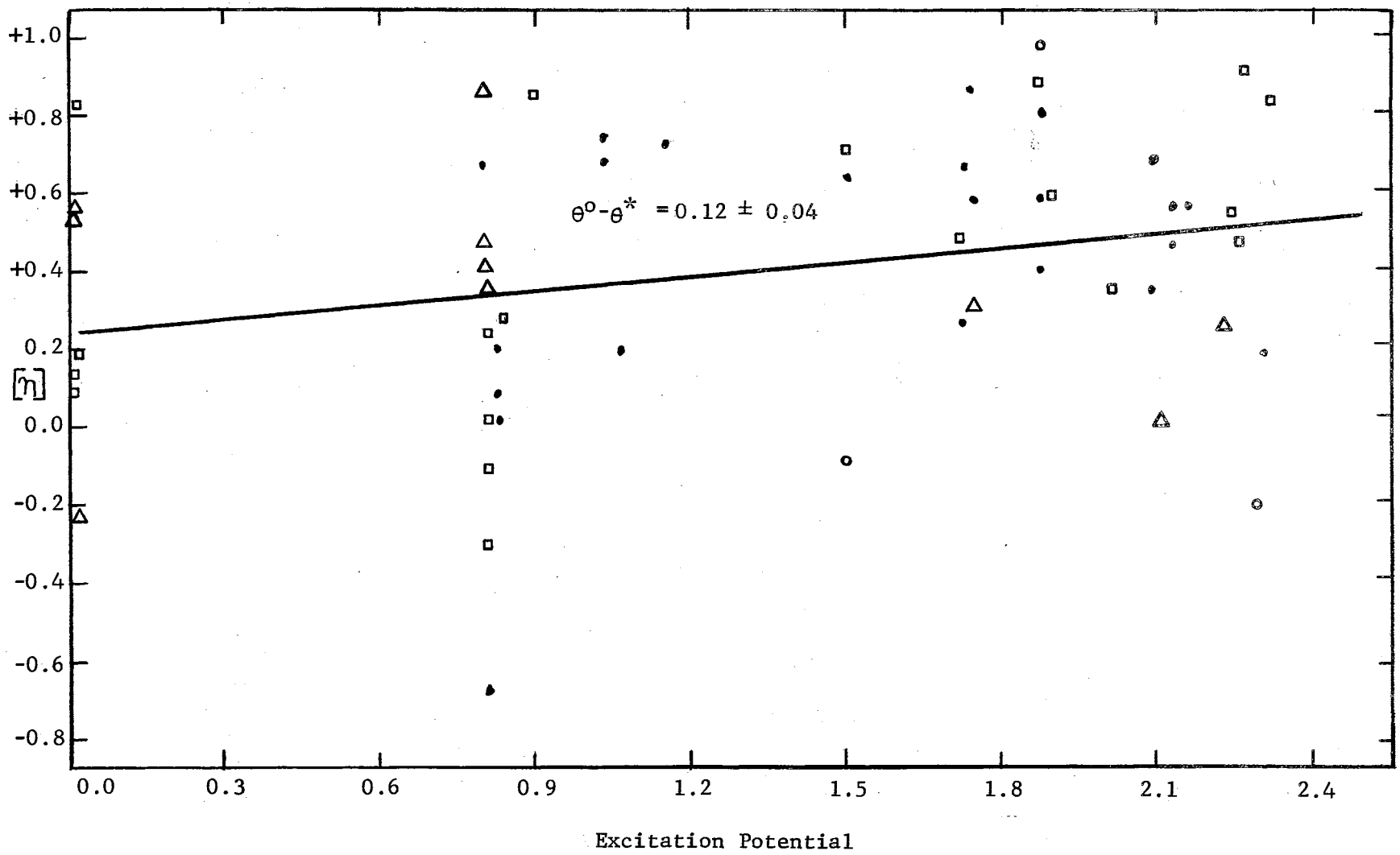

Figure 10. Plot of $[\eta]$ vs. Excitation Potential for Ti I.

TABLE XXI

DIFFERENTIAL CURVE OF GROWTH DATA DERIVED FROM Ti II LINES

λ RMT	log $\frac{W^*}{\lambda}$	log η^*	log $\frac{W^o}{\lambda}$	log η^o	log η^o/η^*	log $\eta^o/\eta^* + \chi(\theta^o-\theta^*)$	Statistical Weight
4300.052	-4.30	-5.00	-4.41	-5.28	-0.28	-0.40	3
4301.928	-4.45	-5.37	-4.46	-5.40	-0.03	-0.15	3
4312.861	-4.39	-5.22	-4.45	-5.37	-0.15	-0.27	3
4316.807	-4.90	-6.90	-5.06	-7.18	-0.28	-0.48	3
4337.916	-4.44	-5.35	-4.69	-6.30	0.95	+0.84	0
4344.291	-4.62	-6.03	-4.76	-6.53	-0.50	-0.61	1
4394.057	-4.60	-5.95	-4.78	-6.61	-0.66	-0.78	2
4395.031	-4.29	-4.97	-4.52	-5.63	-0.65	-0.76	2
4395.848	-4.71	-6.37	-4.86	-6.81	-0.23	-0.35	3
4409.519	-5.08	-7.21	-5.12	-7.28	-0.07	-0.19	2
4417.718	-4.53	-5.67	-4.66	-6.20	-0.52	-0.64	2
4421.949	-4.85	-6.80	-4.94	-6.98	-0.18	-0.38	2
4443.802	-441	-5.28	-4.56	-5.77	-0.49	-0.60	3
4450.487	-4.51	-5.59	-4.76	-6.51	-0.92	-1.03	2
4468.493	-4.37	-5.18	-4.57	-5.84	-0.66	-0.77	3
4533.966	-4.25	-4.89	-4.62	-6.03	-1.14	-1.26	0
4563.761	-4.37	-5.17	-4.58	-5.87	-0.69	-0.81	3
4568.312	-5.00	-7.08	-5.26	-7.48	-0.40	-0.52	2
4571.971	-4.27	-4.93	-4.56	-5.80	-0.87	-1.03	2
4708.663	-4.84	-6.77	-5.01	-7.10	-0.33	-0.45	1
4779.986	-4.76	-6.53	-4.80	-6.66	-0.13	-0.33	3
4805.105	-4.49	-5.50	-4.59	-5.93	-0.43	-0.63	1
5129.143	-4.57	-5.84	-4.86	-6.82	0.02	-0.17	1
5185.90	-4.83	-6.74	-4.95	-7.00	-0.26	-0.45	2
5336.809	-4.80	-6.66	-4.88	-6.86	-0.20	-0.36	2
5381.020	-4.88	-6.86	-4.98	-7.04	-0.18	-0.34	3
5418.802	-4.96	-7.01	-5.04	-7.14	-0.13	-0.29	3

Weighted Average $[\eta] = -0.36$

Weighted Average $[\eta] + \chi(\theta^o-\theta^*) = -0.22$

Partition Function μ^o ($T = 5140^oK$) = 53.4 μ^* ($T = 5730^oK$) = 56.5

$[\mu] = \log 53.4/56.5 = -0.024$

Total Velocity $[v] = -0.16$

TABLE XXI (Continued)

Continuous Absorption Coefficient	$[k_\lambda] = +0.06$
Relative Abundance	$\log \frac{N^o}{N^*} = -0.22 - 0.024 - 0.16 + 0.06 = -0.344$

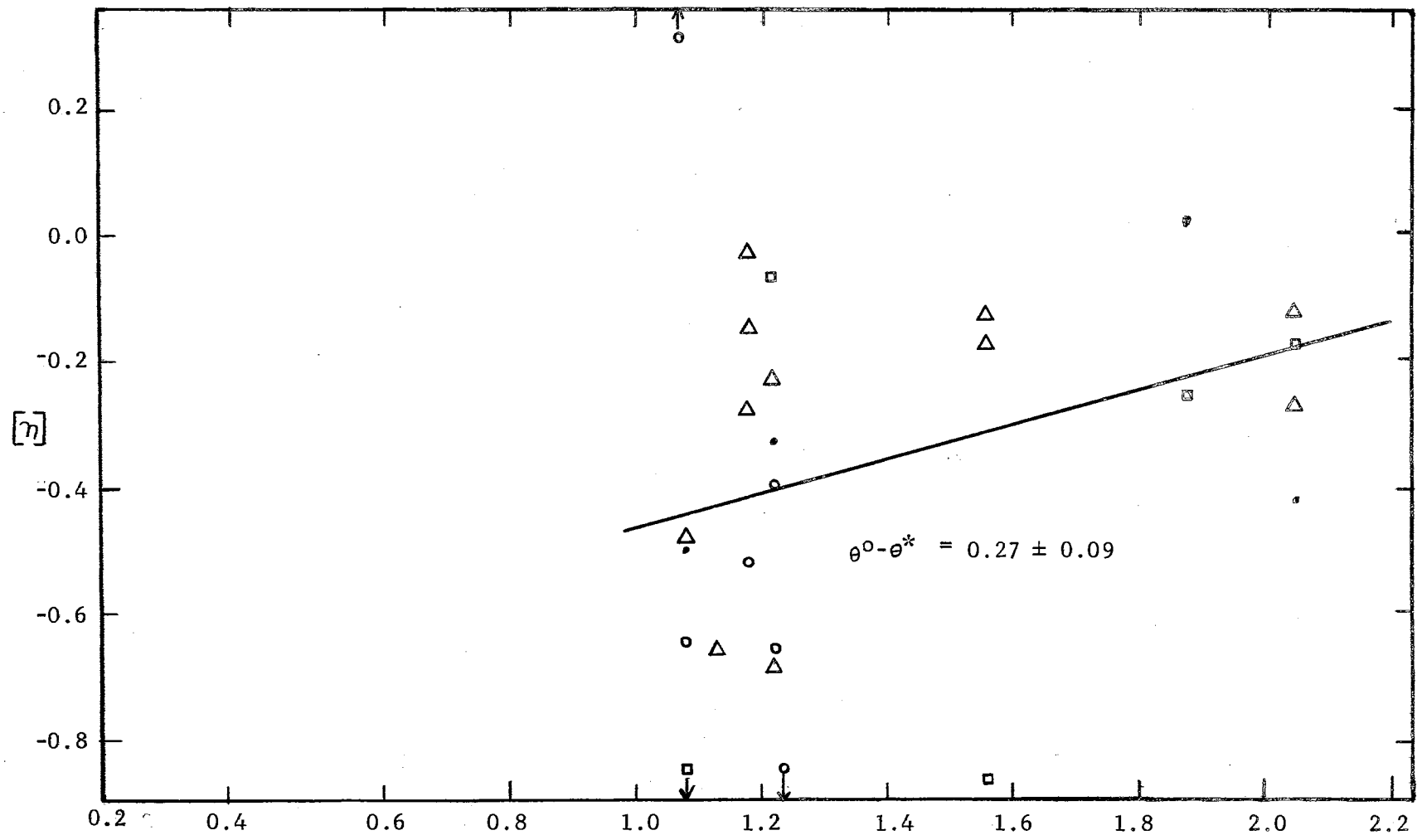

Figure 11. Plot of $[\eta]$ vs. Excitation Potential for Ti II.

TABLE XXII

DIFFERENTIAL CURVE OF GROWTH DATA DERIVED FROM V I LINES

λ RMT	$\log \frac{W^*}{\lambda}$	$\log \eta^*$	$\log \frac{W^o}{\lambda}$	$\log \eta^o$	$\log \eta^o/\eta^*$	$\log \eta^o/\eta^* + \chi(\theta^o-\theta^*)$	Statistical Weight
4095.486	-5.33	-7.56	-5.15	-7.31	+0.25	+0.36	1
4111.785	-5.95	-8.19	-4.59	-5.90	+0.29	+0.32	1
4113.518	-5.44	-7.67	-5.71	-7.95	-0.28	+0.16	1
4115.185	-5.24	-7.44	-4.62	-6.04	+0.40	+0.43	1
4341.832	-5.34	-7.57	-6.46	-	-	-	0
4379.238	-4.80	-6.66	-4.60	-5.95	+0.71	+0.74	2
4389.974	-4.91	-6.92	-4.72	-6.40	+0.52	+0.55	3
4406.641	-5.26	-7.48	-4.75	-6.51	+0.97	+1.00	2
4408.204	-5.24	-7.45	-4.78	-6.58	+0.87	+0.90	1
4437.837	-5.66	-7.90	-5.22	-7.41	+0.49	+0.52	1
4444.207	-5.37	-7.60	-5.16	-7.32	+0.28	+0.31	1
4452.008	-5.36	-7.59	-5.31	-7.52	+0.07	+0.26	1
4469.710	-5.65	-7.89	-5.40	-7.63	+0.26	+0.44	1
4553.056	-5.24	-7.45	-6.36	-	-	-	0
4560.710	-5.45	-7.68	-5.78	-8.02	-0.34	-0.15	1
4577.173	-5.05	-7.16	-5.26	-7.48	-0.32	-0.32	1
4686.926	-5.77	-8.01	-6.37	-	-	-	0
5234.088	-5.49	-7.73	-5.98	-8.22	-0.49	-0.26	1

Weighted Average	$[\eta] = 0.34$
Weighted Average	$[\eta] + \chi(\theta^o-\theta^*) = 0.41$
Partition Function	μ^o ($T = 5140^oK$) = 1.69 μ^* ($T = 5730^oK$) = 1.73
	$[\mu] = \log 1.69/1.73 = -0.009$
Total Velocity	$[v] = -0.16$
Continuous Absorption Coefficient	$[k_\lambda] = 0.06$
Relative Abundance	$\log \frac{N^o}{N^*} = 0.41 - 0.01 - 0.16 + 0.06 = 0.30$

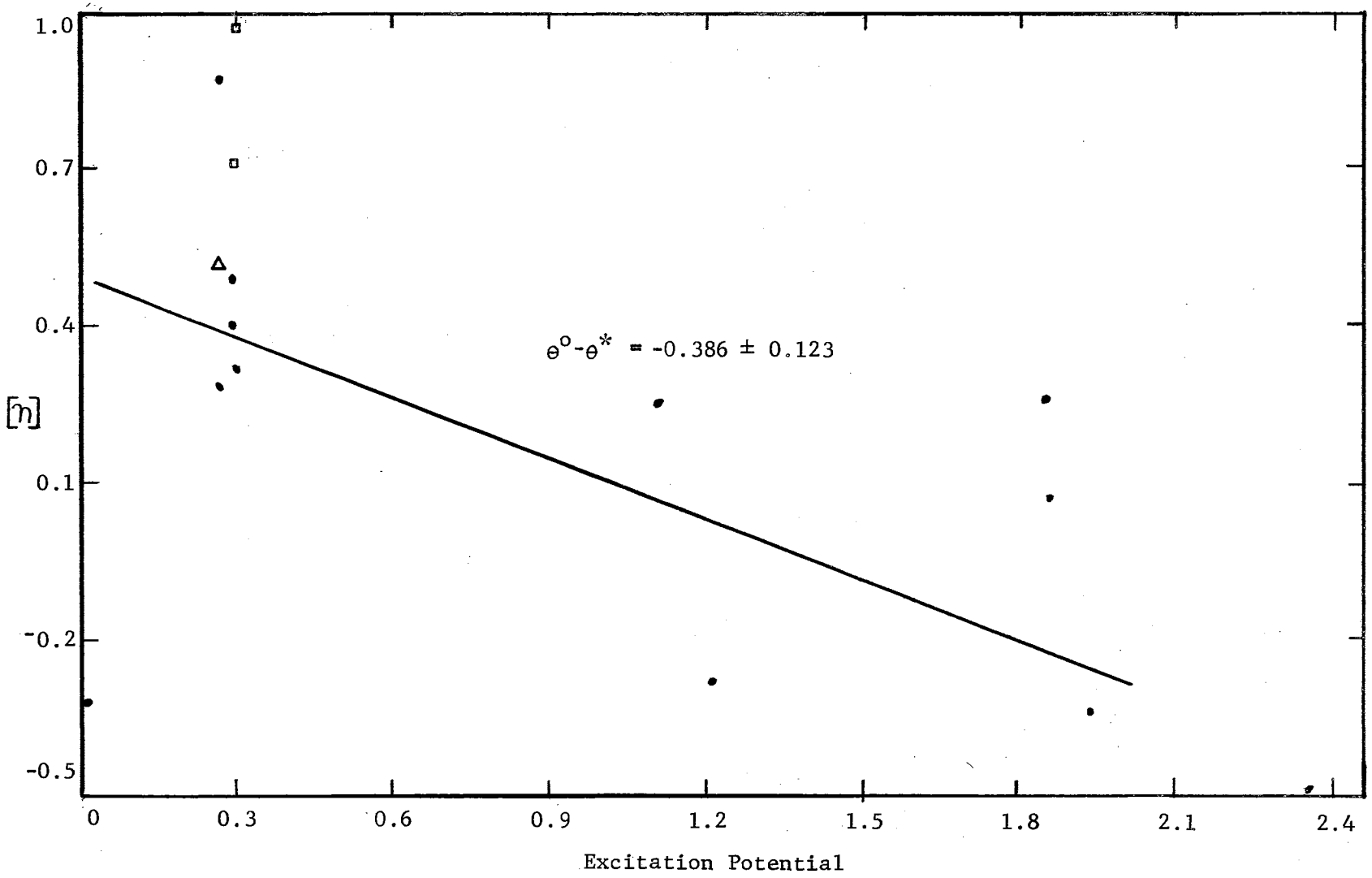

Figure 12. Plot of $[\eta]$ vs. Excitation Potential for V I.

TABLE XXIII

DIFFERENTIAL CURVE OF GROWTH DATA DERIVED FROM V II LINES

λ RMT	$\log \frac{W^*}{\lambda}$	$\log \eta^*$	$\log \frac{W^o}{\lambda}$	$\log \eta^o$	$\log \eta^o/\eta^*$	$\log \eta^o/\eta^* + \chi(\theta^o-\theta^*)$	Statistical Weight
4002.940	-4.71	-6.38	-4.82	-6.71	-0.33	-0.19	1
4005.712	-4.55	-5.76	-4.67	-6.25	-0.49	-0.31	1
4023.388	-4.81	-6.69	-4.78	-6.60	+0.09	+0.27	1
4036.779	-4.93	-6.96	-5.12	-7.26	-0.30	-0.15	2
4039.574	-5.30	-7.53	-5.65	-7.89	-0.36	-0.18	1
4065.070	-5.02	-7.11	-4.90	-6.89	+0.22	+0.60	2
4178.390	-5.11	-7.40	-5.22	-7.42	-0.02	+0.15	1
4183.435	-4.87	-6.84	-4.73	-6.45	+0.39	+0.59	0
4225.228	-5.15	-7.32	-5.12	-7.27	+0.05	+0.25	2
4232.065	-5.26	-7.48	-4.98	-7.03	+0.45	+0.85	1
4234.251	-5.39	-7.62	-5.78	-8.02	-0.40	-0.23	1

Weighted Average $[\eta] = -0.13$

Weighted Average $[\eta] + \chi(\theta^o-\theta^*) = 0.14$

Partition Function μ^o ($T = 5140^oK$) = 1.665 μ^* ($T = 5730^oK$) = 1.695

$[\mu] = \log 1.665/1.695 = -0.007$

Total Velocity $[v] = -0.16$

Continuous Absorption Coefficient $[k_\lambda] = 0.06$

Relative Abundance

$$\log \frac{N^o}{N^*} = 0.14 - 0.01 - 0.16 + 0.06 = 0.03$$

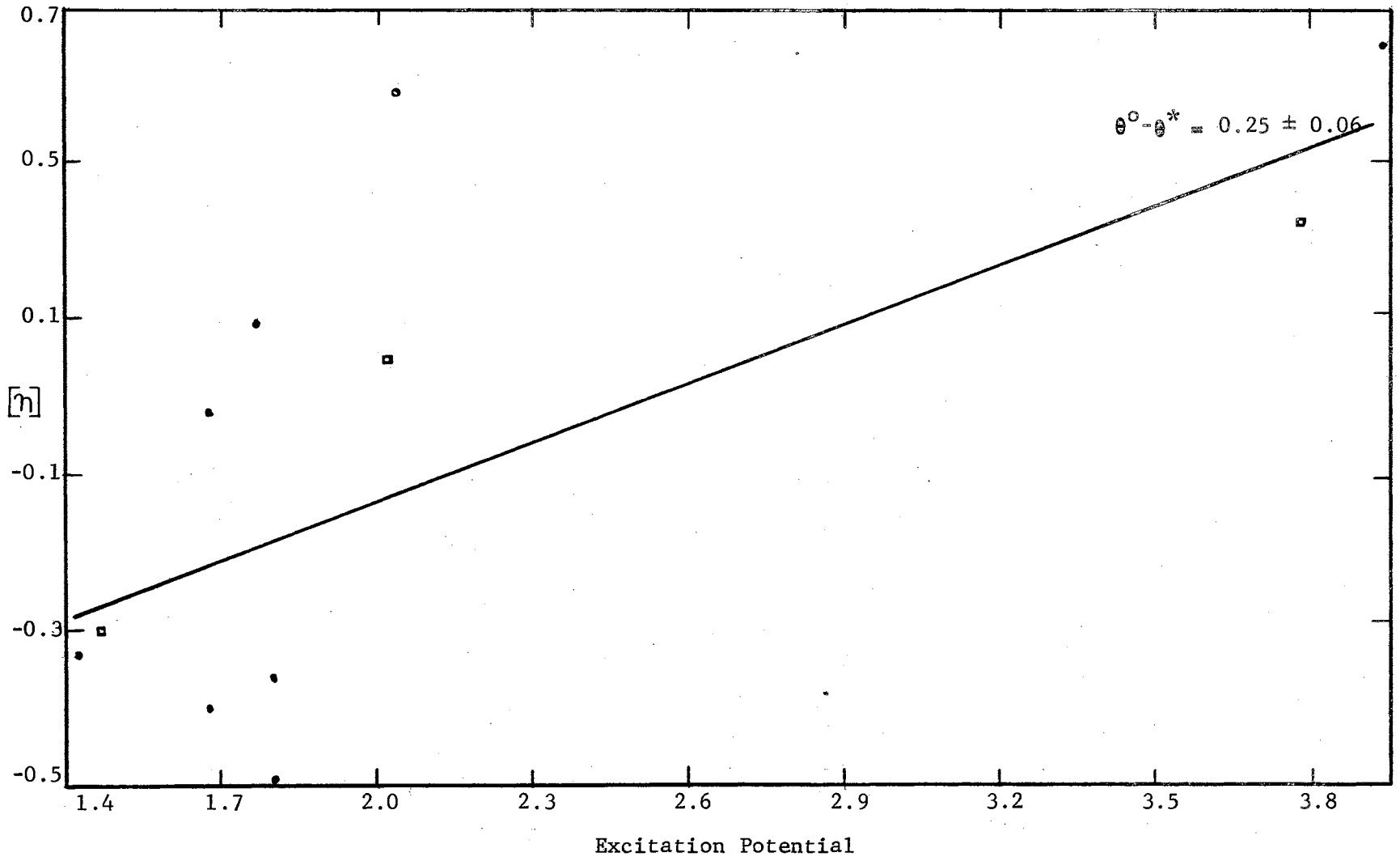

Figure 13. Plot of [η] vs. Excitation Potential for V II.

TABLE XXIV

DIFFERENTIAL CURVE OF GROWTH DATA DERIVED FROM Cr I LINES

λ RMT	log $\frac{W^*}{\lambda}$	log η^*	log $\frac{W^o}{\lambda}$	log η^o	log η^o/η^*	log $\eta^o/\eta^* + \chi(\theta^o-\theta^*)$	Statistical Weight
4001.444	-5.04	-7.14	-4.77	-6.56	0.58	0.97	2
4022.263	-5.42	-7.65	-4.86	-6.82	0.83	1.22	0
4039.100	-5.15	-7.31	-4.98	-7.05	0.26	0.64	2
4065.716	-5.85	-8.09	-5.46	-7.69	0.40	0.81	1
4120.613	-5.40	-7.63	-5.29	-7.52	0.11	0.38	1
4126.521	-5.43	-7.66	-4.94	-6.98	0.68	0.93	1
4197.234	-5.58	-7.82	-5.30	-7.58	0.24	0.62	1
4208.357	-6.03	-8.26	-5.42	-7.65	0.61	0.99	1
4209.368	-5.45	-7.68	-5.16	-7.33	0.35	0.73	1
4211 349	-5.60	-7.84	-5.32	-7.55	0.29	0.59	1
4254.346	-4.37	-5.18	-5.03	-4.44	0.74	0.74	0
4272.910	-5.42	-7.65	-5.12	-7.28	0.37	0.66	1
4274.803	-4.40	-5.25	-5.34	-5.10	0.15	0.15	1
4289.721	-4.29	-4.97	-5.27	-4.93	0.14	0.04	1
4337.566	-4.67	-6.24	-4.69	-6.32	-0.08	0.02	1
4339.450	-4.90	-6.90	-4.72	-6.41	0.49	0.59	1
4339.718	-5.23	-7.44	-4.80	-6.66	0.78	0.88	1
4344.507	-4.65	-6.15	-4.64	-6.13	0.02	0.12	1
4346.833	-5.18	-7.36	-5.05	-7.16	0.20	0.50	1
4351.051	-4.96	-7.01	-4.68	-6.28	0.73	0.83	2
4373.254	-5.66	-7.90	-4.99	-7.06	0.84	0.94	1
4381.112	-5.93	-8.17	-5.21	-7.41	0.76	1.03	1
4384.977	-4.98	-7.04	-4.74	-6.47	0.57	0.67	3
4387.496	-5.08	-7.21	-4.86	-6.81	0.40	0.70	3
4410.304	-5.79	-8.03	-5.50	-7.74	0.29	0.59	1
4412.250	-5.57	-7.81	-5.18	-7.36	0.45	0.55	1
4458.538	-5.10	-7.24	-5.02	-7.10	0.14	0.44	3
4511.903	-5.09	-7.22	-5.16	-7.33	-0.11	0.20	1
4535.146	-5.50	-7.74	-5.24	-7.45	0.29	0.54	1
4545.956	-4.73	-6.45	-4.79	-6.64	0.19	0.29	2
4591.394	-4.90	-6.90	-4.89	-6.88	0.02	0.12	3
4600.752	-4.73	-6.45	-4.76	-6.53	-0.08	0.02	2
4616.137	-4.82	-6.72	-4.81	-6.69	0.03	0.13	2
4626.188	-4.85	-6.80	-4.84	-6.76	0.04	0.14	2
4639.538	-5.12	-7.27	-5.49	-7.73	-0.46	-0.15	1
4646.174	-4.55	-5.76	-4.78	-6.61	-0.85	-0.75	0
4649.461	-5.49	-7.73	-5.36	-7.60	0.13	0.38	1
4651.285	-4.88	-6.86	-4.84	-6.79	0.17	0.27	3
4652.158	-4.79	-6.63	-4.76	-6.53	0.10	0.20	2
4708.040	-5.08	-7.21	-4.96	-7.01	0.20	0.51	3
4718.429	-4.93	-6.96	-4.90	-6.90	0.06	0.38	3
4724.416	-5.58	-7.82	-5.24	-7.45	0.37	0.68	1
4730.711	-5.21	-7.40	-5.04	-7.14	0.26	0.57	1
4745.308	-5.66	-7.90	-5.60	-7.84	0.06	0.33	1
4756.113	-4.94	-6.98	-4.90	-6.90	0.08	0.39	3

TABLE XXIV (Continued)

λ RMT	log $\frac{W^*}{\lambda}$	log η^*	log $\frac{W^o}{\lambda}$	log η^o	log η^o/η^*	log η^o/η^* $+\chi(\theta^o-\theta^*)$	Statistical Weight
4764.294	-5.30	-7.53	-5.26	-7.48	0.05	0.40	1
4836.857	-5.56	-7.80	-5.48	-7.72	0.08	0.39	2
4922.267	-4.50	-5.55	-4.70	-6.36	0.19	0.50	1
4936.344	-5.08	-7.21	-5.06	-7.18	0.03	0.34	2
4954.811	-4.92	-6.94	-4.96	-7.01	-0.07	0.24	2
4964.928	-5.22	-7.42	-5.15	-7.32	0.10	0.19	1
5110.751	-5.66	-7.90	-5.28	-7.51	0.39	0.66	1
5206.039	-4.50	-5.55	-4.39	-5.22	0.33	0.42	2
5238.971	-5.43	-7.66	-5.52	-7.75	-0.09	0.18	1
5243.395	-5.28	-7.51	-5.44	-7.67	-0.16	0.18	1
5247.564	-4.98	-7.04	-4.84	-6.77	0.27	0.37	3
5296.686	-4.84	-6.77	-4.75	-6.56	0.21	0.31	2
5297.360	-4.81	-6.68	-4.78	-6.60	0.08	0.37	2
5298.269	-4.56	-5.80	-4.68	-6.27	-0.47	-0.37	1
5329.12	-4.97	-7.02	-4.84	-6.76	0.26	0.55	3
5345.807	-4.80	-6.66	-4.70	-6.34	0.32	0.42	2
5348.319	-4.99	-7.06	-4.76	-6.54	0.52	0.62	3
5390.394	-5.31	-7.54	-5.65	-7.89	-0.35	-0.02	1
5409.791	-4.66	-6.20	-5.54	-5.78	0.42	0.52	2
5712.778	-5.79	-8.03	-5.52	-7.76	0.27	0.57	1

Weighted Average $[\eta] = 0.23$

Weighted Average $[\eta] + \chi(\theta^o-\theta^*) = 0.43$

Partition Function μ^o ($T = 5140^oK$) = 11.1 μ^* ($T = 5730^oK$) = 12.2

$[\mu] = \log 11.1/12\ 2 = -0.041$

Total Velocity $[v] = -0.16$

Continuous Absorption Coefficient $[k_\lambda] = 0.06$

Relative Abundance $\log \frac{N^o}{N^*} = 0.43 - 0.04 - 0.16 + 0.06 = 0.29$

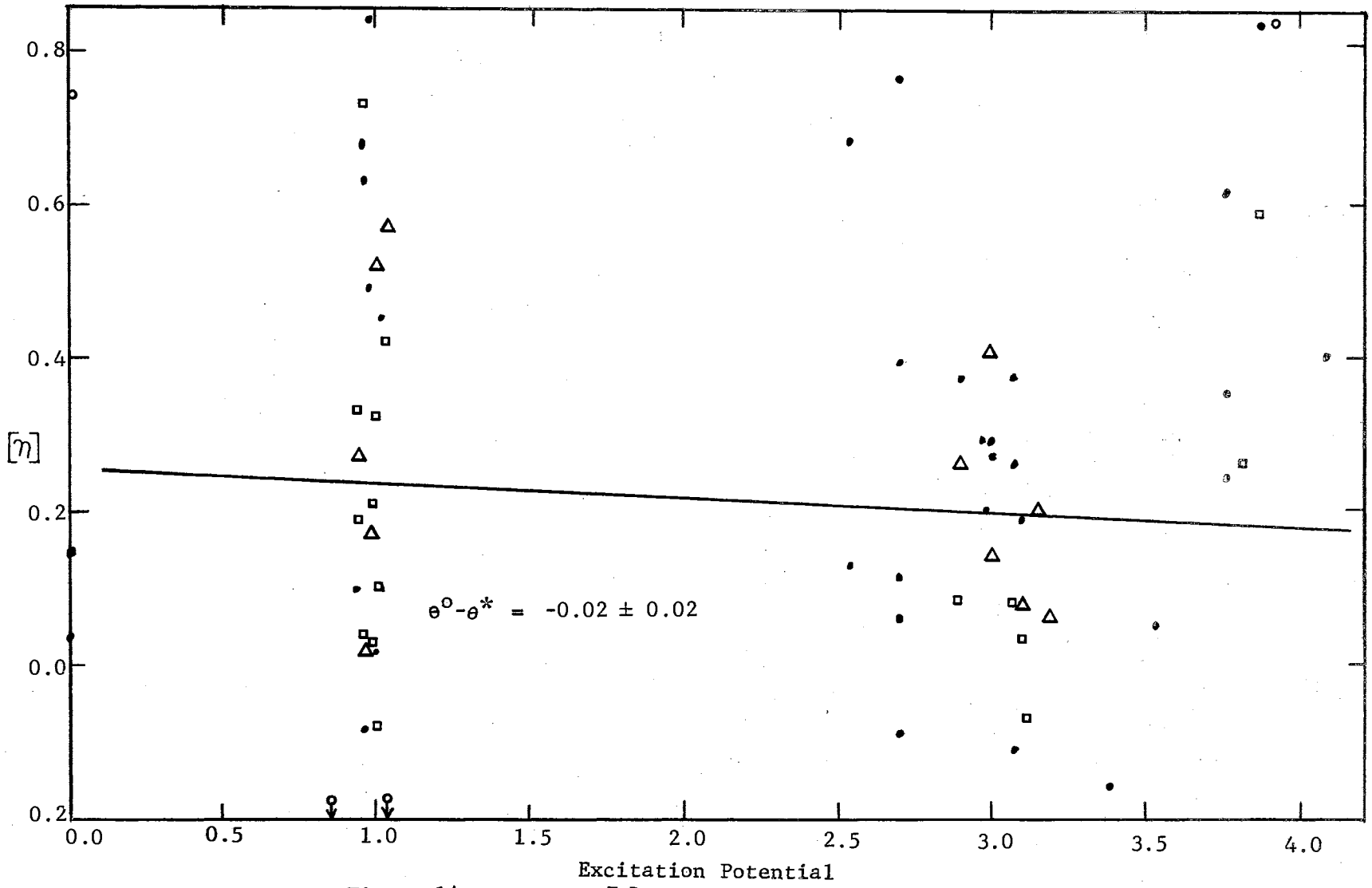

Figure 14. Plot of $[\eta]$ vs. Excitation Potential for Cr I.

TABLE XXV

DIFFERENTIAL CURVE OF GROWTH DATA DERIVED FROM Cr II LINES

λ RMT	$\log \frac{W^*}{\lambda}$	$\log \eta^*$	$\log \frac{W^o}{\lambda}$	$\log \eta^o$	$\log \eta^o/\eta^*$	$\log \eta^o/\eta^* + \chi(\theta^o-\theta^*)$	Statistical Weight
4242.38	-4.55	-5.80	-4.42	-5.30	0.30	0.68	0
4252.62	-5.00	-7.08	-5.15	-7.32	-0.24	0.14	3
4261.92	-4.76	-6.53	-4.60	-5.95	0.58	0.96	0
4275.57	-4.64	-5.98	-4.83	-6.75	-0.77	-0.39	1
4555.02	-4 67	-6.23	-5.07	-7.19	-0.86	-0.46	2
4558.659	-4.50	-5.55	-4.84	-6.76	-1.21	-0.80	1
4588.217	-4.61	-5.99	-4.84	-6.77	-0.78	-0.38	1
4592.09	-4.88	-6.86	-5.02	-7.11	-0.25	-0.16	1
4616.64	-4 98	-7.04	-5.10	-7 23	-0.19	0.21	2
4634.11	-4.75	-6.50	-4.94	-6.98	-0.48	-0.07	1
4812.35	-4.96	-7.01	-5.07	-7.20	-0.19	0.19	3
4848.24	-4.67	-6.24	-4.97	-7.03	-0.79	-0.41	2
4876.41	-4.60	-5.97	-5.08	-7.20	-1.23	-0.85	1
5237.35	-5.01	-7.09	-5.03	-7.12	-0.03	0.38	2
5305.85	-5.08	-7.21	-5.32	-7.55	-0.24	0.14	2
5334.88	-5.18	-7.36	-5.22	-7.42	-0.06	0.34	2
5502.05	-5.12	-7.27	-5.38	-7.61	-0.34	0.07	2

Weighted Average $[\eta] = -0.42$

Weighted Average $[\eta] + \chi(\theta^o-\theta^*) = -0.04$

Partition Function μ^o (T = 5140°K) = 7.3 μ^* (T = 5730°K) = 8.2

$[\mu] = \log 7.3/8.2 = -0.06$

Total Velocity $[v] = -0.16$

Continuous Absorption Coefficient $[k_\lambda] = 0.06$

Relative Abundance

$$\log \frac{N^o}{N^*} = -0.04 - 0.06 - 0.16 + 0.06 = -0.20$$

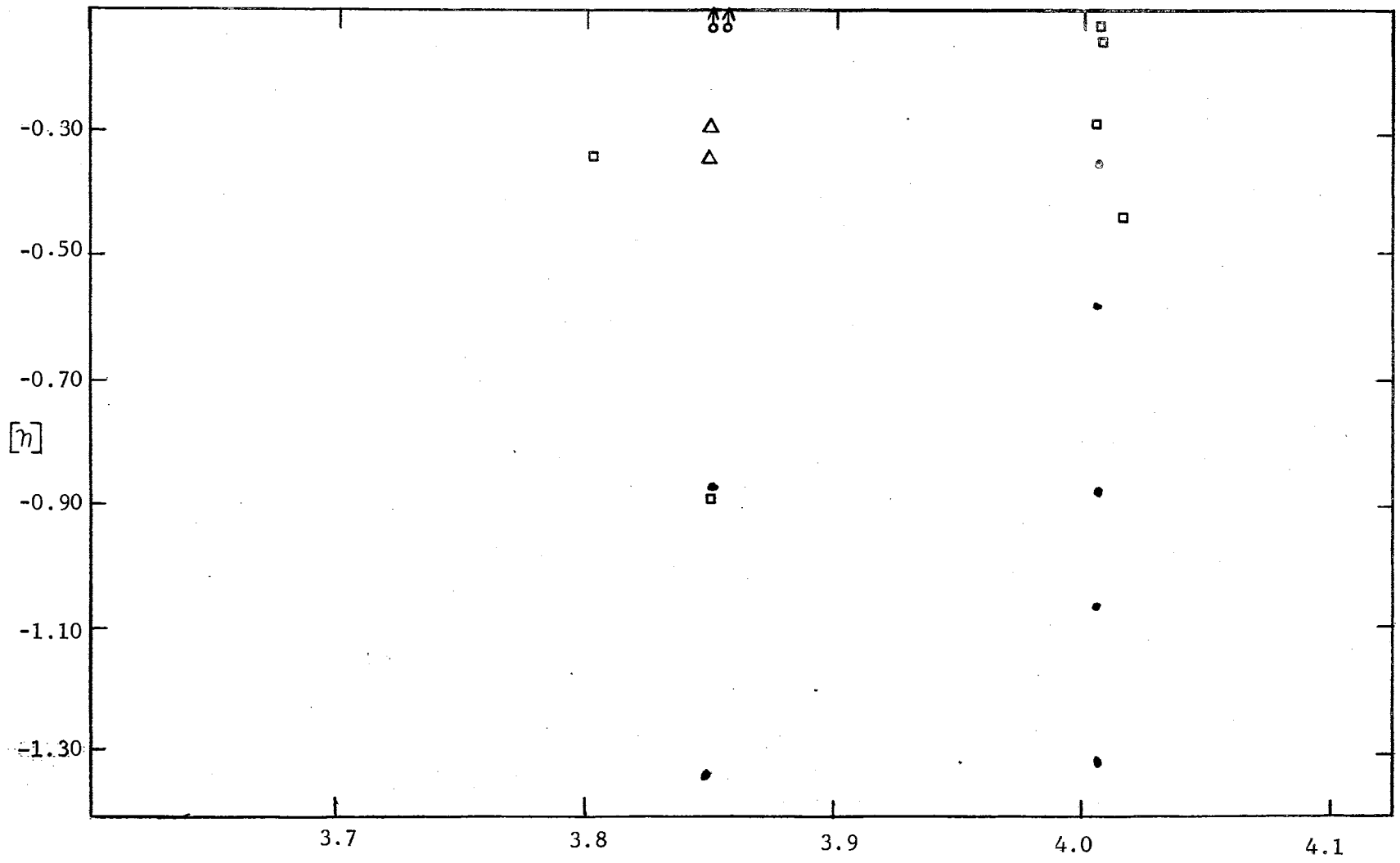

Figure 15. Plot of [η] vs. Excitation Potential for Cr II.

TABLE XXVI

DIFFERENTIAL CURVE OF GROWTH DATA DERIVED FROM Mn I LINES

λ RMT	log $\frac{W^*}{\lambda}$	log η^*	log $\frac{W^o}{\lambda}$	log η^o	log η^o/η^*	log $\eta^o/\eta^* + \chi(\theta^o-\theta^*)$	Statistical Weight
4018.102	-4.45	-5.37	-4.46	-5.40	-0.03	0.18	1
4030.755	-4.15	-4.66	-4.09	-4.56	0.10	0.10	1
4033.073	-4.25	-4.88	-4.18	-4.71	0.17	0.17	2
4034.490	-4.35	-5.12	-4.28	-4.95	0.17	0.17	3
4055.543	-4.56	-5.80	-4.55	-5.77	0.03	0.24	2
4059.392	-5.12	-7.27	-4.84	-6.77	0.50	0.81	2
4070.279	-5.09	-7.22	-4.79	-6.64	0.58	0.80	3
4070.422	-4.67	-6.24	-4.60	-5.93	0.31	0.53	1
4082.944	-4.87	-6.84	-4.64	-6.11	0.73	0.95	3
4257.659	-5.46	-7.69	-4.88	-6.87	0.82	1.11	2
4265.924	-5.27	-7.50	-4.84	-6.77	0.73	1.02	1
4453.005	-5.39	-7.62	-4.99	-7.06	0.56	0.85	1
4457.045	-5.59	-7.83	-5.07	-7.20	0.63	0.94	1
4470.138	-5.29	-7.52	-4.96	-7.01	0.51	0.80	2
4502.220	-5.21	-7.40	-4.96	-7.01	0.39	0.68	2
4709.715	-5.19	-7.38	-4.88	-6.86	0.52	0.81	3
4739.108	-5.28	-7.51	-4.92	-6.96	0.55	0.84	2
4754.042	-4.57	-5.84	-4.56	-5.80	0.04	0.27	2
4765.859	-4.85	-6.79	-4.82	-6.73	0.06	0.35	2
4766.430	-4.75	-6.50	-4.73	-6.44	0.06	0.35	2
4783.420	-4.48	-5.45	-4.48	-5.47	-0.02	0.21	3
4823.516	-4.43	-5.32	-4.46	-5.41	-0.09	0.14	3

Weighted Average $[\eta] = 0.67$

Weighted Average $[\eta] + \chi(\theta^o-\theta^*) = 0.55$

Partition Function μ^o (T = 5140°K) = 6.70 μ^* (T = 5730°K) = 7.15

$[\mu] = \log 6.70/7.15 = -0.03$

Total Velocity $[v] = -0.17$

Continuous Absorption Coefficient $[k_\lambda] = 0.06$

Relative Abundance

$$\log \frac{N^o}{N^*} = 0.55 - 0.03 - 0.17 + 0.06 = 0.41$$

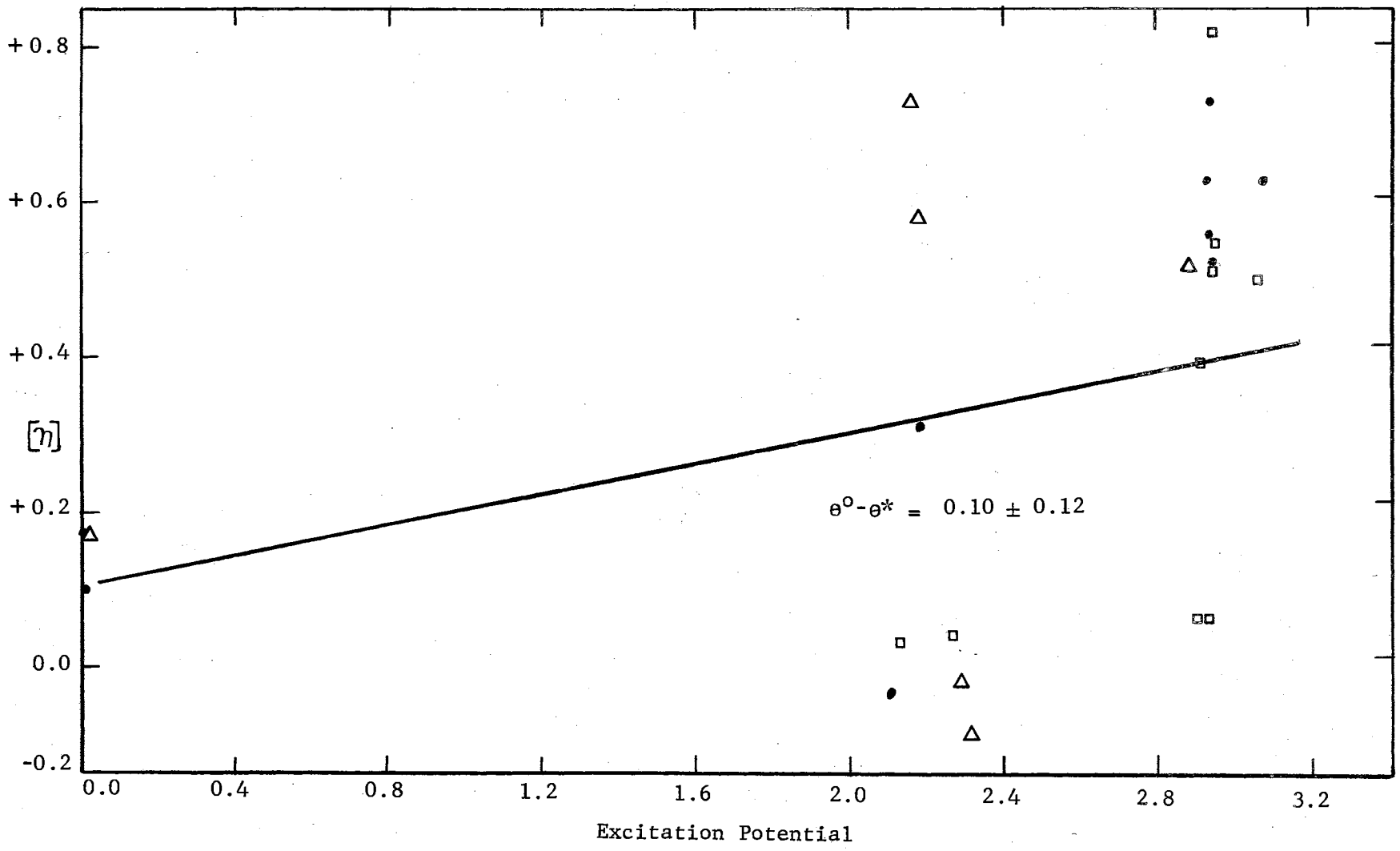

Figure 16. Plot of $[\eta]$ vs. Excitation Potential for Mn I.

TABLE XXVII

DIFFERENTIAL CURVE OF GROWTH DATA DERIVED FROM Mn II LINES

λ RMT	$\log \frac{W^*}{\lambda}$	$\log \eta^*$	$\log \frac{W^o}{\lambda}$	$\log \eta^o$	$\log \eta^o/\eta^*$	$\log \eta^o/\eta^* + \chi(\theta^o-\theta^*)$	Statistical Weight
4530.034	-5.36	-7.59	-6.96	—	—	—	0
4652.816	-5.97	-8.21	-6.49	—	—	—	0
4755.728	-5.38	-7.59	-5.26	-7.48	0.13	0.67	1
5299.278	-5.16	-7.33	—	—	—	—	0

Weighted Average $[\eta] = 0.13$

Weighted Average $[\eta] + \chi(\theta^o-\theta^*) = 0.67$

Partition Function μ^o (T = 5140°K) = 8.00 μ^* (T = 5730°K) = 8.35

$[\mu] = \log 8.00/8.35 = -0.02$

Total Velocity $[v] = 0.17$

Continuous Absorption Coefficient $[k_\lambda] = 0.06$

Relative Abundance

$$\log \frac{N^o}{N^*} = 0.67 - 0.02 - 0.17 + 0.06 = 0.54$$

TABLE XXVIII

DIFFERENTIAL CURVE OF GROWTH DATA DERIVED FROM Fe I LINES

λ RMT	log $\frac{W^*}{\lambda}$	log η^*	log $\frac{W^o}{\lambda}$	log η^o	log η^o/η^*	log η^o/η^* $+\chi(\theta^o-\theta^*)$	Statistical Weight
4005.246	-4.15	-4.46	-3.98	-4.36	0.30	0.45	0
4009.714	-4.59	-5.91	-4.52	-5.62	0.29	0.51	1
4045.815	-3.86	-4.14	-3.60	-3.50	0.64	0.79	0
4062.446	-4.62	-6.03	-4.62	-6.03	0.00	0.28	1
4063.597	-4.01	-4.45	-3.72	-3.98	0.56	0.71	0
4071.740	-4.09	-4.56	-3.76	-3.96	0.60	0.76	0
4107.492	-4.68	-6.72	-4.52	-5.62	0.35	0.63	1
4134.681	-4.53	-5.68	-4.51	-5.58	0.10	0.38	1
4143.871	-4.19	-4.75	-3.94	-4.29	0.46	0.61	0
4147.673	-4.60	-5.95	-4.58	-5.86	-0.09	0.06	1
4154.502	-4.53	-5.68	-4.52	-5.63	0.05	0.33	1
4175.640	-4.61	-5.99	-4.58	-5.87	0.12	0.40	1
4181.758	-4.43	-5.32	-4.45	-5.38	-0.06	0.22	2
4187.044	-4.51	-5.39	-4.31	-5.04	0.55	0.79	1
4187.802	-4.37	-5.18	-5.27	-4.93	0.25	0.49	1
4191.436	-4.45	-5.38	-4.36	-5.15	0.23	0.48	1
4199.098	-4.50	-5.55	-4.36	-5.15	0.40	0.70	1
4202.031	-4.27	-4.93	-4.11	-4.59	0.34	0.49	1
4206.702	-4.56	-5.80	-4.54	-5.72	0.08	0.08	1
4216.186	-4.49	-5.50	-4.51	-5.61	-0.11	-0.08	1
4219.364	-4.48	-5.45	-4.46	-5.40	0.05	0.41	2
4222.219	-4.55	-5.76	-4.37	-5.18	0.58	0.82	1
4227.434	-4.26	-4.91	-4.36	-5.15	-0.24	0.09	1
4233.608	-4.43	-5.45	-4.15	-4.67	-0.22	0.03	2
4235.942	-4.31	-5.03	-4.04	-4.45	0.58	0.82	2
4238.816	-4.48	-5.45	-4.44	-5.34	0.11	0.44	2
4247.432	-4.44	-5.35	-4.42	-5.30	0.05	0.38	2
4248.228	-4.66	-6.20	-4.64	-6.11	0.09	0.40	1
4250.125	-4.43	-5.32	-4.09	-4.56	0.76	1.01	0
4250.790	-4.38	-5.20	-4.02	-4.43	0.77	0.92	0
4260.479	-4.28	-4.95	-4.86	-4.13	0.82	1.06	0
4271.159	-4.37	-5.18	-4.24	-4.88	0.30	0.54	2
4271.764	-4.19	-4.75	-3.76	-3.96	0.79	0.94	0
4282.406	-4.47	-5.42	-4.47	-5.42	0.00	0.22	2
4291.466	-4.68	-6.27	-4.71	-6.36	-0.09	-0.09	1
4325.765	-4.07	-4.52	-3.73	-3.94	0.58	0.74	0
4337.049	-4.44	-5.35	-4.56	-5.79	-0.44	0.29	1
4352.737	-4.44	-5.35	-4.49	-5.49	-0.14	0.08	1
4369.774	-4.52	-5.63	-4.43	-5.33	0.30	0.60	2
4375.932	-4.50	-5.55	-4.46	-5.40	0.15	-0.15	1
4383.547	-4.04	-4.45	-3.64	-3.76	0.69	0.84	0
4389.244	-5.00	-7.08	-4.82	-6.71	0.37	0.37	2
4404.752	-4.15	-4.66	-3.69	-3.85	0.81	0.96	0
4415.125	-4.20	-4.77	-4.02	-4.43	0.34	0.50	0

TABLE XXVIII (Continued)

λ RMT	$\log \frac{W^*}{\lambda}$	$\log \eta^*$	$\log \frac{W^o}{\lambda}$	$\log \eta^o$	$\log \eta^o/\eta^*$	$\log \eta^o/\eta^* + \chi(\theta^o-\theta^*)$	Statistical Weight
4427.312	-4.45	-5.38	-4.52	-5.63	-0.25	-0.25	1
4430.618	-4.57	-5.84	-4.58	-5.89	-0.05	0.17	1
4442.343	-4.51	-5.58	-4.42	-5.29	0.29	0.51	1
4443.197	-4.57	-5.84	-4.67	-6.24	-0.40	-0.12	1
4447.722	-4.52	-5.63	-4.40	-5.25	0.38	0.60	1
4454.383	-4.61	-5.99	-4.72	-6.41	-0.42	-0.14	1
4461.654	-4.36	-5.15	-4.58	-5.89	-0.74	-0.73	0
4466.554	-4.47	-5.42	-4.56	-5.76	-0.34	-0.36	1
4489.741	-4.60	-5.95	-4.74	-6.48	-0.53	-0.52	1
4494.568	-4.45	-5.38	-4.51	-5.58	-0.20	0.02	1
4531.152	-4.23	-4.84	-4.63	-6.08	-1.24	-1.09	0
4602.944	-4.59	-5.91	-4.68	-6.26	-0.35	-0.20	1
4736.780	-4.54	-5.72	-4.52	-5.62	0.10	0.42	1
4859.748	-4.53	-5.68	-4.65	-6.18	-0.50	-0.21	1
4871.323	-4.40	-5.25	-4.33	-5.07	0.18	0.46	1
4872.144	-4.41	-5.28	-4.40	-5.25	0.03	0.32	1
4890.762	-4.40	-5.25	-4.34	-5.12	0.13	0.42	2
4891.496	-4.32	-5.05	-4.20	-4.75	0.30	0.58	2
4918.999	-4.38	-5.20	-4.25	-4.88	0.32	0.60	1
4920.509	-4.26	-4.91	-4.02	-4.43	0.48	0.76	0
5001.871	-4.47	-5.42	-4.47	-5.44	-0.02	0.37	1
5005.720	-4.54	-5.72	-4.56	-5.81	-0.09	0.30	1
5006.126	-4.54	-5.72	-4.42	-5.30	0.42	0.70	1
5049.825	-4.64	-6.11	-4.60	-5.93	0.18	0.07	1
5051.636	-4.51	-5.59	-4.66	-6.18	-0.59	-0.50	1
5068.774	-4.64	-6.11	-4.60	-5.93	0.18	0.47	1
5083.342	-4.63	-6.07	-4.73	-6.43	-0.36	-0.26	1
5110.414	-4.50	-5.55	-4.61	-6.00	-0.45	-0.45	1
5133.692	-4.56	-5.80	-4.49	-5.51	0.05	0.47	1
5191.460	-4.53	-5.68	-4.51	-5.60	0.08	0.38	1
5192.350	-4.55	-5.76	-4.47	-5.42	0.34	0.64	1
5194.943	-4.69	-6.30	-4.62	-6.02	0.28	0.43	1
5216.278	-4.63	-6.07	-4.68	-6.28	-0.21	-0.05	1
5225.533	-4.95	-7.00	-4.88	-6.87	0.13	0.14	1
5232.946	-4.43	-5.32	-4.18	-4.73	0.59	0.88	1
5250.650	-4.81	-6.69	-4.70	-6.35	0.34	0.56	1
5266.562	-4.57	-5.84	-4.32	-5.05	0.79	1.09	0
5269.541	-4.42	-5.30	-4.04	-4.44	0.86	0.95	0
5281.796	-4.70	-6.34	-4.51	-5.58	0.76	1.06	1
5283.628	-4.52	-5.63	-4.40	-5.24	0.39	0.71	1
5307.365	-4.85	-6.80	-4.79	-6.63	0.17	0.33	1
5324.185	-4.50	-5.55	-4.20	-4.77	0.78	1.10	0
5328.042	-4.30	-5.00	-4.15	-4.67	0.33	0.42	2
5339.935	-4.72	-6.41	-4.52	-5.63	0.78	1.10	1
5364.874	-4.77	-6.56	-4.61	-5.99	0.57	1.01	1
5367.470	-4.75	-6.50	-4.54	-5.66	-0.16	0.28	1

TABLE XXVIII (Continued)

λ RMT	log $\frac{W^*}{\lambda}$	log η^*	log $\frac{W^o}{\lambda}$	log η^o	log η^o/η^*	log η^o/η^* $+\chi(\theta^o-\theta^*)$	Statistical Weight
5369.965	−4.66	−6.20	−4.47	−5.42	0.78	1.21	1
5383.374	−4.60	−5.95	−4.42	−5.30	0.65	1.18	1
5393.174	−4.69	−6.30	−4.54	−5.74	0.56	0.88	1
5397.131	−4.50	−5.55	−4.35	−5.14	0.41	0.50	1
5404.144	−4.47	−5.42	−4.35	−5.14	0.28	0.72	2
5405.778	−4.51	−5.59	−4.31	−5.02	0.57	0.67	1
5410.913	−4.70	−6.34	−4.51	−5.59	0.75	1.19	1
5424.072	−4.54	−5.72	−4.36	−5.14	0.58	1.01	1
5429.699	−4.38	−5.20	−4.28	−4.95	0.25	0.35	2
5434.527	−4.53	−5.68	−4.47	−5.42	0.26	0.36	1
5445.045	−4.72	−6.41	−4.65	−6.15	0.26	0.70	1
5446.920	−4.39	−5.22	−4.36	−5.15	0.07	0.17	2
5497.519	−4.50	−5.55	−4.63	−6.08	-0.53	-0.43	0
5501.469	−4.58	−5.87	−4.68	−6.27	-0.40	-0.30	1
5506.782	−4.55	−5.76	−4.68	−6.27	-0.51	-0.41	1
5569.625	−4.65	−6.16	−4.53	−5.71	0.45	0.79	1
5572.849	−4.58	−5.87	−4.44	−5.34	0.53	0.87	1
5576.097	−4.81	−6.69	−4.69	−6.32	0.37	0.71	1
5586.763	−4.46	−5.40	−4.36	−5.14	0.26	0.59	1
5615.652	−4.42	−5.30	−4.29	−4.98	0.32	0.65	1
5762.992	−4.71	−6.38	−4.76	−6.52	-0.14	0.28	1
6024.066	−4.90	−6.90	−4.71	−6.38	0.52	0.97	1
6065.487	−4.79	−6.63	−4.72	−6.41	0.22	0.48	1
6137.696	−4.73	−6.44	−4.68	−6.26	0.18	0.44	1
6230.728	−4.67	−6.24	−4.59	−5.93	0.31	0.56	1
6246.334	−4.91	−6.92	−4.75	−6.50	0.42	0.78	1
6252.561	−4.76	−6.53	−4.76	−6.53	0.00	0.24	1
6265.140	−4.99	−7.06	−4.94	−6.98	0.08	0.30	1
6301.515	−4.79	−6.63	−4.74	−6.46	0.17	0.53	1
6318.022	−4.90	−6.90	−4.78	−6.61	0.29	0.53	1
6393.605	−4.74	−6.47	−4.64	−6.12	0.35	0.59	1
6411.658	−4.71	−6.38	−4.67	−6.23	0.15	0.51	1
6421.355	−4.84	−6.77	−4.75	−6.51	0.26	0.49	1
6430.851	−4.84	−6.77	−4.76	−6.53	0.24	0.46	1
6494.985	−4.70	−6.34	−4.57	−5.82	0.52	0.76	1

Weighted Average	$[\eta] = 0.16$
Weighted Average	$[\eta] + \chi(\theta^o-\theta^*) = 0.41$
Partition Function	μ^o (T = 5140°K) = 28.7 μ^* (T = 5730°K) = 31.2
	$[\mu]$ = log 28.7/31.2 = -0.036
Total Velocity	$[v] = -0.17$
Continuous Absorption Coefficient	$[k_\lambda] = 0.06$

TABLE XXVIII (Continued)

Relative Abundance	$\log \frac{N^o}{N^*} = 0.41 - 0.036 - 0.17 + 0.06 = 0.26$

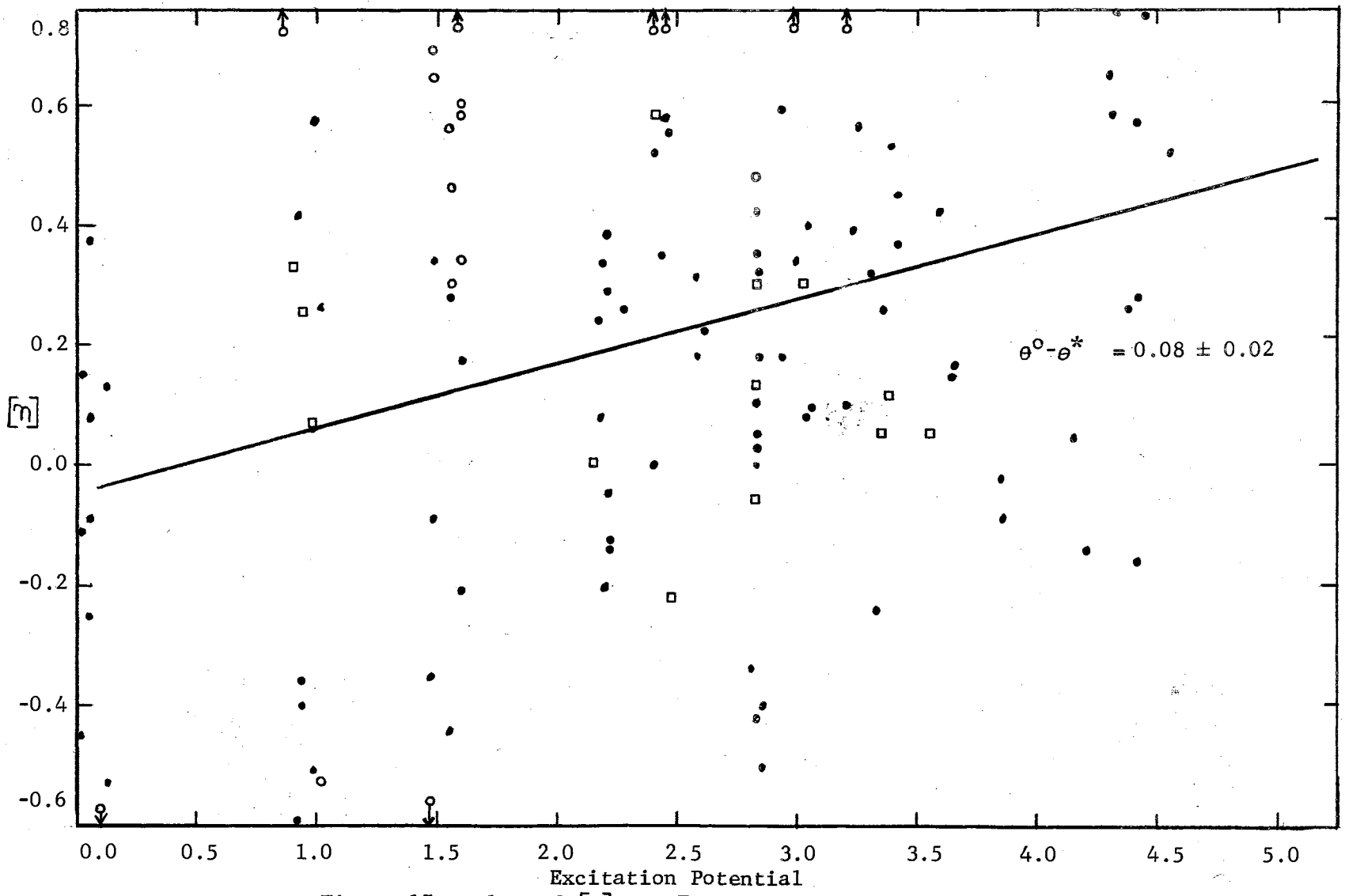

Figure 17. Plot of $[\eta]$ vs. Excitation Potential for Fe I.

TABLE XXIX

DIFFERENTIAL CURVE OF GROWTH DATA DERIVED FROM Fe II LINES

λ RMT	$\log \frac{W^*}{\lambda}$	$\log \eta^*$	$\log \frac{W^o}{\lambda}$	$\log \eta^o$	$\log \eta^o/\eta^*$	$\log \eta^o/\eta^* + \chi(\theta^o-\theta^*)$	Statistical Weight
4122.638	-4.48	-5.49	-4.82	-6.70	-1.21	-0.95	0
4128.735	-4.92	-6.93	-4.92	-6.93	0.00	0.26	1
4178.855	-4.76	-6.23	-4.72	-6.41	-0.18	0.08	1
4273.317	-4.65	-6.16	-4.68	-6.26	-0.10	0.17	2
4303.166	-4.64	-6.10	-4.62	-6.03	0.07	0.34	1
4369.404	-4.95	-7.00	-5.02	-7.11	-0.11	0.17	2
4384.33	-4.45	-5.36	-4.15	-4.68	0.68	0.94	0
4416.817	-4.61	-5.97	-4.76	-6.53	-0.56	-0.28	1
4491.401	-4.55	-5.76	-4.83	-6.74	-0.98	-0.70	1
4508.283	-4.52	-5.60	-4.78	-6.61	-1.01	-0.73	1
4576.331	-4.61	-5.99	-4.92	-6.93	-0.94	-0.66	2
4583.829	-4.59	-5.91	-4.59	-5.89	0.02	0.30	1
4620.513	-4.86	-6.82	-4.99	-7.06	-0.24	0.04	1
4666.750	-4.64	-6.11	-5.02	-7.11	-1.00	1.28	0
4731.439	-4.55	-5.77	-4.78	-6.60	-0.83	-0.54	1
4923.921	-4.30	-5.00	-4.47	-5.42	-0.42	-0.13	1
5018.437	-4.24	-4.85	-4.38	-5.20	-0.35	-0.06	1
5132.67	-5.22	-7.42	-5.33	-7.56	-0.14	0.14	1
5169.030	-4.20	-4.77	-4.52	-5.66	-0.89	-0.60	1
5197.569	-4.62	-6.03	-4.81	-6.69	-0.66	-0.34	2
5234.620	-4.64	-6.11	-4.81	-6.68	-0.57	-0.25	1
5264.801	-4.94	-6.98	-5.07	-7.20	-0.22	0.10	2
5284.092	-4.88	-6.86	-4.90	-6.89	-0.03	0.26	2
5325.559	-4.95	-6.99	-5.08	-7.20	-0.21	0.11	2
5362.864	-4.73	-6.43	-4.69	-6.30	0.13	0.45	1
5414.089	-5.29	-7.52	-5.24	-7.45	0.07	0.39	1
5425.269	-4.98	-7.04	-5.06	-7.16	-0.12	0.20	1
6247.562	-4.94	-6.98	-5.10	-7.25	-0.27	0.12	2
6416.905	-5.04	-7.13	-5.20	-7.40	-0.27	0.12	1
6432.654	-5.00	-7.09	-5.23	-7.43	-0.24	0.05	1
6456.376	-4.65	-6.16	-4.97	-7.02	-0.86	-0.47	0

Weighted Average	$[\eta] = -0.34$
Weighted Average	$[\eta] + \chi(\theta^o-\theta^*) = -0.03$
Partition Function	μ^o (T = 5140°K) = 44.4 μ^* (T = 5730°K) = 47.1
	$[\mu] = \log 44.4/47.1 = -0.025$
Total Velocity	$[v] = -0.17$
Continuous Absorption Coefficient	$[k_\lambda] = 0.06$
Relative Abundance	$\log \frac{N^o}{N^*} = -0.03 - 0.025 - 0.17 + 0.06 = -0.165$

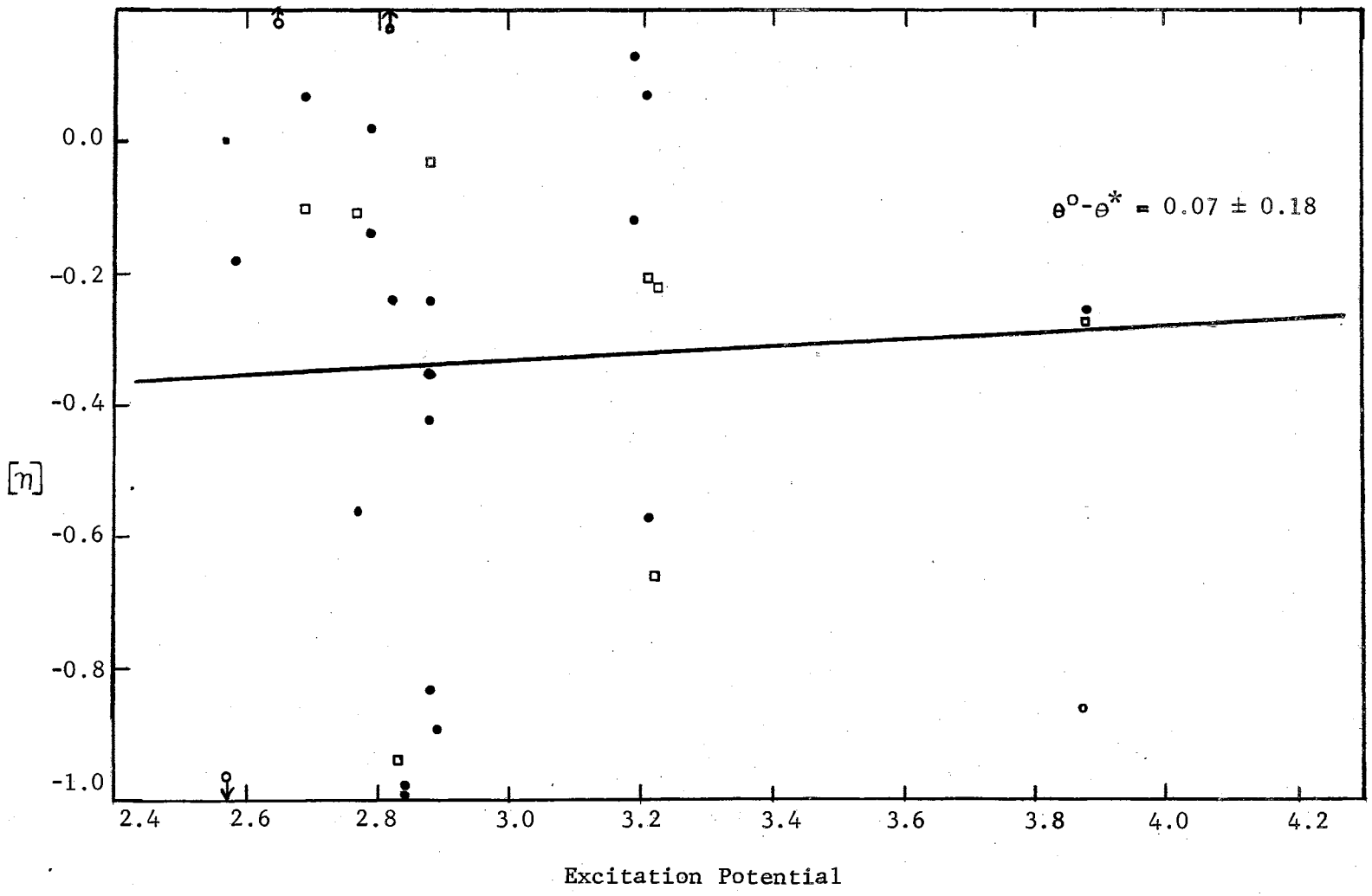

Figure 18. Plot of $[\eta]$ vs. Excitation Potential for Fe II.

TABLE XXX

DIFFERENTIAL CURVE OF GROWTH DATA DERIVED FROM Co I LINES

λ RMT	$\log \frac{W^*}{\lambda}$	$\log \eta^*$	$\log \frac{W^o}{\lambda}$	$\log \eta^o$	$\log \eta^o/\eta^*$	$\log \eta^o/\eta^* + \chi(\theta^o-\theta^*)$	Statistical Weight
4020.898	-5.14	-7.30	-4.70	-6.34	-0.96	1.00	3
4092.386	-4.56	-5.80	-4.58	-5.87	-0.07	0.02	1
4110.532	-5.04	-7.14	-4.63	-6.07	1.07	1.17	2
4121.318	-4.66	-6.20	-4.52	-5.63	0.57	0.66	1
4517.094	-5.29	-7.52	-5.20	-7.40	0.12	0.43	1
4693.190	-5.48	-7.72	-5.44	-7.56	0.37	0.69	1
4727.936	-5.54	-7.78	-5.74	-7.98	-0.20	-0.18	1
5156.366	-5.01	-7.10	-5.71	-7.95	-0.85	-0.45	1
5212.699	-5.54	-7.78	-5.40	-7.63	0.15	0.50	1
5342.703	-5.77	-8.01	-5.26	-7.47	0.54	0.94	1
5343.383	-5.34	-7.57	-4.92	-6.93	0.64	1.04	1
5369.591	-5.51	-7.75	-5.12	-7.28	0.47	0.64	1

Weighted Average $[\eta] + \chi(\theta^o-\theta^*) = 0.64$

Partition Function μ^o (T = 5140°K) = 32.22 μ^* (T = 5730°K) = 35.15

$[\mu] = \log 32.22/35.15 = -0.04$

Total Velocity $[v] = -0.15$

Continuous Absorption Coefficient $[k_\lambda] = 0.06$

Relative Abundance $\log \frac{N^o}{N^*} = 0.64 - 0.04 - 0.15 + 0.06 = 0.51$

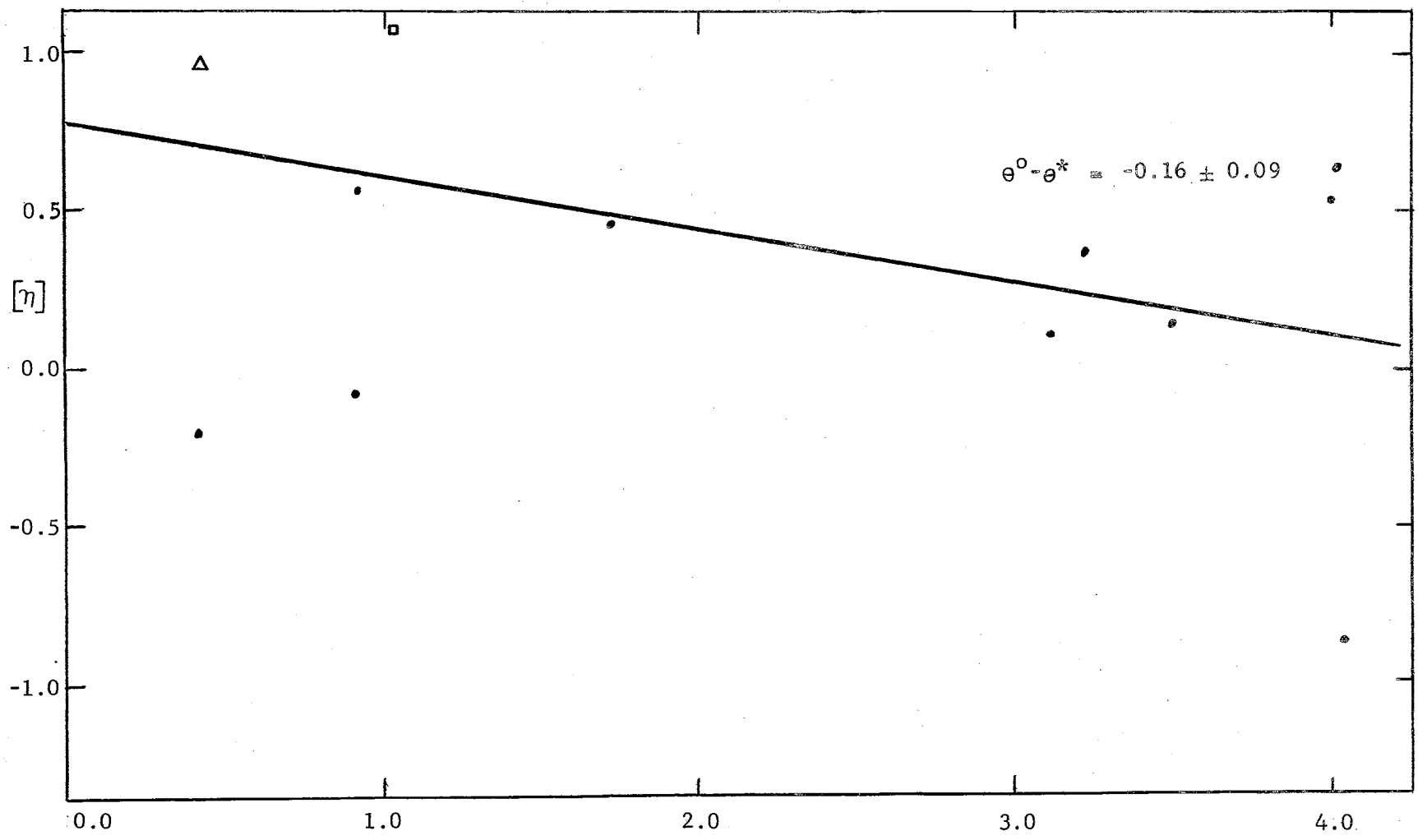

Figure 19. Plot of [η] vs. Excitation Potential for Co I.

TABLE XXXI

DIFFERENTIAL CURVE OF GROWTH DATA DERIVED FROM Ni I LINES

λ RMT	$\log \frac{W^*}{\lambda}$	$\log \eta^*$	$\log \frac{W^o}{\lambda}$	$\log \eta^o$	$\log \eta^o/\eta^*$	$\log \eta^o/\eta^* + \chi(\theta^o-\theta^*)$	Statistical Weight
4462.460	-4.89	-6.88	-4.86	-6.81	0.07	+0.41	3
4470.483	-4.82	-6.72	-4.81	-6.70	0.02	+0.36	2
4604.994	-4.81	-6.69	-4.87	-6.84	-0.15	+0.20	1
4606.231	-5.31	-7.54	-5.07	-7.20	0.34	+0.70	1
4648.659	-4.79	-6.63	-4.84	-6.77	-0.14	+0.20	2
4686.218	-5.13	-7.28	-4.96	-7.00	0.28	+0.64	2
4714.421	-4.54	-5.72	-4.55	-5.77	-0.05	+0.29	2
4715.778	-4.95	-7.00	-4.84	-6.77	0.23	+0.58	3
4756.519	-4.85	-6.79	-4.80	-6.66	0.13	+0.48	3
4806.996	-5.14	-7.30	-4.84	-6.76	0.54	+0.91	3
4829.028	-4.69	-6.30	-4.72	-6.42	-0.12	+0.23	2
4866.267	-4.87	-6.84	-4.86	-6.83	0.01	+0.36	1
4873.437	-4.97	-7.02	-4.95	-7.00	0.02	+0.39	1
4904.413	-4.93	-6.96	-4.73	-6.45	0.51	+0.86	1
4918.363	-4.98	-7.04	-4.82	-6.71	0.33	+0.71	2
4935.830	-5.27	-7.50	-4.88	-6.86	0.64	+1.03	1
4980.161	-4.71	-6.38	-4.64	-6.15	0.23	+0.59	1
4984.126	-4.74	-6.47	-4.74	-6.46	0.01	+0.39	1
5000.335	-4.81	-6.69	-4.85	-6.80	-0.11	+0.25	1
5012.464	-4.96	-7.01	-4.95	-6.99	0.02	+0.39	2
5017.591	-4.71	-6.38	-4.76	-6.51	-0.13	+0.22	1
5035.374	-4.77	-6.56	-4.66	-6.21	0.35	+0.71	1
5080.523	-4.70	-6.34	-4.74	-6.46	-0.12	+0.24	1
5081.111	-4.88	-6.86	-4.75	-6.49	0.37	+0.75	2
5084.081	-4.85	-6.80	-4.74	-6.46	0.34	+0.71	1
5099.946	-4.82	-6.72	-4.81	-6.69	0.03	+0.40	1
5115.397	-4.90	-6.90	-4.85	-6.79	0.11	+0.49	2
5146.478	-4.71	-6.38	-4.83	-6.74	-0.36	+0.01	2
5155.764	-4.90	-6.90	-4.82	-6.72	0.18	+0.57	3
5176.565	-5.19	-7.38	-4.96	-7.02	0.36	+0.75	3
5578.734	-5.32	-7.55	-5.08	-7.20	0.35	+0.52	1
5592.283	-5.41	-7.64	-5.00	-7.13	0.51	+0.70	1

Weighted Average $[\eta] + \chi(\theta^o-\theta^*) = 0.51$

Partition Function μ^o (T = 5140°K) = 3.12 μ^* (T = 5730°K) = 32.4

$[\mu] = \log 31.2/32.4 = -0.016$

Total Velocity $[v] = -0.17$

Continuous Absorption Coefficient $[k_\lambda] = 0.06$

Relative Abundance

$$\log \frac{N^o}{N^*} = 0.51 - 0.016 - 0.17 + 0.06 = 0.394$$

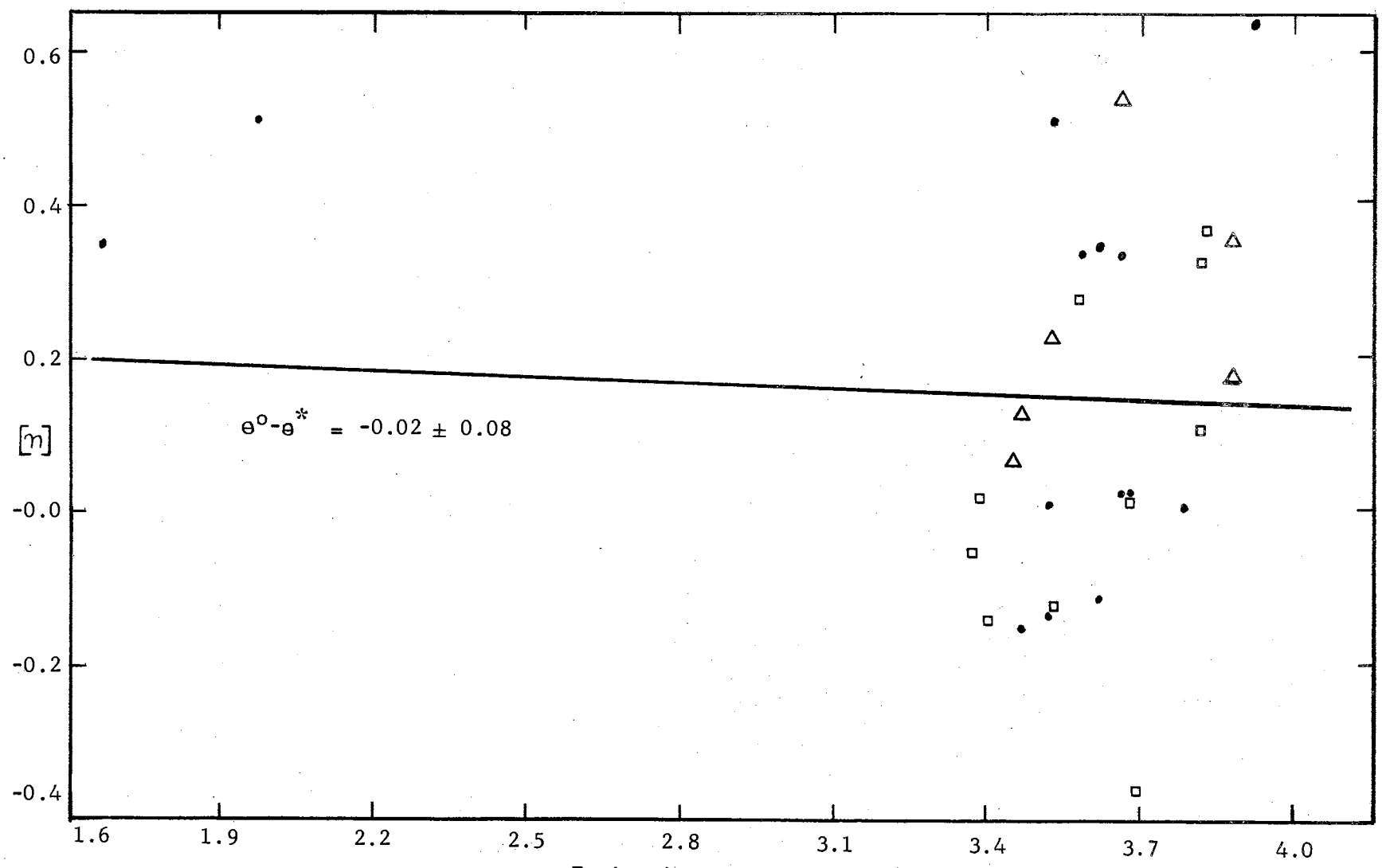

Figure 20. Plot of [η] vs. Excitation Potential for Ni I.

TABLE XXXII

DIFFERENTIAL CURVE OF GROWTH DATA DERIVED FROM Cu I LINES

λ RMT	$\log \frac{W^*}{\lambda}$	$\log \eta^*$	$\log \frac{W^o}{\lambda}$	$\log \eta^o$	$\log \eta^o/\eta^*$	$\log \eta^o/\eta^* + \chi(\theta^o-\theta^*)$	Statistical Weight
5218.202	-5.14	-7.30	-5.04	-7.14	0.16	0.54	1
Weighted Average		$[\eta] + \chi(\theta^o-\theta^*) = 0.54$					
Partition Function		μ^o (T = 5140°K) = 24.99 μ^* (T = 5730°K) = 25.21					
		$[\mu] = \log 24.99/25.21 = 0.00$					
Total Velocity		$[v] = -0.17$					
Continuous Absorption Coefficient		$[k_\lambda] = 0.06$					
Relative Abundance		$\log \frac{N^o}{N^*} = 0.54 - 0.00 \quad -0.17 + 0.06 = 0.43$					

TABLE XXXIII

DIFFERENTIAL CURVE OF GROWTH DATA DERIVED FROM Zn I LINES

λ RMT	$\log \frac{W^*}{\lambda}$	$\log \eta^*$	$\log \frac{W^o}{\lambda}$	$\log \eta^o$	$\log \eta^o/\eta^*$	$\log \eta^o/\eta^* + \chi(\theta^o-\theta^*)$	Statistical Weight
4722.159	-4.98	-7.04	-4.88	-6.86	0.18	0.58	1
4810.534	-4.78	-6.60	-4.76	-6.53	0.07	0.48	1
Weighted Average		$[\eta] + \chi(\theta^o-\theta^*) = 0.53$					
Partition Function		Not Available					
Total Velocity		$[v] = -0.17$					
Continuous Absorption Coefficient		$[k_\lambda] = 0.06$					
Relative Abundance		$\log \frac{N^o}{N^*} = 0.53 - 0.17 + 0.06 = 0.42$					

TABLE XXXIV

DIFFERENTIAL CURVE OF GROWTH DATA DERIVED FROM Sr I LINES

λ RMT	$\log \frac{W^*}{\lambda}$	$\log \eta^*$	$\log \frac{W^o}{\lambda}$	$\log \eta^o$	$\log \eta^o/\eta^*$	$\log \eta^o/\eta^* + \chi(\theta^o-\theta^*)$	Statistical Weight
4607.331	-5.26	-7.49	-5.11	-7.25	0.24	0.24	1
Weighted Average		$[\eta]$ = 0.24					
Weighted Average		$[\eta] + \chi(\theta^o-\theta^*)$ = 0.24					
Partition Function		μ^o (T = 5140°K) = 1.31		μ^* (T = 5730°K) = 1.41			
		$[\mu]$ = log 1.31/1.41 = -0.03					
Total Velocity		$[v]$ = -0.18					
Continuous Absorption Coefficient		$[k_\lambda]$ = 0.06					
Relative Abundance		$\log \frac{N^o}{N^*}$ = 0.24 - 0.03 - 0.18 + 0.06 = 0.09					

TABLE XXXV

DIFFERENTIAL CURVE OF GROWTH DATA DERIVED FROM Sr II LINES

λ RMT	$\log \frac{W^*}{\lambda}$	$\log \eta^*$	$\log \frac{W^o}{\lambda}$	$\log \eta^o$	$\log \eta^o/\eta^*$	$\log \eta^o/\eta^* + \chi(\theta^o-\theta^*)$	Statistical Weight
4077.714	-4.08	-4.54	-4.08	-4.54	0.0	0.0	1
4215.524	-4.24	-4.86	-4.26	-4.90	-0.04	-0.04	1
Weighted Average		$[\eta] = -0.02$					
Weighted Average		$[\eta] + \chi(\theta^o-\theta^*) = -0.02$					
Partition Function		μ^o (T = 5140°K) = 2.23 μ^* (T = 5730°K) = 2.30					
		$[\mu] = \log 2.23/2.30 = -0.01$					
Total Velocity		$[v] = -0.18$					
Continuous Absorption Coefficient		$[k_\lambda] = 0.06$					
Relative Abundance		$\log \frac{N^o}{N^*} = -0.02 - 0.01 - 0.18 + 0.06 = -0.16$					

TABLE XXXVI

DIFFERENTIAL CURVE OF GROWTH DATA DERIVED FROM Y I LINES

λ RMT	$\log \frac{W^*}{\lambda}$	$\log \eta^*$	$\log \frac{W^o}{\lambda}$	$\log \eta^o$	$\log \eta^o/\eta^*$	$\log \eta^o/\eta^* + \chi(\theta^o-\theta^*)$	Statistical Weight
4047.64	-5.65	-7.89	-5.33	-7.56	0.33	0.33	1
4477.45	-5.48	-7.71	-5.76	-7.99	-0.28	-0.15	1
Weighted Average		$[\eta] = 0.02$					
Weighted Average		$[\eta] + \chi(\theta^o-\theta^*) = 0.09$					
Partition Function		μ^o (T = 5140°K) = 13.27 μ^* (T = 5730°K) = 14.14					
		$[\mu] = \log 13.27/14.14 = -0.03$					
Total Velocity		$[v] = -0.185$					
Continuous Absorption Coefficient		$[k_\lambda] = 0.06$					
Relative Abundance		$\log \frac{N^o}{N^*} = 0.09 - 0.03 - 0.185 + 0.06 = -0.065$					

TABLE XXXVII

DIFFERENTIAL CURVE OF GROWTH DATA DERIVED FROM Y II LINES

λ RMT	$\log \frac{W^*}{\lambda}$	$\log \eta^*$	$\log \frac{W^o}{\lambda}$	$\log \eta^o$	$\log \eta^o/\eta^*$	$\log \eta^o/\eta^* + \chi(\theta^o-\theta^*)$	Statistical Weight
4358.73	-4.02	-7.12	-4.76	-6.54	0.58	0.68	0
4398.02	-4.81	-6.69	-4.98	-7.04	-0.35	-0.34	2
4883.69	-4.65	-6.15	-4.98	-7.04	-0.89	-0.78	2
5087.42	-4.86	-6.83	-5.11	-7.25	-0.42	-0.31	1
5200.42	-5.05	-7.20	-5.15	-7.31	-0.11	-0.01	2
5402.85	-5.41	-7.64	-5.65	-7.89	-0.25	-0.12	1

Weighted Average $[\eta] = -0.42$

Weighted Average $[\eta] + \chi(\theta^o-\theta^*) = -0.34$

Partition Function μ^o (T = 5140°K) = 16.70 μ^* (T = 5730°K) = 17.44

$[\mu] = \log 16.70/17.44 = -0.02$

Total Velocity $[v] = -0.185$

Continuous Absorption Coefficient $[k_\lambda] = 0.06$

Relative Abundance $\log \frac{N^o}{N^*} = -0.34 - 0.02 - 0.185 + 0.06 = -0.485$

TABLE XXXVIII

DIFFERENTIAL CURVE OF GROWTH DATA DERIVED FROM Zr II LINES

λ RMT	$\log \frac{W^*}{\lambda}$	$\log \eta^*$	$\log \frac{W^o}{\lambda}$	$\log \eta^o$	$\log \eta^o/\eta^*$	$\log \eta^o/\eta^* + \chi(\theta^o-\theta^*)$	Statistical Weight
4050.32	-5.06	-7.18	-5.30	-7.53	-0.35	-0.28	2
4096.63	5.23	7.44	4.96	7.01	0.43	-0.40	1
4156.24	4.49	5.50	5.60	5.97	-0.47	0.49	1
4208.99	4.97	7.03	4.96	7.01	0.02	0.09	2
4317.32	5.46	7.69	5.52	7.76	-0.07	0.00	2
4333.28	5.44	7.67	5.49	7.73	-0.06	-0.18	1

Weighted Average $[\eta] + \chi(\theta^o-\theta^*) = -0.01$

Partition Function μ^o (T = 5140°K) = 48.66 μ^* (T = 5730°K) = 51.34

$[\mu] = \log 48.66/51.34 = -0.02$

Total Velocity $[v] = -0.19$

Continuous Absorption Coefficient $[k_\lambda] = 0.06$

Relative Abundance

$$\log \frac{N^o}{N^*} = -0.01 - 0.02 - 0.19 + 0.06 = -0.16$$

TABLE XXXIX

DIFFERENTIAL CURVE OF GROWTH DATA DERIVED FROM Ba II LINES

λ RMT	$\log \frac{W^*}{\lambda}$	$\log \eta^*$	$\log \frac{W^o}{\lambda}$	$\log \eta^o$	$\log \eta^o/\eta^*$	$\log \eta^o/\eta^* + \chi(\theta^o-\theta^*)$	Statistical Weight
4554.033	-4.22	-4.81	-4.46	-5.39	-0.58	-0.58	1
6496.896	-4.58	-5.87	-4.80	-6.65	-0.78	-0.72	1
Weighted Average		$[\eta] + \chi(\theta^o-\theta^*) = -0.65$					
Partition Function		μ^o (T = 5140°K) = 4.31 μ^* (T = 5730°K) = 4.72					
		$[\mu] = \log 4.31/4.72 = -0.04$					
Total Velocity		$[v] = -0.20$					
Continuous Absorption Coefficient		$[k_\lambda] = 0.06$					
Relative Abundance		$\log \frac{N^o}{N^*} = -0.65 - 0.04 - 0.20 + 0.06 = -0.83$					

TABLE XL

DIFFERENTIAL CURVE OF GROWTH DATA DERIVED FROM La II LINES

λ RMT	$\log \frac{W^*}{\lambda}$	$\log \eta^*$	$\log \frac{W^o}{\lambda}$	$\log \eta^o$	$\log \eta^o/\eta^*$	$\log \eta^o/\eta^* + \chi(\theta^o-\theta^*)$	Statistical Weight
4042.91	-5.16	-7.33	-5.35	-7.58	-0.25	-0.16	1
4086.72	-4.84	-6.79	-4.99	-7.06	-0.27	-0.27	1
4238.38	-5.25	-7.46	-5.40	-7.63	-0.17	-0.13	1
4333.76	-4.90	-6.90	-5.09	-7.22	-0.32	-0.30	1
Weighted Average		$[\eta] + \chi(\theta^o-\theta^*) = -0.21$					
Partition Function		μ^o (T = 5140°K) = 32.87 μ^* (T = 5730°K) = 33.07					
		$[\mu] = \log 32.87/33.07 = 0.00$					
Total Velocity		$[v] = -0.20$					
Continuous Absorption Coefficient		$[k_\lambda] = 0.06$					
Relative Abundance		$\log \frac{N^o}{N^*} = -0.21 + 0.00 - 0.20 + 0.06 = 0.05$					

TABLE XLI

DIFFERENTIAL CURVE OF GROWTH DATA DERIVED FROM Ce II LINES

λ RMT	$\log \frac{W^*}{\lambda}$	$\log \eta^*$	$\log \frac{W^o}{\lambda}$	$\log \eta^o$	$\log \eta^o/\eta^*$	$\log \eta^o/\eta^* + \chi(\theta^o-\theta^*)$	Statistical Weight
4014.899	-5.52	-7.76	-5.07	-7.20	-0.56	-0.51	1
4073.477	-5.53	-7.77	-5.35	-7.58	-0.19	-0.19	1
4083.233	-5.53	-7.77	-5.20	-7.39	-0.38	-0.31	1
4113.726	-5.62	-7.86	-5.53	-7.77	-0.09	-0.04	1
4137.646	-5.41	-7.64	-5.10	-7.24	-0.40	-0.40	1
4399.203	-5.80	-8.04	-5.90	-8.14	-0.10	-0.07	1
4418.784	-5.64	-7.88	-5.41	-7.64	-0.24	-0.20	1
4486.909	-5.61	-7.85	-5.61	-7.85	0.00	0.02	1
4562.360	-5.10	-7.24	-5.39	-7.66	0.42	0.42	1
4628.160	-5.46	-7.69	-5.51	-7.75	-0.06	-0.06	1
5274.244	-5.72	-7.96	-5.90	-8.14	-0.18	-0.12	1

Weighted Average	$[\eta] + \chi(\theta^o-\theta^*) = -0.13$
Partition Function	Not Available
Total Velocity	$[v] = -0.20$
Continuous Absorption Coefficient	$[k_\lambda] = 0.06$
Relative Abundance	$\log \frac{N^o}{N^*} = -0.13 - 0.20 + 0.06 = -0.27$

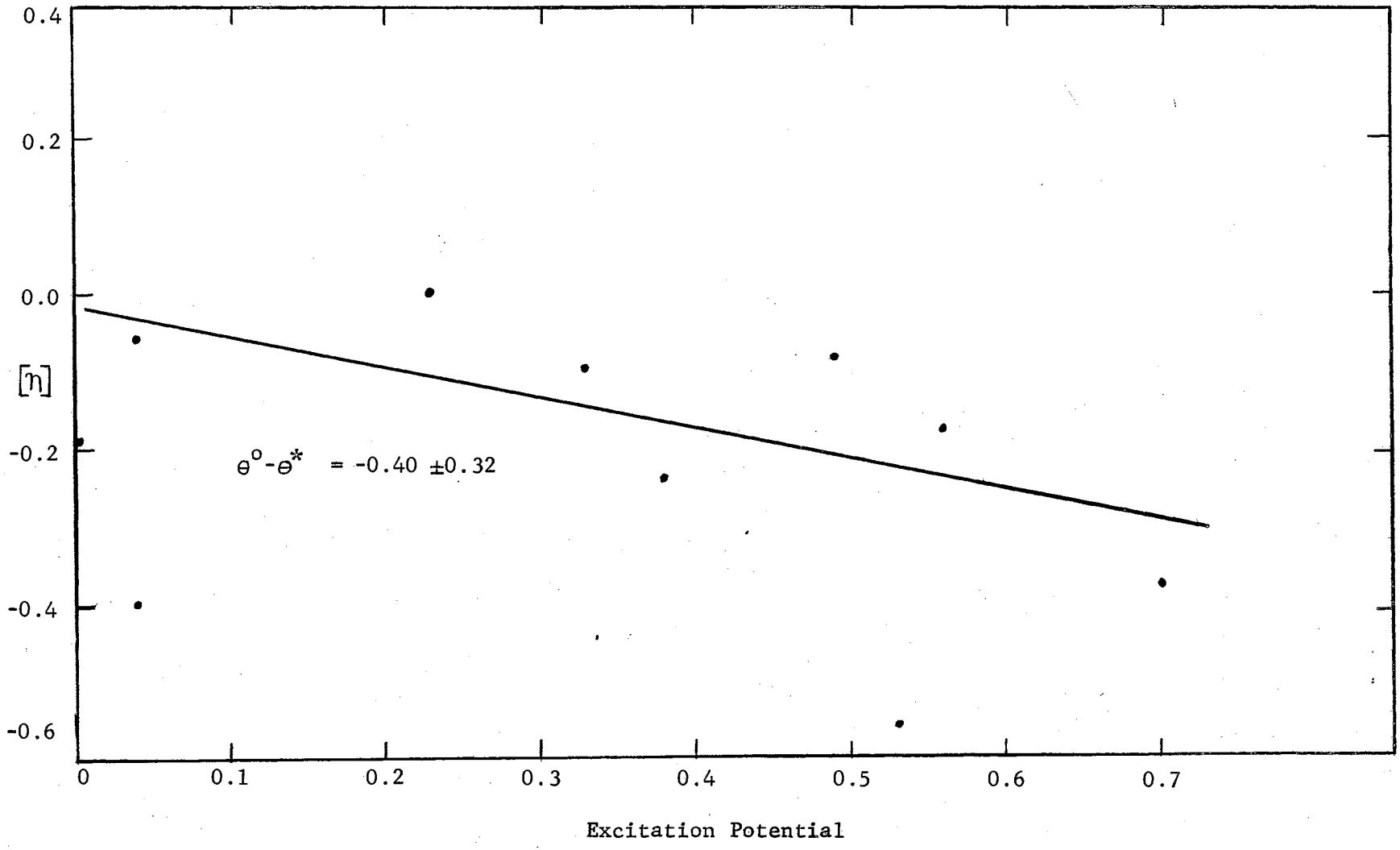

Figure 21. Plot of $[\eta]$ vs. Excitation Potential for Ce II.

TABLE XLII

DIFFERENTIAL CURVE OF GROWTH DATA DERIVED FROM Nd II LINES

λ RMT	$\log \frac{W^*}{\lambda}$	$\log \eta^*$	$\log \frac{W^o}{\lambda}$	$\log \eta^o$	$\log \eta^o/\eta^*$	$\log \eta^o/\eta^* + \chi(\theta^o-\theta^*)$	Statistical Weight
4021.330	-5.52	-7.76	-5.40	-7.63	-0.13	-0.10	1
4358.169	-5.34	-7.57	-5.06	-7.18	-0.39	-0.36	2
4462.985	-5.54	-7.78	-5.47	-7.77	-0.00	0.06	1
Weighted Average			$[\eta] + \chi(\theta^o-\theta^*) = -0.19$				
Partition Function			Not Available				
Total Velocity			$[v] = -0.20$				
Continuous Absorption Coefficient			$[k_\lambda] = 0.06$				
Relative Abundance			$\log \frac{N^o}{N^*} = -0.19 - 0.20 + 0.06 = -0.33$				

TABLE XLIII

DIFFERENTIAL CURVE OF GROWTH DATA DERIVED FROM Sm II LINES

λ RMT	$\log \frac{W^*}{\lambda}$	$\log \eta^*$	$\log \frac{W^o}{\lambda}$	$\log \eta^o$	$\log \eta^o/\eta^*$	$\log \eta^o/\eta^* + \chi(\theta^o-\theta^*)$	Statistical Weight
4334.153	-5.46	-7.69	-5.34	-7.57	-0.12	-0.09	1
4467.342	-5.75	-7.99	-5.76	-8.00	-0.01	0.06	1
Weighted Average		$[\eta] + \chi(\theta^o-\theta^*) = -0.01$					
Partition Function		Not Available					
Total Velocity		$[v] = -0.20$					
Continuous Absorption Coefficient		$[k_\lambda] = 0.06$					
Relative Abundance		$\log \frac{N^o}{N^*} = -0.01 - 0.20 + 0.06 = -0.15$					

TABLE XLIV

DIFFERENTIAL CURVE OF GROWTH DATA DERIVED FROM Eu II LINES

λ RMT	$\log \frac{W^*}{\lambda}$	$\log \eta^*$	$\log \frac{W^o}{\lambda}$	$\log \eta^o$	$\log \eta^o/\eta^*$	$\log \eta^o/\eta^* + \chi(\theta^o-\theta^*)$	Statistical Weight
4129.73	-5.06	-7.18	-4.89	-6.85	-0.33	-0.33	1
Weighted Average	$[\eta] + \chi(\theta^o-\theta^*) = -0.33$						
Partition Function	Not Available						
Total Velocity	$[v] = -0.20$						
Continuous Absorption Coefficient	$[k_\lambda] = +0.06$						
Relative Abundance	$\log \frac{N^o}{N^*} = -0.33 - 0.20 + 0.06 = -0.47$						

TABLE XLV

DIFFERENTIAL CURVE OF GROWTH DATA DERIVED FROM Gd II LINES

λ RMT	$\log \frac{W^*}{\lambda}$	$\log \eta^*$	$\log \frac{W^o}{\lambda}$	$\log \eta^o$	$\log \eta^o/\eta^*$	$\log \eta^o/\eta^* + \chi(\theta^o-\theta^*)$	Statistical Weight
4130.372	-5.47	-7.70	-5.57	-7.82	-0.12	-0.05	1

Weighted Average	$[\eta] + \chi(\theta^o-\theta^*) = -0.05$
Partition Function	Not Available
Total Velocity	$[v] = -0.20$
Continuous Absorption Coefficient	$[k_\lambda] = +0.06$
Relative Abundance	$\log \frac{N^o}{N^*} = -0.05 - 0.20 + 0.06 = -0.19$

Results for Mg I

Only seven lines are available from levels at 2.70 and 4.33 eV. The lines cover a wide range of equivalent widths from 41 mA on the linear portion of the curve of growth to 566 mA which is well onto the damping region. Several independent measures of the equivalent width of each line are available for all but two lines and the values of $[\eta] + \chi(\theta^{o} - \theta^{*})$ which are obtained after correction for excitation potential show a small dispersion; therefore all of the lines in Table XIII were given a weight of unity in the computation of the mean value of $[\eta] + \chi(\theta^{o} - \theta^{*})$.

Results for Mg II

Only one line is observable on two tracings with an equivalent width of 5 mA. Since the corresponding solar equivalent width is only 12 mA, the reliability of the point is poor. The value of the partition function for Mg II is not available. Since the abundance calculated in Table XIV differs greatly from that calculated by Greenstein (1948) it may be concluded that the reliability of the data is low.

Results for Si I

Only four lines are available for Si I and for three of them only one measurement is available. The other point was measured twice. However, all points lie on the linear portion of the curve of growth and the values of $[\eta] + \chi(\theta^{o} - \theta^{*})$ which are obtained show little scatter. Consequently, the abundance calculated in Table XV is considered reliable.

Results for Si II

As seen from an inspection of Table XVI the two lines which arise from the very high excitation potential of 8.09 eV are observable on only one tracing. One point lies on the linear portion of the curve of growth, the other on the knee of the curve. In spite of the sparcity of the data, a calculation of the electron pressure gives the value of $P_e^* = 0.95\ P_e^o$ which is in fair agreement with the values obtained from elements with better data, and therefore indicates that the data for Si II is reasonably accurate.

Results for Ca I

Twenty-one lines of Ca I were measured by Peebles and are listed in Table XVII. The equivalent widths range from 36 mA to a value of 400 mA, a value that is so far out on the damping portion of the curve of growth that a weight of zero was assigned. Only one tracing is available for those lines which tend to be concentrated on the flat portion of the curve of growth. Yet the dispersion of the points about the straight line fitted by the least squares method to the plot of $[\eta]$ versus excitation potential, illustrated in Figure 8, is less than average, ± 0.26. Since the range of excitation potential covered is small, only extending from 1.88 eV to 2.51 eV, the F value calculated for the slope of the curve is not significant.

Results for Sc I

Only three lines are observable for Sc I with very low values of equivalent width, 9, 10, and 17 mA. The quality of the lowest two

values is affected by the fact that the equivalent width measured in the sun is also very low and thus the systematic errors in the measurements can become quite large. The only reliable line listed in Table XVIII, at λ4023.688, has an equivalent width of 17 mA based on the average of three tracings, and the corresponding line in the solar spectrum is 57 mA which is large enough to be free from any substantial systematic error. Upon applying the correction factor for excitation potential the value of ±0.06 which is calculated for the 4743.814A line is more closely in agreement with the 4023.688A line than the one at 4553.152A which differs from the most reliable line by a factor of almost unity in the logarithm. Therefore, the 4753,152A line was given zero weight in the abundance analysis, and the abundance of Sc I is based upon only two lines. An attempt to calculate a relative electron pressure from Sc data produced a result which greatly differed from the value adopted from better quality data, therefore indicating that the Sc I data are poor.

Results for Sc II

The observational data available for Sc II in Table XIX are of much higher quality than that which is available for Sc I. This is the reverse of the situation which prevails for most elements in which the unionized state usually has the better data. Reference to Table 3-1 of Aller (1963) shows why this is true; most of the Scandium in a star such as in the sun is in the ionized state. For Sc II there are 11 lines that are observable over a range of equivalent widths that cover the linear and flat portions of the curve of growth. Several tracings are available for most of the lines and the 4314.084A line is measurable on

a total of seven tracings with individual values ranging from 139 mA to 267 mA. In Figure 9 is given the plot of $[\eta]$ versus excitation potential. A distinct trend is followed by 9 of the 11 points. These nine points are in two clusters that cover a narrow range of excitation potential at 0.60 and 1.49 eV and show a positive slope. However, the other two points at 0.31 and 1.76 eV do not follow this trend and tend to reduce the calculated least squares value of the slope of +0.14 which is close to the average value of +0.10. The F value calculated for the least squares fit is not significant, however.

Results for Ti I

The equivalent widths of some 55 lines of Ti I were measured by Peebles over the moderate range of excitation potentials from 0.0 to 2.3 electron volts, as illustrated in Figure 10. The general quality of the data listed in Table XX is high and is reflected in the deviation of the points about the regression line, $\pm$0.32, a value quite close to average. Since few of the lines fall on the flat or damping portions of the curve of growth, many have high statistical weights of two or three. The least squares calculated value of the slope is +0.12, very close to the adopted value of +0.10 and the F value is significant at the five percent level.

Results for Ti II

The 27 lines of Ti II given in Table XXI were the only ones measured by Peebles for an element in its ionized state. The data is of very good quality with a large number of points given statistical weights of two or three. The slope of the plot of $[\eta]$ versus

excitation potential (Figure 11) is 0.27 and has a significant F value; however, the points only cover a small range of excitation potential from 1.1 eV to 2.05 eV and so the slope is not considered accurate. The dispersion of the points about the regression line has the low value of $\pm$0.24 and the electron pressure calculated from Ti data is only slightly lower than the adopted average value.

Results for V I

Eighteen lines are given in Table XXII for V I, but three of the lines have such a low value of equivalent width in the sun that they fall below the cutoff point on the Cowley's curve of growth. Although it would be possible to simply extend the linear portion of the curve to lower values of $\log W/\lambda$ and $\log \eta$, the systematic errors for the measurement of the equivalent widths of such faint lines are so large that it was decided to simply assign them zero weight. The remaining lines tend to be of moderate equivalent width; for many of them only one measurement was available. This is reflected in the slightly higher-than-average deviation of the lines, $\pm$0.37. When $[\eta]$ is plotted against the excitation potential as given in Figure 12, the graph runs over the moderate span from 0.3 to 2.4 eV with the F value being significant and the slope having the very large negative value of -0.39. The value of the relative electron pressure calculated from the V I data comes very close to the adopted average value, a fact which indicates that the basic quality of the data is high.

Results for V II

The equivalent widths of the 11 lines that are available for the

study of V II are listed in Table XXIII. Most of the points fall on the linear portion of the curve of growth but many are found on only one tracing. The dispersion has a low value of ± 0.18 and the slope has the large positive value of 0.248 with a highly significant F value of 19.90. However, examination of the plot of $[\eta]$ versus excitation potential given in Figure 13 shows that nine of the points have excitation potentials between 1.4 and 2.1 eV with the two points having large values of $[\eta]$ at 3.78 and 3.96 eV being responsible for the large slope. Since each of the two lines was measured on only one tracing and is of only moderate equivalent width, and the range of excitation potentials covered is within the same range as the other elements studied, the existence of such a large difference in excitation temperatures between θ Ursae Majoris and the sun for V II is based on meager evidence and the average value of +0.10 will be adopted instead.

Results for Cr I

Cr I has 65 lines which cover a wide range of equivalent widths from 0.0 to 4.0 eV listed in Table XXIV. The general quality of the data is high with most of the lines falling on the linear portion of the curve of growth. In spite of the fact that the dispersion is ± 0.26, slightly below average, the least squares fit of a straight line to the plot of $[\eta]$ versus excitation potential, shown in Figure 14, yields an F value that is not significant. The hypothesis of the test for which the F value is calculated is that there will be a statistically significant reduction in the sum of squares of the deviations of the points from the calculated regression line as opposed to the sum of squares calculated with respect to a horizontal line with zero slope passing

through the mean value of the data. Since the calculated regression line has such a small slope, no significant reduction in the sum of squares was made and, thus, the value of Fisher's F was not significant.

Results for Cr II

Seventeen lines are listed in Table XXV for Cr II. The values of equivalent width are large enough to avoid systematic error. Although six lines fall on the flat portion of the curve of growth, the dispersion of the points about the regression line has the very large value of ± 0.41. The plot of $[\eta]$ versus excitation potential given in Figure 15 shows that all of the points occur in two intervals of excitation potential at around 3.8 to 3.85 eV and at 4.05 eV. Since Fisher's F has the low value of 0.05 and the variation of the data with excitation potential displays little trend, no line has been drawn in Figure 15.

Results for Mn I

Twenty-two lines are listed in Table XXVI for Mn I, covering a range of equivalent widths from 11 mA to 286 mA. Since all of the lines are in the wavelength region between 4000A and 4900A, several measurements are available for determining the equivalent width of each line. Consequently, the data are of good quality with an average value of disposition; most of the statistical weights of the lines are greater than one. A significant F value is calculated for the slope of +0.10, but an inspection of Figure 16 shows that, except for three points at 0.0 eV, all of the other points lie in the narrow range of excitation potential between 2.1 and 2.9 eV.

Results for Mn II

Of the four lines which are listed in Table XXVII for Mn II, a value of $[\eta]$ could only be obtained from one of them. Two of the others had such low values of equivalent width in the sun that they did not fall on the Cowley's curve of growth. It seems reasonable that the equivalent widths of these lines should be low since they are from levels at 10.62 and 10.74 eV, values so high that the energy levels would not be expected to be very highly populated. The third line does not have a value of the equivalent width in the sun listed in either the Utrecht or Canberra tables so no value of $[\eta]$ may be derived from it.

Results for Fe I

As has been the case in most curve of growth studies, the best statistical data in this work was obtained from the lines of Fe I. The 115 observable lines of Fe I are the most numerous of all the elements, and the equivalent widths cover the linear, flat, and damping regions of the curve of growth. Because of the wealth of data which is available, a more rigerous standard of acceptance was applied to the data and many lines were given zero weight which would have been allowed to influence the results if such a large number of lines had not been available from which to select. An inspection of Table XXVIII shows that lines having large equivalent widths in θ Ursae Majoris and the sun, and which consequently lie far out on the damping region of the curve of growth, tend to have more positive values of $[\eta] + \chi(\theta^{o} - \theta^{*})$ than do lines that lie on the flat or linear portions of the curve.

This is interpreted as being due to the fact that the damping constants of θ Ursae Majoris and the sun are different and consequently the curves of growth do not match on the far end of the damping portion. The fact that $[\eta] + \chi(\theta^{o} - \theta^{*})$ tends to be positive indicates that the damping constant of θ Ursae Majoris is greater than that of the sun. This conclusion is verified by the computation of Peebles that $\log a = -1.8$ for θ Ursae Majoris and of Greenstein that $\log a = -2.3$ for the sun.

The excitation potentials cover as large a range as any of the elements, and run from 0.0 to 4.5 eV as can be seen from an inspection of Figure 17. The value of Fisher's F calculated for $(\theta^{o} - \theta^{*})$ is significant and the numerical value of the excitation temperature difference, 0.08, is very close to the adopted mean value of 0.10. The standard deviation of a measurement from the regression line, $\pm$0.29, is also close to the average value of $\pm$0.30. In summary, Fe I provides data which are quite suitable for the use of the curve of growth technique, and in adequate abundance to enable a good statistical analysis to be performed.

Results for Fe II

The 33 lines listed in Table XXIX for Fe II represent the largest amount of observable data collected in this study for an element in the ionized state. The range of equivalent widths is such that lines are available from the linear portion of the curve of growth to the high end of the damping portion; but the excitation potentials are limited to a restricted region. The majority of the points cover the range of 2.6 to 3.2 eV with three points at 3.9 eV as shown in Figure 18.

Consequently, it is not surprising to find that the excitation temperature difference which was calculated by the least squares method does not have a significant F value. The dispersion of the points is a nominal $\pm$0.34. The relative electron pressure calculated in Table XI for Fe data gives a value which is close to the average value that was adopted.

Results for Co I

The 12 observable lines of Co I which are listed in Table XXX fall on the linear part of the curve of growth. More than one measurement is available for the majority of points but the values of the average equivalent widths are generally low enough so that systematic error affects the accuracy of the data; this is evidenced by the dispersion of the points in Figure 19 being $\pm$0.51, the highest value of all the elements for which calculations were made. A wide range of excitation potentials is covered from 0.43 to 4.0 eV, and a value for the differential excitation temperature of -0.165 is calculated. This is one of the few negative values calculated which comes from good quality data, but the F value just misses being significant at the five percent level. If it were not for the fact that the dispersion of the points has a high value and that the data consists of only 12 lines, the existance of this negative value of slope would have to be given greater consideration.

Results for Ni I

The 32 lines of Ni I which are listed in Table XXXI fall on the linear and flat portions of the curve of growth and have measurements

of the equivalent widths of the lines taken sufficiently often to give confidence in the data and produce good values of the statistical weight. As shown in Figure 20, the vast majority of the points are concentrated between 3.4 and 3.9 eV with only two points at 1.67 and 1.94 eV. Consequently, the F value for the difference in excitation temperature is not significant although the dispersion of the points has the low value of $\pm$0.23.

Results for Cu I

In Table XXXII the only line recorded for Cu I has an equivalent width of 38 mA. Since the line falls on the linear portion of the curve of growth and two measurements are available, a modest amount of confidence can be placed in the value of $[\eta] + (\theta^{o} - \theta^{*}) = +0.54$ which is derived.

Results for Zn I

Two lines are available for Zn I, one of which is on the linear portion of the curve of growth and the other on the flat portion. Since the values of $[\eta] + \chi(\theta^{o} - \theta^{*})$ are in close agreement, and two measurements are available for one line and four for the other, the data seem adequate to derive an abundance. No value for the partition function was available for inclusion in the calculation of the abundance in Table XXXIII.

Results for Sr I

In Table XXXIV only one line is available for Sr I from the linear portion of the curve of growth. The equivalent width is derived from

only one measurement but the value of the electron pressure calculated from the Sr data indicates that the data from this line are reliable.

Results for Sr II

Two lines are listed in Table XXXV for Sr II from the damping portion of the curve of growth. Even though data from the damping portion is subject to a large error in the value of $[\eta]$, the absence of any other lines requires us to make the abundance calculations with this data if any information on Sr II is to be obtained.

Results for Y I

In Table XXXVI are listed the only two lines that are observable for Y I; only one measurement is available for each. The equivalent widths are so small that considerable systematic error is likely to be involved. Consequently, the available data for Y I are poor. The poor quality of the Y data is reflected in the fact that the electron pressure calculated from this data differs greatly from the value adopted from the other elements.

Results for Y II

Six lines are listed in Table XXXVII for Y II and each has more than one measurement available. However, a large difference in the value of $[\eta]$ as compared with the other five points, and a large discrepancy between the Utrecht and Canberra values of W^o, force the assignment of zero weight to the line at 4358.73A. The other points fall mainly on the linear portion of the curve of growth but cover such a small portion of excitation potential that the F value was not

significant for the slope.

Results for Zr II

Six lines are listed in Table XXXVIII for Zr II; half of them are of sufficient quality to receive a statistical weight of two. But since five of the lines are close together in excitation potential, the F value for the slope was not significant. The dispersion of the points, however, is a very low ± 0.20.

Results for Ba II

Two lines with large equivalent widths are listed in Table XXXIX for Ba II; one line is in the damping region, the other on the flat portion of the curve of growth. Although only two measurements were made for one line and one for the other, the values of $[\eta] + \chi(\theta^{o} - \theta^{*})$ obtained from the pair agree reasonably well.

Results for La II

Four lines are given in Table XL for La II, the equivalent width of each being measured at least twice and all lying on the linear portion of the curve of growth. A limited span of excitation potential is covered but the computed values of $[\eta] + \chi(\theta^{o} - \theta^{*})$ are in good agreement.

Results for Ce II

Although the partition function for Ce II is not available, an inspection of Table XLI shows that 11 data points are available having low values of equivalent width. In Figure 21 a plot of $[\eta]$ versus

excitation potential reveals that the calculated slope of -0.40 is based upon data covering the small range of excitation potential from 0.0 to 0.7 eV. Therefore, the value of Fisher's F is not significant but the low scatter of points about the regression line indicates that the calculated abundance will be accurate.

Results for Nd II

The three lines given for Nd II in Table XLII permit a determination of the abundance to be made if the partition function term, which is not available, is neglected.

Since two of the lines come from the linear portion of the curve of growth reasonable confidence may be placed in the accuracy of the calculated abundance.

Results for Sm II

The two lines of Sm II in Table XLIII are of low equivalent widths in both the sun and the star so large systematic errors are possible in the determination of $[\eta]$. The line is measured in the star once and the other line only two times. Therefore, the data are not of good quality.

Results for Eu II

The one line available for Eu II is measured on only one microphotometer tracing and the value of the partition function is not available. Therefore, the abundance calculated in Table XLIV is not reliable.

Results for Gd II

Since the one line of Gd II given in Table XLV measures 14 mA in the star on one tracing, and 11 mA in the sun, the abundance which has been computed neglecting the partition function rests on a very tenuous observational basis.

CHAPTER V

CONCLUSIONS

In this chapter the conclusions reached in this study will be summarized and a comparison of the results will be made with those of Peebles and Greenstein.

Summary of Physical Properties of θ Ursae Majoris

The difference in the values of θ_{exc} between the sun and θ Ursae Majoris was determined from fitting straight lines by the least squares method to plots of $[\eta]$ versus excitation potential. Making use of a value of the statistical parameter known as Fisher's F that is significant at the 5 percent level as an acceptance criterion, an average value of $\theta^{o} - \theta^{*} = +0.10 \pm 0.03$ for the reciprocal temperature was calculated from the slopes of the elements Fe I, Ti I and Mn I.

The mean electron pressure in θ Ursae Majoris was determined relative to the sun by using data from the elements Fe, Ti, V and Cr in two stages of ionization in the differential Saha equation. Since the ionization temperature and the electron pressure cannot in practice be determined simultaneously from the differential Saha equation with data from several elements, it is better to assume an ionization temperature and use the information from two stages of ionization of the elements to calculate the electron pressure. An attempt to determine the ionization temperature by an analysis of the pseudo-equivalent widths of the HΥ

profile is described in Appendix A, but resulted in a large spread of values. Assuming that the ionization temperatures in the sun and the star were equal to the effective temperatures, and statistically weighting the results according to the number and quality of the lines for the elements, a mean electron pressure was obtained for θ Ursae Majoris that was 1.17 times as great as that in the sun.

Since experimental values of log c/v were only available in the sun and the star for the elements Ca I, Ti I, Ti II, Cr I, Fe I and Ni I, it was necessary to use total velocities that were theoretically calculated from the effective temperature and the values of turbulent velocity. As an inspection of Table X indicates, the agreement between the theoretically calculated values of log v^{o}/v^{*} and the values experimentally derived from Wright's (1948) solar velocities and Peebles' average values for θ Ursae Majoris is satisfactory for only half of the cases. Therefore, the theoretically calculated values were used exclusively in the computations.

The partition function correction was calculated from tabulated values given in Aller (1963) using the solar excitation temperature of $5143^{o}K$ and the value determined in this study for θ Ursae Majoris of $5730^{o}K$.

A study of the 115 lines of Fe I shows that the values of $[\eta]$ that are obtained from lines of large equivalent width (greater than 300 mA) tend to be significantly larger than those of smaller equivalent width. This observation supports the conclusion that the damping constants have different values in the sun and θ Ursae Majoris and that the values of $[\eta]$ derived from lines of large equivalent width will tend to be in error. Therefore, in cases where enough lines of small equivalent width

were available to give adequate statistics, lines of large equivalent width have been given zero weight.

Peebles found values of log a = -1.8 for both scattering models and -1.3 for both absorption models. Greenstein's value of $\Gamma/\gamma_{cl} = 1.7$ corresponds to a value of log a = -2.3, but is influenced by the fact that Greenstein's lines of large equivalent width are systematically smaller than those of Peebles and of this paper.

TABLE XLVI

PHYSICAL PARAMETERS OF θ URSAE MAJORIS DETERMINED FROM CURVE OF GROWTH ANALYSES

Parameter	Greenstein	Peebles	This Work
θ^{o}_{exc}	1.04	Not Used	0.98
θ^{*}_{exc}	0.98	Numerous Values	0.88
θ^{*}_{ion}	0.87	0.81[1]	0.81[1]
log c/v^{*}	5.44	5.04 (Fe I-NBS)	Not Obtained
log P^{*}_{e}	1.20[2]	1.31 (Ti I-NBS)	1.07
log k^{*}_{λ}	-1.00	Not Used	-0.70
log a^{*}	-2.3	-1.8 Both Scattering Models -1.3 Both Scattering Models	Not Obtained
Type of Analysis	Differential Curve of Growth	Absolute Curve of Growth	Differential Curve of Growth

[1]Derived from the effective temperature.

[2]Derived for $\theta_{ion} = 0.80$.

In Table XLVI are summarized for comparison the physical properties of θ Ursae Majoris as measured by Greenstein (1948), Peebles (1964) and this work. Part of the difference between the values of θ^*_{exc} obtained by Greenstein and this work is due to the fact that different values of excitation temperature were assumed for the sun; the values of θ_{ion} differ because of the difference in the choice of depths at which line formation was assumed to occur. Greenstein uses a value of $\tau = 0.25$ whereas Peebles and this work take the value at $\tau = 0.6$. There is good agreement between the values of log c/v^* obtained for iron by Peebles and Greenstein; good agreement is obtained by all three authors on the value of the electron pressure.

Numerical values of the damping constant were not obtained in this work but the results of the analysis of iron indicate that the damping constants in the sun and θ Ursae Majoris are not the same. The fact that Peebles and Greenstein do not obtain the same numerical values may be related to the fact that there is a systematic difference in the lines of large equivalent widths between the two sets of data.

Comparison With the Work of Peebles

A direct comparison of the results of this study with that of Peebles is not possible at this time because neither the S-S nor the M-E model enables the abundance of the element to be calculated directly in terms of the number of atoms per unit volume.

In the S-S model the abundance-related quantity appearing in the abscissa of the curve of growth is the product NH, where N is the number of atoms per unit volume and H is the depth of the reversing layer

characterizing the model. Unless an adequate theory is available that will give a prediction of the depth of the reversing layer for each separate element for the particular stellar atmosphere under study as a function of excitation and ionization, it is not possible to determine N. In the M-E theory the abundance of the element enters the abscissa of the curve of growth through the term $N/\rho\bar{k}$ where ρ is the density and $\bar{k}$ is the mean continuous absorption coefficient per gram of stellar material. Again $1/(\rho\bar{k})$, which is a measure of the geometrical depth of the atmosphere corresponding to infinite optical depth in the continuum, may vary strongly with optical depth and, at best, only an average value can be obtained. Therefore, until a model atmosphere study is made of θ Ursae Majoris to enable values of H, ρ and $\bar{k}$ to be calculated for the models used by Peebles, it will not be possible to make a direct comparison of the density of atoms produced in this study with the values produced by Peebles which represents the number of atoms in a one square centimeter column in the line of sight.

Comparison of Results With Greenstein

A comparison of the abundances obtained in this study with those of Greenstein is not directly possible because different calculations were used to determine the correction for continuous optical absorption. Moreover, Greenstein's abundance results are not in a form which can conveniently be compared with the results found in this study. He defines a quantity, $\Delta \log \xi$, which can be converted into a form comparable with those of this paper if $\log k_\lambda^\circ/k_\lambda^*$ is added to the negative of the term. Greenstein used -0.46 for the $[k_\lambda]$ term while the value employed here is +0.06. For a direct comparison of the results of the

two different investigations, Greenstein's results are "normalized" by using the value of the absorption coefficient of this study. It should be noted that Greenstein does not make the small correction for the change in partition function with temperature between the star and the sun.

A comparison of the results is given in Table XLVII where it can be seen that this study has obtained a value of +0.26 for the relative abundance of Fe I while Greenstein's normalized value is +0.49. Since the best data should be obtainable for Fe I the difference between these two figures is indicative of the amount of agreement between the two works. Selecting elements in which more than 10 lines are available for study in both works, the largest difference between the values of abundance was obtained for Fe II, for which Greenstein's derived value of -0.50 is based on 30 lines and this work resulted in a value of -0.16 based on 21 lines. A typical difference in the abundance obtained for elements with more than 10 lines was about 0.25, a figure consistent with that obtained for Fe I.

In conclusion, it is noted that θ Ursae Majoris has a chemical composition differing very little from the solar values. However, there is a definite trend suggesting that the metal content of the star is somewhat less than that of the sun. Differences in the absorption coefficients obtained here and by Greenstein suggest that a further study of this star using the model atmospheres approach should prove fruitful.

TABLE XLVII

COMPARISON OF VALUES OF ABUNDANCES BETWEEN GREENSTEIN AND THIS WORK

Element	Mangold		Greenstein		
	No. of Lines	$\log \frac{N^o}{N^*}$	No. of Lines	$-\Delta \log \xi$	$\log \frac{N^{o\#}}{N^*}$
Na I	4:	0.26	-	-	-
Mg I	7	0.94	5	0.45	0.51
Mg II	1:	1.26	-	-	-
Si I	4	0.70	-	-	-
Si II	2	0.33	-	-	-
Ca I	21	0.14	10	0.25	0.31
Sc I	3:	0.23	-	-	-
Sc II	11	-0.39	8	-0.35	-0.29
Ti I	55	0.17	13	0.14	0.20
Ti II	27	-0.34	26	-0.54	-0.48
V I	13	0.30	6	0.73	0.79
V II	11	0.03	4:	-0.30	-0.24
Cr I	15	0.29	10	0.28	0.34
Cr II	17	-0.20	9	-0.49	0.43
Mn I	22	0.41	7	0.45	0.51
Mn II	4:	0.54	-	-	-
Fe I	115	0.26	121	0.43	0.49
Fe II	30	-0.16	21	-0.56	-0.50
Co I	12	0.51	3	0.70	0.76
Ni I	32	0.39	9	0.08	0.14
Cu I	1:	0.43	-	-	-
Zn I	2	0.42	2	-0.05	0.01
Sr I	1:	0.09	-	-	-
Sr II	2:	-0.16	3	0.01	0.07
Y I	2:	-0.07	-	-	-
Y II	6:	-0.49	5	-0.45	-0.39
Zr II	5	-0.16	7	-0.15	-0.09
Ba II	2:	-0.83	2	-0.23	-0.17
La II	4	0.05	9	-0.34	-0.28
Ce II	11	-0.27	8	-0.32	-0.26
Nd II	3	-0.33	3:	-0.50	-0.44
Sm II	2:	-0.15	4	-0.50	-0.44
Eu II	1:	-0.47	-	-	-
Gd II	1:	-0.19	4:	-0.40	-0.34

#Normalized with value of [k_λ] used in this paper.

:Colon behind number of lines indicates low quality data.

REFERENCES

Allen, C. W. 1934, Mem. Comm. Obs. Canberra, Vol. 1, No. 5.

_____. 1938, ibid., Vol. 2, No. 6.

_____. 1963, Astrophysical Quantities (2d ed.; London: The Athlone Press).

Aller, L. H. 1963, Astrophysics (2d ed.; New York: The Ronald Press Company).

Aller, L. H., and Greenstein, J. L. 1960, Ap. J. Suppl., 5, 139.

Baker, J. G. 1936, Ap. J., 84, 474.

Cayrel, G., and Cayrel, R. 1963, Ap. J., 137, 431.

Conti, P. S. 1967, Ap. J., 148, 105.

Corliss, C. H., and Bozman, W. R., Experimental Transition Probabilities for Spectral Lines of 70 Elements (NBS Mono. No. 53 [Washington: Government Printing Office]).

Cowley, C. R., and Cowley, A. P. 1964, Ap. J., 140, 713.

Greenstein, J. L. 1948, Ap. J., 107, 151.

_____. 1960, Stellar Atmospheres, ed. J. L. Greenstein (Chicago: The University of Chicago Press), pp. 199, 246.

Goldberg, L., Muller, E. A., and Aller, L. H. 1960, Ap. J. Suppl., 5, 1.

Gunn, J. E., and Kraft, R. P. 1963, Ap. J., 137, 301.

Helfer, H. L., Wallerstein, G., and Greenstein, J. L. 1959, Ap. J., 129, 700.

_____. 1963, Ap. J., 138, 97.

Hunger, K. 1956, Zs. f. Ap., 39, 36.

Hynek, J. A. 1951, Astrophysics (New York: McGraw-Hill Book Company, Inc.).

Johnson, H. L., and Morgan, W. W. 1953, Ap. J., 117, 313.

REFERENCES (Continued)

Koelbloed, D. 1967, Ap. J., 149, 299.

Keenan, P. C., and Morgan, W. W. 1951, Astrophysics, ed. J. A. Hynek (New York: McGraw-Hill Book Co.), pp. 12, 27.

King, R. B., and King, A. S. 1938, Ap. J., 87, 24.

Minnaert, M., and Slob, C. 1931, Proc. Amsterdam Acad. 34, Part I, 542.

Menzel, D. H. 1936, Ap. J., 84, 462.

Moore, C. E. 1959, Revised Multiplet Table (NBS Tech. Note 36 [Washington: Government Printing Office]).

Munch, G. 1960, Stellar Atmospheres, ed. J. L. Greenstein (Chicago: The University of Chicago Press).

Pannekoek and van Albada 1946, Pub. Astr. Inst. Amsterdam, No. 6, p. 1.

Peebles, H. O. 1964, Ph. D. Thesis, Oklahoma State University, unpublished.

Pierce, A. K., and Aller, L. H. 1952, Ap. J., 116, 175.

Schroeder, L. W. 1958, Ph. D. Thesis, Indiana University, unpublished.

Searle, L. S., and Oke, J. B. 1962, Ap. J., 126, 266.

Searle, L. S., Sargent, W. L. W., and Jugaku, J. 1963, Ap. J., 137, 268.

Steel, R. G. D., and Torrie, J. H. 1960, Principles and Procedures of Statistics (New York: McGraw-Hill Book Company, Inc.).

Swensson, J. W. 1946, Ap. J., 103, 207.

Thackeray, A. 1936, Ap. J., 84, 433.

Unsold, A. 1938, Physik der Sternatmospharen (Berlin: Springer).

Utrecht Staff 1960, Preliminary Photometric Catalogue of Fraunhofer Lines, Rech. Astr. Obs. Utrecht, Vol. 15.

Wallerstein, G., Greenstein, J. L., Parker, R., Helfer, H. L., and Aller, L. H. 1963, Ap. J., 137, 280.

Wright, K. O. 1948, Pub. Dom. Ap. Obs. Victoria, VIII, No. 1.

_____. 1962, Astronomical Techniques, ed. W. A. Hiltner (Chicago: The University of Chicago Press), p. 83.

_____. 1966, Abundance Determinations in Stellar Spectra, I. A. U. Symposium No. 26 (New York: Academic Press), pp. 15, 35.

Wrubel, M. H. 1949, Ap. J., 109, 66.

A P P E N D I C E S

APPENDIX A

REVIEW OF METHODS USED IN THE LITERATURE FOR DIFFERENTIAL CURVE OF GROWTH ANALYSES

In this Appendix the methods which other investigators have reported in the literature for the determination of abundances and the physical parameters characterizing the outer layers of stellar atmospheres will be reviewed. As has been stated in Chapter IV, one must be aware of the simplifying assumptions made in a differential curve of growth analysis and have an understanding of the true nature of the line formation process. A review of differential curve of growth studies performed by other authors shows that in practice a differential curve of growth analysis needs to be supplemented by data gathered by techniques outside of the differential method itself. The principal sources of information for the supplementary data come from calculations based upon the theory of model atmospheres. The authors of the papers, some of the techniques used, and the methods used to determine some of the important parameters are listed in Table XLVIII.

It is essential to have some knowledge of the techniques of model atmospheres to be able to understand the approximations which are made in a differential curve of growth analysis. This is especially true for the formation of lines of ionized elements, and lines arising from levels at high excitation potentials, which are generally formed at greater depths in the atmosphere than lines from neutral elements. Since the

TABLE XLVIII

DIFFERENTIAL CURVE OF GROWTH TECHNIQUES USED BY OTHER AUTHORS

Author(s) (Date)	Method of Analysis	Excitation Temperature Source	Effective Temperature Source	Values of Solar Constants
Greenstein (1948)	differential COG & model atmospheres	Fe I	not used	$\theta_{ion} = 0.95$ $\log P_e = 0.80$ at $\tau = 0.25$
Aller & Greenstein (1960)	differential COG	assume Fe I abundance equal to sun	photoelectric scan of continuum	$\theta_{ion} = 0.89$ $\log P_e = 1.30$
Cayrel & Cayrel (1963)	differential COG & model atmospheres	not explained	photoelectric scan, color index, T_{exc}, & model atmospheres	$\theta_{exc} = 0.97$ $\log P_e = 1.3$
Gunn & Kraft (1963)	differential COG	Fe I	not used	$\theta_{exc} = 1.04$ $\theta_{ion} = 0.89$ $\log P_e = 1.30$
Searle, Sargent, & Jugaku (1963)	differential COG	Fe I & Ti I	not used	not given
Wallerstein et. al. (1963)	differential COG	Fe I	6 color photometry	$\theta_{eff} = 0.83$
Koelbloed (1967)	differential & absolute COG & model atmos.	Fe I	from T_{exc} through Conti's models; photoelectric scan of continuum	$\theta_{exc} = 0.98$ $\log P_e = 1.00$

TABLE XLVIII (Continued)

Author(s) (Date)	Ionization Temperature and Electron Pressure	Source of Largest Error	Determination of Abundance
Greenstein (1948)	assume $T_{ion} = T_{exc}$; differential Saha eq. in single layer approximation		relative to the same element in the sun
Aller & Greenstein (1960)	differential Saha eq. in single layer approximation	determination of temperature	relative to the same element in the sun
Cayrel & Cayrel (1963)	assume $T_{ion} = T_{exc}$; differential Saha eq. in single layer approximation		relative to the same element in the sun
Gunn & Kraft (1963)	pseudo-equivalent widths of H	error in values of $[\eta]$	relative to the same element in the sun
Searle, Sargent, & Jugaku (1963)	strength of Fe II lines; degree of ionization of Fe; profile analysis of the wings of H		relative to abundance of Fe I
Wallerstein et. al. (1963)	T_{ion} is average of T_{exc}, T_{eff} and shift of COG relative to Fe	determination of temperature	
Koelbloed (1967)	differential Saha eq. in single layer approximation; model atmosphere calculations		with respect to abundance of hydrogen; used because of model atmos. technique

differential curve of growth technique only gives results relative to the sun, it is necessary to have a solar model atmosphere in order to be able to choose values of the ionization temperature and electron pressure at a representative depth for line formation. The numerical value of the continuous optical absorption coefficient will be determined from the ionization temperature and electron pressure. The differential curve of growth technique gives as a result only the difference in the excitation temperature between the sun and the star. In order to obtain the absolute value of the excitation temperature the absolute value of the solar excitation temperature, which is available from a model atmosphere or absolute curve of growth constructed from solar data, must be used. Through model atmosphere calculations it is possible to determine the ionization temperature from the analysis of the profiles of lines such as that of Hγ. Model atmospheres can also be used to relate the values of ionization temperature to effective temperature and effective temperature to the luminosity and surface gravity of the star. The determination of the effective temperature is done most accurately by a photoelectric scan of the continuum after correcting for line blanketing. Other techniques involve six color photometry or UBV data, or an estimate of the temperature simply from the spectral class of the star. It is necessary to have accurate measurements of the effective temperature of both the sun and the star if these are used as equivalent to the ionization temperatures in the Saha equation. Therefore, the authors reviewed in this Appendix frequently make use of stellar information gathered from sources outside of the differential curve of growth method itself.

Determination of Abundances

The determination of the abundances may be done relative to the sun on an element-by-element basis comparing each element in the star relative to its abundance in the sun. However, another possibility is to make the determination of the abundance with respect to Fe I in the star which can be well determined because of the high quality data which is available. Then the shift of the Fe I curve with respect to the sun is determined in order to relate the stellar to the solar abundances. The direct comparison is made by most authors but Searle, Sargent, and Jugaku (1963) and Wallerstein et al, (1963) work with respect to iron. Koelbloed (1967) makes a determination of the abundance of the element with respect to hydrogen because of the model atmosphere calculations which he uses to determine abundances.

Excitation Temperature

In the curve of growth analysis it is assumed that the distribution of the electrons over the energy states in the atoms follows the Boltzmann equation. In combining data from lines arising from different excitation potentials it is necessary to make a correction involving the excitation temperature or the corresponding value of $\theta_{exc} = 5040/T_{exc}$. In a differential curve of growth analysis the difference in the values of θ between sun and star, $(\theta^{\circ}_{exc} - \theta^{*}_{exc})$ is found from the slope of the straight line passed through a plot of $\log \eta^{\circ}/\eta^{*}$ against excitation potential. In practice it is difficult to find elements other than Fe I which cover a large enough span of excitation potential and have enough lines observable for an adequate statistical analysis. Of the

authors cited in this Appendix, only Searle, Sargent and Jugaku (1963), who obtained data from Ti II, used any element other than Fe I to determine θ_{exc}. The value of excitation temperature found for Fe I was assumed to hold for all of the other atoms and ions.

After determining the difference in excitation temperature between the sun and star, the absolute value of θ^{*}_{exc} can be obtained by using a value of θ°_{exc} obtained from a solar curve of growth. Wright (1948) obtained a value of $4875^{\circ}K$, corresponding to $\theta^{\circ}_{exc} = 1.03$, for the mean excitation temperature of the sun. The specific value obtained for Fe I was $5100^{\circ}K$ or $\theta_{exc} = 0.99$. These excitation temperatures were obtained using the f-values of King and King (1938) which were taken in a low temperature arc that did not provide information on the lines which arise from levels with high excitation potential. Many authors have noted, e.g., Cowley and Cowley (1964), that lines arising from higher excitation potentials tend to have higher excitation temperatures and correspondingly lower values of θ_{exc}. Therefore, it is not surprising to find that the Cowleys obtain an average effective temperature for the sun for all elements of $\theta_{eff} = 0.98$ using the f-values of Corliss and Bozman which were taken in a higher temperature furnace and extend to levels having higher values of excitation potential. Unfortunately the exact value of θ°_{exc} obtained from Fe I is not available since a breakdown of excitation potential by element is not included in the Cowleys' work.

Ionization Temperature

The determination of the ionization temperature is not nearly so straightforward as the determination of the excitation temperature and many diverse techniques have been reported in the literature for estimating this parameter. The ionization temperature is used in the Saha equation along with the abundance information from several elements in the unionized and first stage of ionization to determine the electron pressure at a representative depth for line formation inside of the stellar atmosphere. Knowledge of the temperature and electron pressure enables a value of the optical absorption coefficient to be selected from theoretically computed tables, such as those given in Allen (1963). Since the numerical value of the optical absorption coefficient is very sensitive to the values of temperature and electron pressure that are used it is important that accurate values of these parameters be determined.

As a first approximation the ionization temperature will be approximately equal in value to the effective temperature and the excitation temperature. The best determinations of the effective temperature are obtained from photoelectric scans of the stellar spectrum, but such detailed information is usually not available and six-color photometry or UBV color indices must be used.

Koelbloed (1967) makes the assumption that the ionization temperature is equal to the excitation temperature, while Aller and Greenstein (1960) use T_{ion} slightly less than T_{eff}. Helfer, Wallerstein and Greenstein (1963) adopt a value of the ionization temperature which lies between the excitation and effective temperatures. Wallerstein et al.

(1963) determine the ionization temperature by taking an average value of the effective temperature as derived from six-color photometry, the excitation temperature derived from Fe I, and a unique method of applying the Saha equation to obtain a direct value of the ionization temperature. On the assumption that the relative abundances of the neutral elements in the star are the same as they are in the sun, the observed shift in the curve of growth of the neutral lines with respect to the Fe I curve $N_{(Fe\ I)}/N_{(X\ I)}$ is plotted against the difference in ionization potential between the element and iron. The slope of a straight line passed through the points determines an ionization temperature. (Note that this does not involve a comparison between the number of neutral and ionized atoms of an element as do other techniques involving the Saha equation.)

Simultaneous Determination of Ionization Temperature and Electron Pressure

Greenstein (1948) gives a technique for the simultaneous determination of θ^*_{ion} and $\log P^*_e$ by using data from two elements observed in two different stages of ionization if the numerical values of the ionization potential are different. Unfortunately the ionization potentials of the observable elements differ by such a small amount that in practice the solutions prove almost indeterminate. If the ionization temperatures can be assumed beforehand, the abundances of several elements in two stages of ionization can be used to calculate the electron pressure from the Saha equation and an average electron pressure determined from the values for several elements. Such a technique was used by Helfer,

Wallerstein and Greenstein (1959) to obtain the electron pressure from Fe, Ti and Cr information.

In an analysis of a star having the same ionization temperature as the sun Aller describes a technique for determining the electron pressure from measurements of the values of $\log \eta^{\circ}/\eta^{*}$ for the neutral and ionized stages of an element. The technique assumes that both sets of lines are in the same wavelength region, so that the absorption coefficient correction is the same, and are produced in the same atmospheric strata so that the temperature, velocity and partition function terms are the same for both neutral and ionized species. Application of the technique to a star that is not of the same temperature as the sun is more difficult than the description that is given in Aller's text (1963) but is simplified if the Saha equation is derived in differential form.

Writing the Saha equation for both the sun and the star, we have

$$\log N_1^{\circ}/N_o^{\circ} = \log 2u_1/u_o + 2.5 \log T_{ion}^{\circ} - \theta_{ion}^{\circ} \chi_i - 0.48 - \log P_e^{\circ}, \quad \text{(A-1)}$$

$$\log N_1^{*}/N_o^{*} = \log 2u_1/u_o + 2.5 \log T_{ion}^{*} - \theta_{ion}^{*} \chi_i - 0.48 - \log P_e^{*}. \quad \text{(A-2)}$$

Subtracting the equation for the star from the one for the sun and assuming that the difference in the ratio of partition functions is negligible, we obtain the equivalent of Equation (7) in the paper by Helfer, Wallerstein and Greenstein (1963).

$$\log N_1^{\circ}/N_0^{\circ} - \log N_1^{*}/N_0^{*} = (\theta^{*}-\theta^{\circ}) \chi_i + 2.5 \log T_{ion}^{\circ}/T_{ion}^{*} - \log P_e^{\circ}/P_e^{*}. \quad \text{(A-3)}$$

The quantity which may be determined from the observable data is the difference in the relative shift of the η values which Aller defines as the quantity

$$\Delta = [\eta_1] - [\eta_o],$$

$$= \log N_1^o/N_1^* - \log N_o^o/N_o^*,$$

$$= \log N_1^o - \log N_1^* - \log N_o^o + \log N_o^*, \qquad \text{(A-4)}$$

$$= (\log N_1^o - \log N_o^o) - (\log N_1^* - \log N_o^*),$$

$$= \log N_1^o/N_0^o - \log N_1^*/N_0^*.$$

The term $\log N_1^o/N_0^o$ may be calculated from the data of Table 8-4, p. 385 of Aller. The left hand side of the differential Saha equation is now given in terms of an observable quantity and the unknowns in the equation are the ionization temperatures and electron pressures in the star and the sun.

$$[\eta_1] - [\eta_o] = (\theta^* - \theta^o)\,\chi_i + 2.5 \log T_{ion}^o/T_{ion}^* - \log P_e^o/P_e^* \qquad \text{(A-5)}$$

Searle, Sargent, and Jugaku (1963) describe three methods that were used to determine representative values of θ and $\log P_e$ for the level of line formation in the atmospheres of three supergiants. Information is obtained from a) the absolute strengths of the Fe II lines; b) the degree of ionization of Fe; and c) the strengths of the Balmer lines. A statistical average of the information from the three techniques, with allowance made for the probable errors of measurement in the data, was then made to obtain the final values of ionization temperature and electron pressure.

Method a) is based upon the determination of the value of the absorption coefficient of the star, k_λ, and a comparison of the experimental value with tables for material of solar composition to determine the probable bands of excitation temperatures and electron pressures. The

assumption is made that all of the iron in both the star and the sun is in the form of Fe II and also that the number of Fe atoms per gram of stellar material is the same. The continuous opacity per gram of stellar material is then determined from the equation

$$\left\langle \log \eta^{\circ} - \log \eta^{*} + \chi_e \left[\theta^{\circ}_{exc} - \theta^{*}_{exc} \right] \right\rangle_{Fe\ II} = \log k^{*}_{\lambda}/k^{\circ}_{\lambda} + \log v^{*}/v^{\circ}. \qquad (A\text{-}6)$$

Estimated errors in the technique were calculated from the estimated uncertainties in the measured values of the excitation temperature and the velocity.

In method b) the degree of ionization of Fe, relative to the sun, is given by

$$\left[\frac{N\ (Fe\ II)}{N\ (Fe\ I)}\right] = \log \frac{N^{*}\ (Fe\ II)}{N^{*}\ (Fe\ I)} - \log \frac{N^{\circ}\ (Fe\ II)}{N^{\circ}\ (Fe\ I)}, \qquad (A\text{-}7)$$

$$= \left\langle \log \eta^{\circ} - \log \eta^{*} + \chi_e \left(\theta^{\circ}_{exc} - \theta^{*}_{exc}\right) \right\rangle_{Fe\ I}$$

$$- \left\langle \log \eta^{\circ} - \log \eta^{*} + \chi_e \left(\theta_{exc} - \theta_{exc}\right) \right\rangle_{Fe\ II},$$

where N is the number of particles per unit volume and the brackets indicate average values. All of the available Fe II lines that were studied came from levels with excitation potentials of about 2.8 eV. The quantities $\log \eta^{\circ} - \log \eta^{*}$ were plotted for the Fe I lines as a function of excitation potential, a value was read off of the mean curve at $\chi_e = 2.8$ eV, and the term $\log \eta^{\circ} - \log \eta^{*} + \chi_e \left(\theta^{\circ}_{exc} - \theta^{*}_{exc}\right)$ was computed. The value of N(Fe II)/N(Fe I) together with the assumed solar values of excitation temperature and electron temperature lead, via the Saha equation, to a band of allowable values of θ_{exc} and electron pres-

sure.

In method c) the profiles of the Hγ lines were measured and compared with model atmosphere calculations for high luminosity F stars made by the authors. In order to avoid errors caused by circumstellar absorption, only data from the wings of the lines was used. The absorption in the wings is a function of the fraction of neutral hydrogen atoms, the quantities θ' and P_e' and the continuous absorption coefficient per gram $k'(\theta', P_e')$ at the wavelength of Hγ. The quantities θ' and P_e' are the values of θ and P_e in the stellar atmosphere at a mean depth of formation of the wings of Hγ. In the calculations it was found that the metallic lines are formed at $\tau \sim 0.2$ while the wings of Hγ at a point on the profile where the absorption is 30% are formed at $\tau \sim 0.5$. It is estimated that the relationship between the primed and unprimed quantities is

$$\theta' = 0.93\,\theta \quad \text{and} \quad \log P_e' = \log P_e + 0.3. \qquad \text{(A-8)}$$

Additional information on θ_{ion} and $\log P_e$ was obtained by fitting the observed profiles to the computed Hγ profiles of Searle and Oke (1962).

Effective Temperatures

The same profiles were also utilized by Gunn and Kraft (1963) to determine the effective temperatures of main sequence stars in the Hyades. In order to exclude the areas in the line wings which would be greatly magnified by an incorrect placement of the continuum, the pseudo-equivalent width of the area under the lines between $(\lambda_o + 10.0)$A and $(\lambda_o - 10.0)$A was used where λ_o is the center of the Hγ profile at

4340.49A. By comparing the measured values of the pseudo-equivalent width with those determined from the computed functions, the effective temperature could be determined. The value of the pseudo-equivalent width is also a relatively insensitive function of the star's surface gravity so this parameter also has to be known to a limited degree of accuracy.

Using this technique, an attempt was made to obtain the value of the effective temperature for θ Ursae Majoris by analysis of the areas contained within the profiles of the HΥ line. For θ Ursae Majoris six microphotometer tracings containing the HΥ profile were available for which the pseudo-equivalent width determination could be made, although tracing 1810 contained only the long-wavelength half of the profile. The following values of the pseudo-equivalent width were obtained from the six tracings.

TABLE XLIX

PSEUDO-EQUIVALENT WIDTHS FOR HΥ

Tracing Number	Pseudo-Eqiuivalent Width
1915	0.232
1914	0.230
1796	0.206
1807	0.200
1810	0.163
1792	0.155

It is noted from an inspection of the values that a grouping in pairs occurs around the values 0.23, 0.20 and 0.16. Adopting Greenstein's value for log g = +3.5 and consulting Figure 3 on Page 305 in the paper of Gunn and Kraft (1963), the observed extreme values of the pseudo-equivalent width could indicate values of the effective tempera-

ture ranging from a maximum value of 6575° K to a minimum value of 6115° K. The mean value of 0.198 for the pseudo-equivalent width corresponds to a temperature of 6405° K which is higher than the effective temperature of 6210° K listed by Hynek (1951) for subgiants of class F6. Although the effective temperatures determined from the pseudo-equivalent widths of the HΥ lines are not inconsistent with the effective temperature determined from the spectral class, the variation between the six tracings is large enough so that the spectral class value of 6210° K is preferred and has been used in the calculations performed in Chapter IV.

Values of the Solar Parameters

In reviewing the literature for values of the solar effective temperature we find predominant agreement on a value of 5725°K or $\theta_{eff} = 0.88$. However, differences exist on the values of the solar electron pressure and ionization temperature. Aller and Greenstein (1960) and Gunn and Kraft (1963) follow the model solar atmosphere of Pierce and Aller (1952) and take values of $\theta^{o}_{ion} = 0.89$ and $\log P^{o}_{e} = 1.30$ at a representative depth for line formation $\tau = 0.35$. In Greenstein's analysis of several F stars in which θ Ursae Majoris was included, line formation occurred at $\tau = 0.25$ and values of $\theta^{o}_{ion} = 0.95$ and $\log P^{o}_{e} = 0.80$ were adopted. Koelbloed (1967) used an intermediate value of the electron pressure of $\log P^{o}_{e} = 1.00$ and takes the ionization temperature equal to the excitation temperature, or $\theta^{o}_{ion} = 0.98$.

Absolute Techniques Using f-values

If the f-values of the lines are known, the effective temperature and the electron pressure may be calculated by the techniques used by Peebles (1964) or given in Aller's text (1963) on page 379. For lines arising from each level of excitation potential Peebles plots

$$\Delta \log X = (\log NH + \log C - \log u + \log c/v) - \theta \chi_e \qquad (A\text{-}9)$$

versus χ_e to get the temperature from the slope of the least squares fit to the data. The value of $\Delta \log X$ is obtained from the horizontal shift necessary to fit the observed to the theoretical curve of growth. The procedure is repeated for a second stage of ionization of the element, and if information is available for two elements with different ionization potentials, both the ionization temperature and the electron pressure may be calculated from the Saha equation. However, Aller restates the objection mentioned in connection with Greenstein's work against using this technique to get both the ionization temperature and the electron pressure. In practice it is better to obtain the ionization temperature from some other source and use the abundance data from several elements to calculate an average electron pressure.

Analysis by Both Curve of Growth and Model Atmosphere Methods

The star ε Virginis was studied by the Cayrels (1963) using both the differential curve of growth technique and a model atmosphere approach. This normal, population I, red giant of spectral class G6, was studied in high dispersion spectra (0.36 to 1.0 mm/A) from which the equivalent widths of 1400 lines were measured. A coarse analysis was made using separate values of the excitation temperature for the neutral and ionized lines and employing the Pierce and Aller (1952) solar curve

of growth. However, it was felt that the coarse analysis failed to take into account the following factors:

"(a) In the solar atmosphere, the ionization of hydrogen begins rather suddenly at about $\tau = 0.5$ and releases a large number of electrons in deep layers. It is likely that this affects the ionized lines more than the neutral ones which are formed in higher layers. (b) Silicon, which is the most important source of electrons in cool stars, is only partially ionized in the upper layers of ϵ Virginis. (c) The wings of hydrogen cannot be predicted properly from a coarse analysis."

To make a comparison between ϵ Virginis and the sun, five observable quantities were selected that depended mainly on the physical parameters (effective temperature, surface gravity, and the hydrogen to metal ratios) and not on individual abundances of the elements. These observable quantities were: "(1) The energy distribution in the continuum, (2) the excitation temperature of Fe I, (3) the strength of the wings of $H\alpha$, (4) the absolute visual magnitude of the star, and (5) the intensity ratio of ionized to neutral lines for an element." Five theoretical model atmospheres for ϵ Virginis were constructed based upon different assumptions of the values of effective temperature, surface gravity and damping constant. The stellar models were computer calculated by numerically integrating four equations relating absorption coefficient, effective temperature, electron pressure and total pressure as functions of optical depth. A comparison was then made between the values of the five observable parameters in ϵ Virginis and the sun. For each element the change in line strength expected from the difference in physical conditions between the sun and star was predicted; any other variation was attributed to a difference in chemical composition.

Determinations were made of macroturbulence and rotational velocity from the half widths of weak lines, microturbulence from the curve of growth of the very numerous lines of Fe I, and surface gravity from an analysis of measurements of the wings of Mg I lines. The effective temperature was derived from the photoelectrically determined colors, the wings of the H α profiles, and the excitation temperature as determined from the variation of displacement with excitation potential of the curves of growth of Fe I and Cr I.

From an analysis of the above data, the most reliable values of the effective temperature, surface gravity and damping constant were chosen and a final definitive model atmosphere computed. The shifts in the curve of growths of the elements between ϵ Virginis and the sun due to the differences in the temperature and gravity were predicted from this model atmosphere. The predicted shift was compared with the observed shift and the residual was attributed to differences in the abundances. An error analysis was made taking into account the contributions from uncertainty in the knowledge of temperature, electron pressure, systematic errors in photometry and random errors in the fitting of the observed to the theoretical curve of growth. The comparison of the predictions of the coarse and fine analyses showed that there were no significant differences between the results predicted by the two, and that the chemical composition of ϵ Virginis was essentially the same as that of the sun.

In his analysis of two high velocity stars, Koelbloed (1967) uses a combination of model atmosphere and both absolute and differential curve of growth techniques. Curves of growth for the elements in the stars were prepared on an absolute basis from the f-values of Corliss and

Bozman (1962) without correcting the ordinate for the velocity of the atoms and ions. The horizontal shift of Fe I in the stellar atmospheres was computed with respect to Fe I as represented by the data used by the Cowleys in constructing their solar curve of growth. For the other elements, the curves of growth for the sun were computed from the Utrecht equivalent widths. The excitation temperature of Fe I was computed by requiring the best fit to the curve of growth of data from different excitation potentials. This value of excitation temperature was used for all of the other elements and ions. Since the experimental values for the excitation temperatures of the ionized species were not well determined, the suggestion was made that a better procedure would have been to calculate excitation temperatures for the ions from model atmospheres.

The determination of effective temperature can usually be done very accurately from a photoelectric scan of the continuous spectrum after correcting for the energy subtracted out by line absorption; but this technique was not applicable in a definitive manner to these stars for two reasons. Since the stars are situated nearly on the galactic equator, the spectra will be affected by reddening due to absorption by intersteller matter, and secondly, accurate stellar models were not available in this temperature region. Nevertheless, the technique was attempted. While the results obtained from the scan of the continuum were not definitive, they were consistent with a value of the effective temperature predicted from the excitation temperature using a model atmosphere for metal deficient stars.

The compatible values for the gravity, and ratio of electron density to hydrogen atom density were related to the effective temperature

through model atmospheres calculated by Conti (1967). By relating the luminosity of the stars to the surface gravity, mass and effective temperature, and determining the electron pressure from the shifts of neutral and ionized Fe, Ti, Cr and V, and using the Saha equation in the single layer approximation, the best values of gravity and ionization temperature were obtained. The abundances of the elements relative to the sun were then computed from the observed shifts in the curves of growth.

In conclusion it may be stated that a differential curve of growth analysis will have to draw on information from model atmospheres, an absolute curve of growth study, or other sources for some of the physical parameters used in performing the calculations and is not capable of providing all of the necessary information itself. This study of Koelbloed (1967) incorporates into the differential curve of growth technique not only a moderately elaborate model atmospheres calculation, but also makes use of the f-values used in the absolute technique.

APPENDIX B

STATISTICAL TECHNIQUES AND DETERMINATION OF ERRORS

Statistical Methods

One of the features of this study has been the use of formal statistical techniques that have not been used by other authors. Peebles and most other authors plot either absolute or relative curves of growth for the star under study for all of the lines arising from each spectral term and visually determine the error involved in horizontally shifting this portion of the curve until it coincides with the curve of the star or the model taken as standard. In contrast, the technique used in this study determines the shift between the curve of growth observed for the star and the curve taken as standard on a line-by-line basis by standard statistical methods which are easily performed on an electronic computer. The traditional method makes use of methods more natural to hand computation and does not make use of rigorous statistical methods. Since the traditional method averages together the scatter in the several lines composing the spectral term and estimates by eye the uncertainty allowed in the shift, a smaller value of uncertainty in the $[\eta]$ term results than in the procedure used in this paper, in which the standard deviation of the values of $[\eta]$ is calculated in agreement with accepted statistical procedures. The difference in reciprocal excitation temperatures is obtained from the slope of a plot of $[\eta]$ versus excitation potential. Using a standard regression analysis

program of the OSU Computing Center, slope of the best least squares linear regression line and its standard deviation, the standard deviation of the points about the regression line, and the statistical significance of the calculated slope, as measured by Fisher's F test, are rapidly evaluated by machine; this enables a quantity of data to be quickly processed that would require a prohibitive amount of hand calculation.

This results in an average value of ± 0.30 for the uncertainty in the value of $[\eta]$ found in this study; Helfer, Wallerstein and Greenstein (1963) using the traditional technique estimate that their maximum error in determining the shifts is in the range of $\pm 0.10 - 0.12$.

This difference in technique also influences the uncertainty that is obtained in the effective temperature but the numerical values that are obtained in this study are comparable with those obtained by Peebles. The computation of the difference in excitation temperatures between the sun and the star for the elements Fe I, Mn I, and Ti I produces an average error in slope of about ± 0.03 in the value of θ_{exc}. If this is converted to a temperature difference (180°), it is of the same size as the errors measured by Peebles for θ Ursae Majoris using the absolute curve of growth technique. The range of excitation temperatures that is covered by data having slopes that are significant at the 5 percent level covers about the same span as the range of temperatures computed by Peebles, as an inspection of Table VII will show. Including the temperatures computed from sources of f-values other than the Bureau of Standards, the temperature extremes are given in Table L.

Although other authors have indicated the quality of the lines used

TABLE L

EXTREMES OF EXCITATION TEMPERATURE

		This Study	Peebles
Unionized	High	Ti I 5860°K	Cr I 6239°K M-E Absorption
	Low	V I 3680°K	Fe I 3730°K M-E Absorption King's f-values
Ionized		Ti II 7100°K	Ti II 8141°K M-E Absorption

in the analysis by rating them as good, poor, slightly blended and other subjective ratings, this study employs a quantitative method of evaluation of the data. The criteria on which the weights were assigned to the lines were the number of profiles measured for a line, the dispersion of the measurements of equivalent width for a line, and the region in which the value of log W/λ intersects the curve of growth. The use of a weighting procedure is justified by noting that to accept all lines on an unweighted basis would be to disregard the fact that the quality of the equivalent widths of the lines differs by large amounts; the use of the weighting procedure is an attempt to make the better quality data have more of an influence on the results. The effect of the weighting procedure upon data is reflected by noting in Table VII that the average difference in reciprocal excitation temperature for an element only changes by a factor of 0.03 if weighted data is substituted for the unweighted. Calculations have shown that the procedure of assigning statistical weights changes the average value of $[\eta]$ by about 0.03 over using equally weighted data. Since the majority of lines were only given weights of unity the weighting procedure did not produce any substantial changes in the values of the results but there is

reason to believe that its use has enabled more accurate results to be calculated from lines of widely differing quality.

Error Analysis

An analysis of the errors involved in the calculations in Chapter IV giving the abundances in terms of the measured quantities will now be performed. Equation (2-18) is repeated for convenience.

$$[N_r] = [\eta] + \chi_{r,s}(\theta^o - \theta^*) + [v] + [u(T)] + [k_\lambda(T,P_e)] . \qquad \text{(B-1)}$$

Assuming that the errors in the quantities on the right hand side of the equation are independently distributed and can be combined in root mean square fashion, the total error in the calculation of the relative abundance in the stellar atmosphere is determined by the r.m.s. sum of the uncertainties of each of the terms on the right hand side of the equation

$$(\delta [N_r])^2 = (\delta [\eta])^2 + (\chi\, \delta (\theta^o - \theta^*))^2 + (\delta [v])^2 + (\delta [u(T)])^2 + (\delta [k_\lambda(T,P_e)])^2 . \qquad \text{(B-2)}$$

The value of the term $\delta[\eta]$ is calculated as the standard deviation of points about the regression line in the least squares computer program used to fit straight lines to the plots of $[\eta]$ versus excitation potential. The average value of the standard deviation of $[\eta]$ for statistically weighted data for the elements on which the least squares analysis was performed was ± 0.30.

The uncertainty in ther term $(\theta^o - \theta^*)$ may be obtained from the uncertainties in the values of the least squares fitted slopes for the elements Fe I, Ti I and Mn I which were used to calculate the average value of $(\theta^o - \theta^*)$. The average value that was obtained for

$\delta(\theta^o - \theta^*) = \pm 0.03$, and, using an average excitation potential of 2.0 eV, the average value of the term $X\delta(\theta^o - \theta^*)$ is calculated to be ± 0.06.

The correction term for the total velocity contains error due to both the uncertainty in the temperature and in the values of the turbulent velocities of the sun and the star. In order to simplify the derivation of the uncertainty in velocity, it will now be demonstrated that one of the error terms is substantially smaller than the other. Considering the error in the velocity of the sun:

$$v^o = \sqrt{\frac{2kT^o}{m} + v_{turb}^{o,2}}. \tag{B-3}$$

$$\frac{\partial v^o}{\partial T^o} = \frac{k}{m}\left(\frac{2kT^o}{m} + v_{turb}^{o,2}\right)^{-\frac{1}{2}}. \tag{B-4}$$

$$\frac{\partial v^o}{\partial v_{turb}} = \frac{1}{2}\left(\frac{2kT^o}{m} + v_{turb}^{o,2}\right)^{-\frac{1}{2}} 2\, v_{turb}^o = \frac{v_{turb}^o}{v^o}. \tag{B-5}$$

$$dv^o = \frac{\partial v^o}{\partial T^o} + \frac{\partial v^o}{\partial v_{turb}}\, dv_{turb}^o,$$

$$= \frac{1}{2v_o}\,\frac{2kT^o}{m}\,\frac{dT^o}{T^o} + \frac{v_{turb}}{v^o}\, dv_{turb}^o. \tag{B-6}$$

Changing from differential to incremental notation, and inserting numerical values for the turbulent, kinetic and total velocities for chromium, it is seen that the term due to the uncertainty in the turbulent velocity is an order of magnitude larger than that due to the uncertainty in the temperature.

$$(\delta v^o)^2 = \left(\frac{v_{th}^2}{2v^o} \cdot \frac{\delta T^o}{T^o}\right)^2 + \left(\frac{v^o_{turb}}{v^o} \cdot \delta v^o_{turb}\right)^2, \qquad (B\text{-}7)$$

$$= \left(\frac{1.63^2}{2 \times 1.7} \cdot .03\right)^2 + \left(\frac{1.4}{1.9} \cdot 0.2\right)^2,$$

$$= (0.013)^2 + (0.147)^2.$$

Regarding the uncertainty in the total velocity to be due entirely to the uncertainty in the turbulent component, an equation for the error in $[v]$ can be shown to be

$$\delta[v] = \left\{ 2.3026^2 \left[\frac{v^o_{turb}}{(v^o)^2} \Delta v_{turb}\right]^2 + 2.3026^2 \left[\frac{v_{turb}}{(v^*)^2} \Delta v^*_{turb}\right]^2 \right\}^{\frac{1}{2}},$$

$$= \left\{ 2.3026^2 \left[\frac{1.4}{1.9^2} \; 0.2\right]^2 + 2.3026^2 \left[\frac{2.4}{2.65^2} \; 0.2\right]^2 \right\}^{\frac{1}{2}},$$

$$= \pm 0.24. \qquad (B\text{-}8)$$

The results of these calculations give a value of $\delta[v]$ which seems rather high. It is based only upon the uncertainty in the turbulent velocity in the sun as measured by the Cowleys' (1964) and upon an error of comparable magnitude for the turbulent velocity in θ Ursae Majoris determined by Peebles for Fe I-NBS data applied to the four atmospheric models. Another method of estimating the error in the total velocity term is to calculate the root mean square difference between the theoretically calculated velocity differences and the experimentally measured velocity differences, given in Table X, for the elements Ca I, Ti I, Ti II, Cr I, Fe I-NBS and Ni I. The value of $\delta[v]$ obtained from

this calculation is ± 0.126. In making a comparison between the theoretically computed and experimentally determined log v^{o}/v^{*} values, it is well to remember that the assumption is made that the lines of all of the elements are formed at levels of the atmosphere that can be characterized by the same values of temperature and turbulent velocity. Since the lines are actually formed at different depths in the atmosphere the assumptions may be incorrect and thus account for the fact that three of the velocities show good agreement and the other three have large variations.

Assuming the same temperature uncertainty of $\delta\theta = \pm 0.03$ for the partition function correction term, a value of $\delta[u] = \pm 0.004$ for a typical element was obtained.

The uncertainty in the value of the continuous absorption coefficient depends upon the uncertainty in both the ionization temperature and the electron pressure. From the standard deviation of the individual values of the electron pressure calculated from the Fe, Ti, Cr and V data given in Table X, the uncertainty in log P_e^{o}/P_e^{*} is calculated to be ± 0.08. Using an uncertainty in the value of θ_{ion} of ± 0.03, the values of log P_e are obtained from Table L of Allen (1963) at a wavelength of $\lambda 5000$. The rate of change of the continuous absorption coefficient with variation in temperature was made between values of $\theta_{ion} = 0.8$ and 0.9, and variation in electron pressure between values of log $P_e = 1.0$ and 2.0. Determining the separate changes in the continuous absorption coefficient to be ± 0.06 for the effect of a ± 0.03 shift in the r.m.s. value of θ_{ion}, and ± 0.08 due to the uncertainty in the electron pressure, the combination of the two sources of error gives

a value of $\delta[k_\lambda] = \pm 0.10$. The value of log P_e may change by ± 0.10 for a 1000 Angstrom variation in wavelength, but since the correction is applied in a differential fashion this source of error will tend to cancel.

To obtain the total error in the determination of the relative number densities of the elements in θ Ursae Majoris, the values for each separate error term are combined in r.m.s. fashion. Substitution in Equation (B-2) gives

$$\delta[N_r] = \left[(0.30)^2 + (0.06)^2 + (0.126)^2 + (0.004)^2 + (0.10)^2\right]^{\frac{1}{2}}, \quad \text{(B-9)}$$

$$= \pm 0.346.$$

It should be noted that the uncertainty in $[\eta]$ is the largest term contributing to the uncertainty in the abundance of an element. The second largest error contribution comes from the correction for the difference in total velocity. The numerical value of the correction was taken as the r.m.s. average of the difference between the theoretically calculated velocity corrections and the experimentally observed data of Peebles (1964) for θ Ursae Majoris and Wright (1948) for the sun. The third largest error contribution comes from the correction for the continuous absorption coefficient due to the uncertainties in the values of the ionization temperature and electron pressure. The uncertainty in the ionization temperature was taken to be equal to the average uncertainty in the excitation temperature and the uncertainty in the electron pressure was determined from the spread of values of $[P_e]$ calculated from the differential Saha equation. All of the other sources of error such as the uncertainty in the correction term for the excitation

potential due to the uncertainty in the differential reciprocal excitation temperature are numerically of negligible size relative to the abundance, total velocity, and absorption coefficient terms.

VITA

Edward Covert Mangold

Candidate for the Degree of

Doctor of Philosophy

Thesis: A DIFFERENTIAL CURVE OF GROWTH ANALYSIS OF THE SPECTRUM OF THE STAR THETA URSAE MAJORIS

Major Field: Physics

Biographical:

Personal Data: Born in Shreveport, Louisiana, August 23, 1936, the son of Charles E. and Bernice M. Mangold.

Education: Attended grade school in Shreveport, Louisiana, and Tulsa, Oklahoma; graduated from Marquette High School, Tulsa, Oklahoma, in May, 1954; attended the de Lasalle Institute in Glencoe, Missouri, in 1954 and 1955; received the Bachelor of Science degree from Rockhurst College in May, 1959, with a major in Physics; received the Master of Science degree in 1964 from the University of Maryland with a major in Physics; completed requirements for the Doctor of Philosophy degree in July, 1968.

Professional Experience: Graduate teaching assistant, University of Maryland, Department of Physics, 1959-60; graduate research assistant, University of Maryland, Department of Physics, 1960-1961 and 1962-1963; Instructor, Department of Natural Sciences and Mathematics, Rockhurst College; 1961-62; Physicist, National Weather Satellite Center; 1963-1965; Graduate Associate, Oklahoma State University Research Foundation Electronics Laboratory, 1965-1968.